Comparative study of dedicated Monte Carlo simulation codes for the performance evaluation of small animal PET systems.

Foteini D. Popota

TESI DOCTORAL UPF / 2014

DIRECTORS DE LA TESI

Dr. Juan Domingo Gispert López (Pasqual Maragall Foundation)

Dr. Javier Pavía Segura (Hospital Clinic, Barcelona)

DEPARTAMENT OF EXPERIMENTAL AND HEALTH SCIENCES

Universitat Pompeu Fabra Barcelona

To my lovely family

"....Πάντα στὸ νοῦ σου νἄχῃς τὴν Ἰθάκη.
Τὸ φθάσιμον ἐκεῖ εἶν' ὁ προορισμός σου.

Ἀλλὰ μὴ βιάζῃς τὸ ταξείδι διόλου.
Καλλίτερα χρόνια πολλὰ νὰ διαρκέσει.
Καὶ γέρος πιὰ ν' ἀράξῃς στὸ νησί,
πλούσιος μὲ ὅσα κέρδισες στὸν δρόμο,
μὴ προσδοκώντας πλούτη νὰ σὲ δώσῃ ἡ Ἰθάκη.

Ἡ Ἰθάκη σ' ἔδωσε τ' ὡραῖο ταξίδι.
Χωρὶς αὐτὴν δὲν θἄβγαινες στὸν δρόμο.
Ἄλλα δὲν ἔχει νὰ σὲ δώσει πιά.

Κι ἂν πτωχικὴ τὴν βρῇς, ἡ Ἰθάκη δὲν σὲ γέλασε.
Ἔτσι σοφὸς ποὺ ἔγινες, μὲ τόση πείρα,
ἤδη θὰ τὸ κατάλαβες ἡ Ἰθάκες τί σημαίνουν."

Κ. Π. Καβάφης
1911

"*…Ten siempre a Itaca en tu mente.*
Llegar allí es tu destino.

Mas no apresures nunca el viaje.
Mejor que dure muchos años
y atracar, viejo ya, en la isla,
enriquecido de cuanto ganaste en el camino
sin aguantar a que Itaca te enriquezca.

Itaca te brindó tan hermoso viaje.
Sin ella no habrías emprendido el camino.
Pero no tiene ya nada que darte.

Aunque la halles pobre, Itaca no te ha engañado.
Así, sabio como te has vuelto, con tanta experiencia,
entenderás ya qué significan las Itacas."

C. P. Cavafis.
1911 - (Antología poética.
Alianza Editorial, Madrid 1999.)

Aknowledgements

It has been a very long and demanding journey but the most rewarding was the journey itself and not the destination.

I would like to express my gratitude to my supervisor Dr. Juan D. Gispert for giving me the opportunity to come to Barcelona and work in this project, which became my PhD Thesis. I thank him for the support and guidance through all these years and for the opportunities to expand my knowledge.

I would like to deeply thank Dr. Javier Pavia for being the co-director of the thesis, for all the support and valuable help.

I also express my gratitude to Dr. Domènec Ros for accepting me in his laboratory, for his help and for giving me the opportunity to work with wonderful people.

Many thanks to Dr. Pablo Aguiar for his valuable help and for the long hours of simulations!

To Dra. Deborah Pareto for the support and lunches through difficult times and not only. To Dr. Raul Herance and Dr. Santiago Rojas for helping me with the experiments. To Dra. Cristina Lois for her support and help.

I would also like to especially thank the support and friendship of Dolors de la Fuente, whom without her valuable help many things would be impossible. Moltes gràcies guapa!

To Samuel España and Dr. Jose Manuel Udias Moinelo for their help and support with the simulation codes.

To my collegues from CRC-CIM, Xavi, Beri, Sandra, Judith, Sergio, Xavi T., Alba, Anna, Ibane, Pili, Olga, Jesus, Cecilia, Natalia, Santi B., Susi, Elia, Nuria, Cristina, Eva, Aida, Ignasi y todos los que puede ser que olvido.

Muito obrigada a minha querida Fran por sua amizade, apoio, risadas, e bons momentos de todos esses anos dentro e fora do trabahlo. Eu sinto faltate muito!!

A todos mis companyeros del clinic... Nuria, Naira, Sebastian, Berta, Cris, Anna, Judith, Paco, Aida, Eloy, Claudia y Carles. Muchisimas gracias por todo lo que hemos pasado, por la auyda, las risas, los momentos de estress, las comidas y mucho mas.. Os echo de menos!

Many many thanks to my lovely friends, Carla, Anna, Mik, Javi y Fran... por todo!

A special thanks goes to Stelios...for always being there for me, with me....for everything. To Majo (τον καλύτερο σκύλο που υπάρχει) for always relaxing me and making me laugh.

To my family, that without their help I wouldn't have come to Barcelona so as to enjoy this trip... Ευχαριστώ για όλα...

Abstract

Positron emission tomography (PET) is a powerful tool for translational research constantly facing the challenge of new technologies. Therefore, technical aspects are becoming more relevant in the design and development of new PET systems. The knowledge of the physical characteristics is the key point especially in the case of small animal imaging. For the optimization of the capabilities of small animal PET systems, their performance has to be evaluated through specific standards and Monte Carlo simulation codes.

In this thesis, in the first part, the performance evaluation of the microPET R4 scanner according to the NEMA NU 4-2008 standards for small animal positron emission tomography is assessed and a comparison against its previous evaluation according to the adapted clinical NEMA NU 2-2001 standards is presented. Differences in the results between NEMA NU 4-2008 and NEMA NU 2-2001 were obtained associated to the use of different phantoms and energy windows. In the second part, dedicated Monte Caro simulation models (using GATE and PeneloPET) of the performance of the R4 system is compared against experimental data. Accurate results were obtained form the simulation codes, whereas PeneloPET proved to be faster than GATE.

Resum

La tomografia per emissió de positrons (PET) és una poderosa eina per a la investigació translacional adreçada constantment al repte de les noves tecnologies. Per tant, els aspectes tècnics són cada vegada més rellevants en el disseny i desenvolupament de nous sistemes de PET. El coneixement de les característiques físiques és el punt clau especialment en el cas de les tècniques d'imatge de petits animals. Per a la optimització de les capacitats dels sistemes de PET per animals de laboratori, el seu rendiment ha de ser avaluat mitjançant protocols específics i codis de simulació de MonteCarlo.

En aquesta tesi, en la primera part, es presenta l'avaluació del rendiment de l'escàner microPET R4 d'acord amb les normes NEMA NU 4-2008 de la tomografia per emissió de positrons petit animal és compara amb l'avaluació anterior realitzada d'acord amb la clínica adaptada NEMA NU 2-2001. Es van obtenir diferències en els resultats entre NEMA NU 4-2008 i NEMA NU 2-2001 associat a la utilització de diferents fantoms i finestres d'energia.

A la segona part, es compara l' exactitud de diferents codis de simulació Monte Carlo (utilitzant GATE i PeneloPET) per avaluar el rendiment del sistema de R4 en relació a les dades experimentals. Tots dos codis van proporcionar resultats exactes si bé PeneloPET va demostrar ser més ràpid que GATE.

Preface

Small animal PET imaging refers to imaging small animals, such as mice and rats, with small, high-resolution PET scanners designed for this reason.

There is a high demand for small animal PET because of the need to study models of diseases since mice and rats are hosts of a large number of related genes.

Since the mid-1990s, small animal PET has been used extensively in non-invasive biomedical research to study small animals longitudinally.

The size difference between human and small animals impose higher performance requirements to small animal PET systems as compared to clinical ones, particularly on spatial resolution and sensitivity. Depending on the specific application, one could trade off spatial resolution for sensitivity or the other way around, but in order to achieve this, the actual performance of each system must be known through specific testing procedures.

Until recently, there were no specific standards to assess the performance of small animal PET systems and their comparison was made by adapting already existing clinical PET standards.

In 2008 the National Electrical Manufacturers association published the NEMA NU 4-2008 standards for small animal PET systems for the evaluation of their performance in terms of spatial resolution, sensitivity, scatter fraction, counting rates and image quality. These standards are meant for comparison of imaging systems under specific operating conditions.

One powerful tool in the development of small animal PET systems is through Monte Carlo simulation codes since many parameters can be optimized like the geometry, crystal size, electronics, shielding etc. It is crucial to determine these parameters, analyze the data and various components of the system so as to evaluate the performance of each system without the actual need of building it in various configurations.
In order to do that, Monte Carlo simulations need to follow specific standards for the performance evaluation of each system and therefore, the NEMA NU 4-2008 standards are the most appropriate ones when small animal systems are to be simulated.

The purpose of this study was two-fold; in the first part the aim was to evaluate the performance parameters of the microPET R4 system using the NEMA NU 4-2008 and to compare it to its previous evaluation according to the adapted clinical NEMA NU 2-2001 standards. This study led to the publication of: Popota F. D., Aguiar P., Herance R. J., et al. **Comparison of the Performance Evaluation of the MicroPET R4 Scanner According to NEMA Standards NU 4-2008 and NU 2-2001.** IEEE Trans Nuc Science, vol 59(5), 1879-1886, 2012.

In the second part the aim was to compare two dedicated Monte Carlo simulation codes for PET systems, GATE and PeneloPET, for the simulation of the performance evaluation of the microPET R4 system under the established standards of NEMA NU 4-2008 with regards to the experimental results obtained in the first part of the thesis. This

comparison has been submitted for publication to Physics in Medicine and Biology. Popota F. D., Aguiar P., España S., et. al. **Monte Carlo simulations versus experimental measurements in a small animal PET system. A comparison in the NEMA NU 4-2008 framework.**

This thesis is submitted to obtain the degree of Doctor at the Pompeu Fabra University. The research conducted herein was under the supervision of Dr. Juan Domingo Gispert López and Javier Pavía Segura, and was conducted at the Centre d' Imatge Molecular (CRC-CIM), Barcelona, Spain and the Unitat de Biofisica i Bioenginyeria, Departament de Ciencies Fisiologiques I Facultat de Medicina, Universidad de Barcelona, Barcelona, Spain.

The PhD was funded by the AMIT project (CEN-20101014) from the CDTI-CENIT program (Ministerio de Ciencia e Innovación) and Fondo de Investigaciones Sanitarias (PI12-00390).

Additional Publications:

Santiago Rojas, Jose Raul Herance, Sergio Abad, Xavier Jimenez, Deborah Pareto, Alba Ruiz, Elia Torrent, Francisca P. Figueiras, Foteini Popota, Francisco J. Fernandez-Soriano, Anna M. Planas, Juan D. Gispert (2011). *Evaluation of hypoxic tissue dynamics with 18F-FMISO PET in a rat model of permanent cerebral ischemia.* Molecular imaging and biology 13(3): 558-564.

Elseline Hoekzema, Santiago Rojas, Raul Herance, Deborah Pareto, Sergio Abad, Xavier Jimenez, Francisca P. Figueiras, Foteini Popota, Alba Ruiz, Nuria Flotats, Francisco J. Fernandez, Milagros Rocha, Mariana Rovira, Victor M. Victor, Juan D. Gispert (2012). *In vivo molecular imaging of the GABA/benzodiazepine receptor complex in the aged rat brain.* Neurobiology of Aging 33(7): 1457-1456.

Elseline Hoekzema, Santiago Rojas, Raúl Herance, Deborah Pareto, Sergio Abad, Xavier Jiménez, Francisca P Figueiras, Foteini Popota, Alba Ruiz, Núria Flotats, Francisco J Fernández, Milagros Rocha, Mariana Rovira, Víctor M Víctor, Juan D Gispert (2011). *[11C]-DASB microPET imaging in the aged rat: Frontal and meso-thalamic increases in serotonin transporter binding.* Experimental Gerontology 46(12): 1020–1025.

E Hoekzema, R Herance, S Rojas, D Pareto, S Abad, X Jiménez, FP Figueiras, F Popota, A Ruiz, È Torrent, FJ Fernández-Soriano, M Rocha, M Rovira, VM Víctor, JD Gispert (2010). *The effects of aging on dopaminergic neurotransmission: a microPET study of [11C]-raclopride binding in the aged rodent brain.* Neuroscience 171(4): 1283–1286.

Conferences:

F. D. Popota, N. P. Martinez, P. Aguiar, S. Madrigal Rojas, D. Ros, A. Cot, J. D. Gispert, J. Pavia (2008). "*Estimation of Scatter Fraction*

of PET imaging in human and small animal systems", XXIV Trobades Científiques de la Mediterrània., Maó.

F. D. Popota, P. Aguiar, Y. Fernandez, C. Lois, D. Pareto, D. Ros, J. Pavia, J. D. Gispert (2009). "*Comparison of NEMA NU 4-2008 vs. NEMA NU 2-2001 for the performance evaluation of the microPET R4 system*", IEEE MIC-NSS Conf Rec M05-151: 2706-2709.

F. D. Popota, P. Aguiar, Y. Fernandez, C. Lois, D. Pareto, D. Ros, J. Pavia, J. D. Gispert (2010). "*Comparison of NEMA NU 4-2008 vs. NEMA NU 2-2001 for the performance evaluation of the microPET R4 system*", CASEIB, Madrid (poster presentation).

Index

List of Abbreviations

3DRP	3D re-projection algorithm
ADC	Analog to Digital Conversion
ACD	Annihilation coincidence detection
ACF	Attenuation Correction Factors
BGO	Bismuth germinate
CFOV	Center of field of view
CPU	Central processing unit
CT	Computed tomography
DOI	Depth of interaction
FBP	Filtered back projection
FORE	Fourier re-binning
FOV	Field if view
FT	Fourier Transform
FWHM	Full Width Half Maximum
FHTM	Full Width Tenth Maximum
GSO(Ce)/GSO	Cerium-doped-gadolinium oxyorthosilicate
LOR	Line of response
LSO(Ce)/LSO	Cerium-doped lutetium oxyorthosilicate
LSF	Line spread function
MC	Monte Carlo
ML-EM	Maximum-likelihood expectation maximazation
MR	Magnetic resonance
NaI(Tl)	Thalium-doped sodium iodide
NECR	Noise equivalent count rate
NEMA	National Electrical Manufacturers Association
OSEM	Ordered subset expectation maximization
PDFs	Probability density functions
PET	Positron Emission Tomography
PMT(s)	Photomultiplier tube(s)
PS-PMT	Position sensitive photomultiplier tube
PSF	Point spread function
PVE	Partial volume effect
RC	Recovery coefficient
RD	Ring difference
ROI	Region of interest
SF	Scatter fraction
SNM	Society of Nuclear Medicine
SNR	Signal to Noise Ratio

SPECT	Single Photon Emission Computed Tomograohy
SSRB	Single slice re-binning

1 | Introduction

1.1 Positron Emission Tomography

Positron emission tomography (PET) is a non-invasive functional imaging technology for quantitatively measuring physiological and biochemical processes *in vivo*. Radioactive compounds used in PET are referred to as radiopharmaceuticals or radiotracers. Generally, they are labeled with short-lived positron-emitting radionuclides such as ^{18}F, ^{11}C, ^{13}N, ^{82}Rb and ^{15}O (Table 1). They are produced in a cyclotron and are then used to label compounds of biological interest. The labeled compound is introduced into the body, usually by intravenous injection and is distributed in tissues in a manner determined by its biochemical properties.

PET Radionuclides	**^{18}F**	**^{11}C**	**^{13}N**	**^{82}Rb**	**^{15}O**
Half-life	110 min	20.4 min	9.96 min	78 s	122 s
Maximum Positron Energy (MeV)	0.63	0.96	1.19	3.35	1.72

Table 1. List of PET radionuclides and their physical properties

This non-invasive nuclear medicine imaging technique results in a 3D image volume of the concentration of the radioisotope, thus mapping biochemical information as a function of the radiotracer used. Also, the tissue concentration of the radiolabeled molecules over time can be measured enabling the application of

pharmacokinetic models to measure the rate of a specific biological process without disturbing it. These unique features, together with the wide variety of biomolecules that can be labeled with positron emitting nuclides, make PET a powerful tool in clinical and research studies. In clinical diagnostic applications PET has been mostly used in oncology, to a lesser extent in neurology, and marginally in cardiology. In clinical research, PET is widely used in neurology, psychiatry and oncology. It has also been used as a translation tool for drug development to evaluate the pharmacokinetics of labeled drugs and the measurement of the effects of drugs on metabolism. PET has also found wide application in pre-clinical studies using small animal models of human disease. The need to perform animal-model studies *in vivo* in living, intact subjects evolved from the fact that the disease could be studied in its natural biological background state including mechanisms that are not present in *in vitro* studies.

1.1.1 Positron Emission and Annihilation

PET imaging is based on the nature of positron and positron decay (Turkington 2001). When a radionuclide decays by positron emission (also known as beta-plus decay or β+), the result is a new nuclide with one fewer proton and one more neutron, as well as the emission of a positron and a neutrino:

$$ {}^{A}_{Z}X_N \rightarrow {}^{A}_{Z-1}Y_{N+1} + e^+ + \nu \qquad \textit{(Eq. 1)} $$

The emitted positron, which is equal in mass and opposite in charge to an electron, slows down through a series of collisions with the

surrounding matter (tissue) and it combines with an electron before it annihilates after travelling a short distance (~ 1mm for 1 MeV in water). The mass of positron and electron is converted to two high energy γ quanta of 511 keV at nearly 180 degrees. This simultaneous emission of two photons in opposite directions is the basis of annihilation coincidence detection (ACD) and imaging in PET (Figure 1).

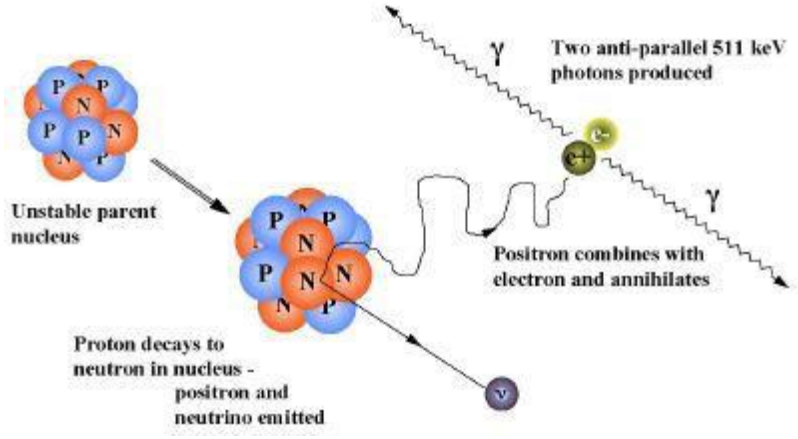

Figure 1. Positron Emission and Annihilation
(www.depts.washington.edu/nucmed/IRL/pet_intro/intro_src/section2.html)

A PET scanner is designed to detect and localize the simultaneous back-to-back photons that are emitted following decay of a radionuclide. Usually, PET detectors are designed forming a ring so as to record as many annihilation photons as possible.

When two photons are simultaneously detected by two pairs of detectors, it can be assumed that the annihilation must have occurred

along the line connecting the two detectors. This line is referred to as the "*line-of-response*" or else "LOR" (Figure 2).

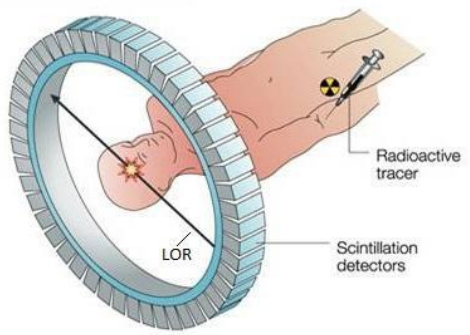

Figure 2. PET detector forming a ring; a coincidence event is assigned to a LOR joining two detectors (West 2004).

1.1.2 Positron Range and Non-colinearity

In PET imaging there are two effects that may lead to errors in determining the line along the annihilation took place (Figure 3). Positrons undergo multiple direction-changing interactions prior to annihilation, following a path in the tissue. This total path length is considerably longer than the *positron range*. From PET imaging perspective it is the average distance from the emitting nucleus to the end of the positron range, measured perpendicular to a line defined by the direction of the annihilation photons. As a consequence, a blurring effect on the final PET image is produced, ranging from a few tenths of a millimeter up to several millimeters, depending on the radionuclide and its maximum energy (Zanzonico 2004). The second

effect is that the annihilation photons almost never are emitted at exactly 180° directions from each-other. This effect, which is due to small residual momentum of the positron when it reaches the end of its range, is known as *non-collinearity*. The angular distribution is approximately guassian with Full Width Half Maximum (FWHM) ~ 0.5 degree. The effect on the spatial resolution is linearly dependent on the separation of the PET detectors and can be estimated as:

$$\Delta_{nc} = 0.0022 * D \qquad \textit{(Eq. 2)}$$

where D is the diameter of the PET scanner (Cherry 2003).

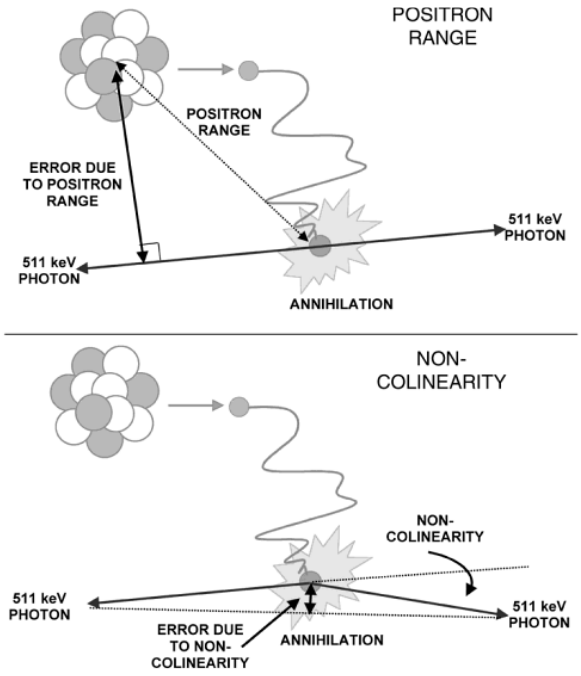

Figure 3: Positron range and non-colinearity (Phelps 2006).

1.1.3 Photon Interaction with Matter

As photons pass through matter they interact with the tissue surrounding them. The type of interaction is a function of the energy of the photons and the atomic number (Z) of the elements composing the matter. The most important interactions are Compton scatter, the photoelectric effect and the pair production, which only occurs with very high photo energies and is therefore not important in clinical nuclear medicine.

a) Compton Scattering

The interaction of Compton scattering takes place between the incident γ-ray and an electron in the absorbing material. It is the most dominant type of interaction in materials with lower atomic numbers, such as human tissue. The incoming photon is deflected through an angle θ with respect to its original direction. The photon transfers a portion of its energy to the electron, which is known as *Compton electron* or *recoil electron*. Because all angles of scattering are possible, the energy transferred to the electron can vary from zero to a large fraction of the γ-ray energy. The energy of the photon after interaction is given by:

$$E' = \frac{E_\gamma}{1+\left(\frac{E}{m_e c^2}\right)(1+cos\theta)} \qquad \textit{(Eq. 3)}$$

where *E* is the energy of the incident photon, *E'* is the energy of the scattered photon, *mec2* is the rest-mass energy of the electron and *ζ* is the angle through which the photon is scattered. The angular

distribution of scattered γ-rays is predicted by the *Klein-Nishina formula* (Knoll 2000).

b) Photoelectric Effect

In the photoelectric absorption process, a photon undergoes an interaction with an absorber atom in which the photon completely disappears. In its place an energetic *photoelectron* is ejected by the atom from one of its bound shells. This electron leaves the atom with energy equal to the energy of the incident γ-ray diminished by the binding energy of the electron. An outer shell electron then fills the inner-shell vacancy and the excess energy is emitted as an X-ray. The photoelectric effect is the dominant type of interaction in materials with higher atomic numbers, such as lead (Z = 82) (Levin 2004).

1.2 Imaging Technology for PET

1.2.1 PET Detectors

A common PET system consists of rings of block detectors. Each block detector is organized into 2D arrays and contains one or more segmented crystals or a collection of small crystals. Photomultiplier tubes (PMT) are placed behind them in order to collect the scintillation light and determine within which detector occurred the event (Figure 4).

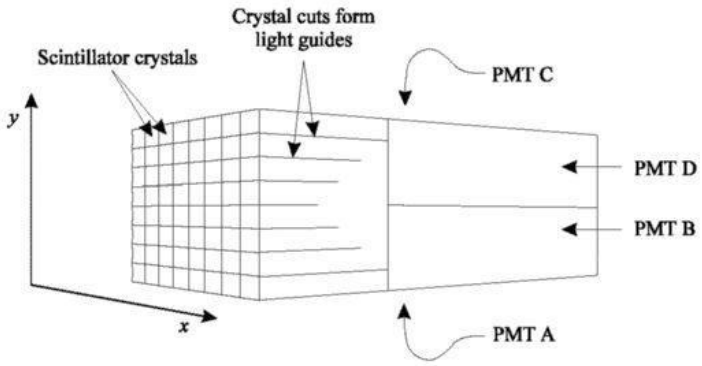

Figure 4. PET camera configuration

((www.depts.washington.edu/nucmed/IRL/pet_intro/intro_src/section2.html).

Generally, the role of PET detectors is to stop an emitted γ-ray and produce a signal that can be utilized by the downstream electronics. This signal must be able to carry information about how much energy has been deposited in the detector, give precise information of the spatial location of the interaction and determine the time difference in arrival of the annihilation photons (*timing resolution*) which is typically in the order of 2 to 6 ns. A typical timing window that is used in PET scanners so as not to reject the annihilation photon pairs is typically 2-3 times the timing resolution, leading to values in the range of 4-18 ns (*coincidence window*). An ideal detector must have a very high efficiency for detecting 511 keV photons, have high stopping power (the 511 keV photons will be absorbed by the detector), have high spatial resolution and high energy and timing resolution.

Scintillation detectors are the most common and successful mode for detection of 511 keV photons in PET imaging. They emit light when

they are excited by radiation of higher energy. The intensity of the scintillation light is important for an accurate determination of the energy of the absorbed radiation. Scintillattion light pulses (flashes) are usually characterized by a fast increase of the intensity in time (*pulse rise time*) followed by an exponential decrease (*fall time*).

There are organic and inorganic scintillators but the advantage of inorganic ones lies to their very good stopping efficiency (high mass density (ρ), their high atomic number (Zeff) and their high energy resolution. Four inorganic scintillators, shown in Table 2, have been widely used in PET scanner so far: the thalium-dopped sodium iodide (Nal(Tl)), bismuth germinate (BGO), cerium-doped lutetium oxyorthosilicate (LSO(Ce) or simply LSO) and cerium-doped gadolinium oxyorthosilicate (GSO(Ce) or simply GSO) (Zanzonico 2004).

	BGO	**LSO**	**GSO**	**NaI(Tl)**
Composition	$Bi_4Ge_3O_{12}$	Lu_2SiO_5	Gd_2SiO_5:Ce	NaI:Tl
Density (g/cm^3)	7.13	7.40	6.71	6.67
Effective atomic number	74	66	59	51
Attenuation coefficient (cm^{-1})	0.92	0.87	0.62	0.34
Light yield	15	75	41	100
Decay constant	300	40	56	230
Refractive index	2.15	1.82	1.85	1.85
Wavelength for max emission	480	420	430	410
Hygroscopic	No	No	No	Yes

Table 2. Physical properties of inorganic scintillators most used in PET (Bailey 2004).

Because PET imaging involves the coincidence detection of the two annihilation photons, it is very important to have an accurate assessment of exactly when a photon interacts in a detector. The accuracy of timing is determined by the decay time and its brightness. A fast, bright scintillator will produce a signal with less timing variation than a slow, dim scintillator. This observation is based on the analysis of the spreads of the average arrival times of the first scintillation photons at the detector. These first photons are the ones which trigger the start of the pulse. The index of refraction determines how efficiently optical photons can be transmitted from the scintillator to the photodetector (Bailey 2004).

1.2.2 Photomultiplier Tubes (PMTs)

The photomultiplier tubes consist of a photocathode and a series of dynodes in an evacuated glass enclosure. When a photon of sufficient energy strikes the photocathode, it ejects a photoelectron due to the photoelectric effect. The photocathode material is usually a mixture of alkali metals, which make the PMT sensitive to photons through the visible region of the electromagnetic spectrum.

The photoelectron is accelerated towards the dynodes, due to the potential difference in each pair of consecutive dynodes, and then towards the multiplier, where electrons are multiplied by means of secondary emission (Knoll 2000). The electron reaches the anode where the accumulation of charge results in a sharp current pulse

indicating the arrival of a photon at the photocathode (Figure 5). An electrical pulse will be generated by the PMT whose amplitude is proportional to the light quanta that reaches the photocathode. This is proportional to the energy deposited.

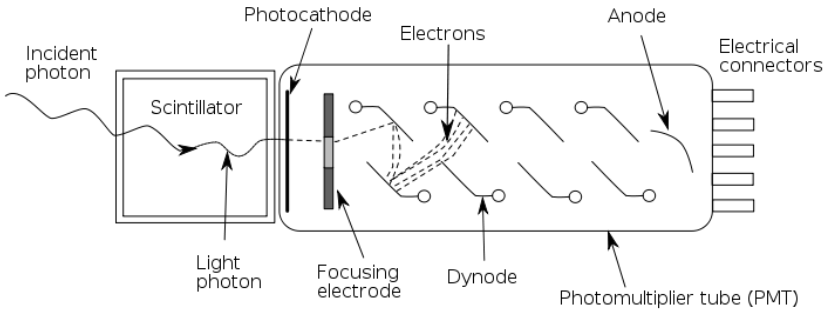

Figure 5. Photomultiplier tube coupled to a scintillator (Engstrom 1978).

Scintillation arrays are usually coupled to a single PMT that must be able to localize the point where the light entered the device. Position sensitive photomultipliers (PS-PMT) are used for this reason. Discriminators are also employed in order to measure the arrival times of different events, so as the best time resolution can be achieved.

Once all pulses have passed the discriminators, the amplitude of the signal must be obtained. This is normally done by the electronics of a PET system that convert the integrated charge in a digital number (*Analog to Digital Conversion or ADC conversion*) that is transmitted and stored in a PC.

1.2.3 Data Organization

Each event is individually written to a file with information about the two locations at which the annihilation photons interacted, meaning the crystal number, the energy and the time the event occurred. This information is stored in a file called *List Mode*. These event packets are then processed and transferred into *LOR histograms* or *sinograms*. Each coincidence event is assigned to a LOR (which joins two detectors) and then is histogrammed into a 2D matrix (sinogram). The matrix is arranged such that each row represents parallel line integrals or a projection of the activity at a particular azimuthal angle (φ). Each column represents the radial offset from the center of the scanner (s). Each element in the matrix (s, φ) records data from radioactivity in the object at location (x,y), which is given by the following relationship:

$$s = x\cos\varphi + y\sin\varphi \qquad \textit{(Eq. 4)}$$

The location of the annihilation can be determined by the sinogram, the distance from the center of the gantry can be determined by the amplitude of the sine wave and its angular location from the phase of the sine wave (Figure 6). Each detector pair corresponds to a particular pixel in the sinogram depending on its orientation angle and distance from the center of the gantry. So, for each coincidence detection, a LOR for that detection is determined, the pixel in the sinogram matrix is located and the value in the pixel is incremented. In the final sinogram, the value in each pixel represents the number of coincidence detections between the detector pair associated with

that LOR. For each slice a separated sinogram is required (Fahey 2002). Each pixel value along the rows of the sinogram matrix is the sum of all of the events along the corresponding LOR. Such a collection of LOR sums is referred to as "*projections (p)*".

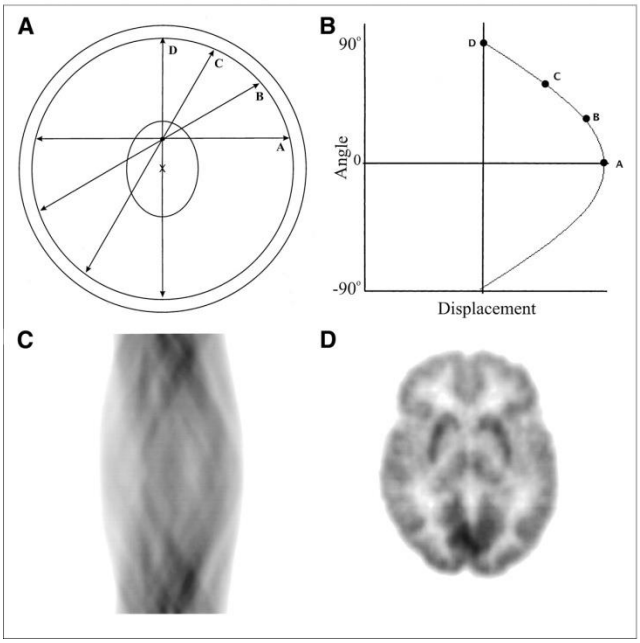

Figure 6. Sinogram formation. (A) Centre of the gantry is noted by the cross (x) and locus of interest is noted by ellipse. Four LORs are passing through locus of interest and are noted as A, B, C and D. (B) These four LORs are plotted in the sinogram where angular orientation is on y-axis and displacement from center of gantry is on x-axis. (C) Sinograms of more complicated objects are composed of many overlapping sine waves. (D) Reconstructed brain image corresponding to sonogram in (C) is shown (Fahey 2002).

1.3 Data Acquisition

1.3.1 Type of Events

Event detection in PET relies on the coincidence detection (*electronic collimation*) and an event can be considered valid if two photons are detected within a pre-defined electronic time window (*coincidence window*), the subsequent LOR formed between them is within a valid acceptance angle of the scanner and if the energy deposited in the crystal by both photons is within the selected energy window. Such coincidence events as referred to as prompt events or "*prompts*". However, there is a terminology used to describe various events in PET since not all prompt events are accepted (Figure 7).

A *single event* is a single photon counted by the detector. The vast majority of events in PET are considered to be single events, typically 90% or more, in which only one of the two annihilation photons is registered. *True coincidence* is an event that derives from a single annihilation and both γ-rays are detected without either of them scatter in the object being scanned. A *scatter coincidence* occurs when one or both of the photons from a single positron annihilation detected within the coincidence timing window have undergone Compton scattering one or more times. This corresponds to a true coincidence since it came from a single positron annihilation, but the resulting LOR will be misplaced causing a reduction in image spatial resolution and image contrast. This causes inconsistencies in the projection data and leads to inaccurate quantification in the final image if not corrected. A *random* or *accidental coincidence* occurs when two nuclei decay at approximately the same time. After

annihilation of both positrons four photons are emitted. Two of these photons, from different annihilations, are counted within the timing window and are considered to have come from the same positron, while the other two are lost. Such randoms are distributed uniformly in time and only the portion of random events included in the prompt window contaminates the primary data set. The random event rate between two detectors *a* and *b* is given by:

$$R_{ab} = 2\tau N_a N_b \qquad \textit{(Eq. 5)}$$

where Na,b is the single event rate incident upon the two detectors and 2τ is the coincidence window width. Multiple events are similar to random events, except that more than two events from more than two annihilations are detected within the coincidence timing window. The event is disregarded due to the ambiguity in deciding which pair of events arises from the same annihilation. Multiple event detection rate is a function of count rate (Bailey 2004, Lewellen 2008).

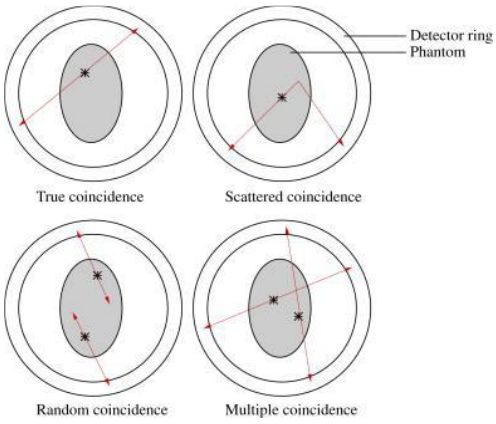

Figure 7. Main coincidence event types in PET.

Prompt events are the sum of true, scatter and random coincidences and only the true coincidences carry spatial information about the distribution of the radiotracer.

1.3.2 2D and 3D acquisitions

Traditionally, PET data acquisitions were based on 2D acquisition mode detection, meaning plane-by-plane LOR detection (Tarantola 2003). To shield out-of-plane coincidence photons that are emitted obliquely and reduce the amount of scatter, septal rings of lead-tungsten can be used. Using the septa, the sensitivity of the system is significantly reduced because a fraction of true coincidence events are rejected.

A large increase in sensitivity, 5 times higher than 2D (Tarantola 2003), can be obtained by removing the septa and by collecting all possible LORs. This approach is called 3D acquisition mode and requires special 3D reconstruction algorithms.

In 3D acquisition mode additional coincidence plane combinations are allowed than in 2D mode. If we consider a scanner having N detector rings; in 3D acquisition mode we will have N direct planes (Figure 8A) and as well N-1 cross planes (Figure 8B) for a total of 2N-1 planes with a center to center spacing of x/2. The representation of all sinograms is facilitated by the use of the *Michelogram* (a square grid) as shown in Figure 8 (C, D). The *ring difference* (RD) specifies the number of rings associated to a sinogram.

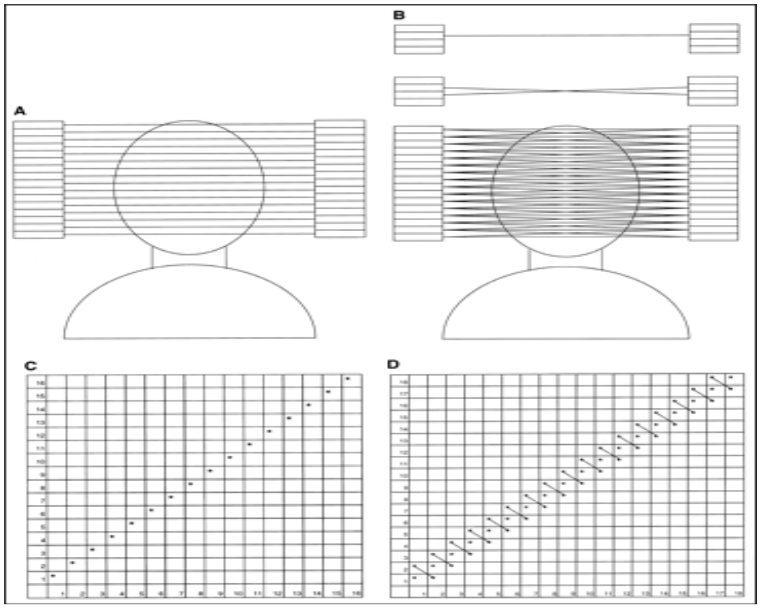

Figure 8. (A) 16 detector rings in coincidence with detectors on the opposite site of the same ring showing "direct" coincidences. (B) "Direct" and "cross" coincidences between detector rings. The michelogram is represented by (C) and (D) where direct coincidences are allowed for the scanner or direct and cross sectional coincidences are used respectively (Fahey 2002).

If ringA and ringB are the ring numbers, the ring difference is given by ringB-ringA. There are positive and negative ring differences. The ring difference of a direct sinogram is zero. A set of merged sinograms with a common average ring difference is called *segment*. This can be calculated by:

$$\text{Number\_of\_segments} = \left(\frac{(2RD)+1}{span}\right) \qquad \textit{(Eq. 6)}$$

Span specifies the number of adjacent LORs that should be grouped together into the same axial angle. Choosing a larger span will not "through away" data, but will reduce the size of the sinogram and will degrade the axial resolution.

However, in 3D mode there is an increase in random and scatter coincidences. To overcome this increase and take full advantage of 3D mode, faster coincidence detection is needed and higher computing power to manage the very high counting rate.

1.3.3 Data Corrections

a) Normalization

In PET scanners there are variations in the response of each crystal detector, resulting in a variation of the detection sensitivity that leads to non-uniform count rates. The process to correct these effects is called *normalization* (Badawi 1999). It is important to accurately correct for normalization in order to achieve good quantification in the final image. It is accomplished by exposing uniformly all detector pairs in 511 keV photon sources (e.g. 68Ge) without a subject in the FOV. Data are collected in 2D and 3D modes and normalization factors are calculated by dividing the average counts in all LORs by the individual detector pair count. The normalization factor is then applied to each detector pair data in the sinogram. The only problem with this method is the long duration of the scan (usually it takes more or less 6 hours) in order to acquire high statistically accuracy of the counts in a blank scan. There is also another approach that involves the splitting of the normalization into different components and treats

each one of them separately. This method is called component-based method (Badawi and Marsden 1999). The normalization coefficients are expressed as a product of factors associated with detector efficiency, dead time, geometric factors, spatial correction, crystal interference and many more.

b) Attenuation Correction

Attenuation correction is one of the most important corrections in PET data as it produces a change in the quantitative values (Muehllehner 2006). Annihilation photons, while travelling through the tissue, are attenuated until they reach the detectors and interact in the subject by Compton interactions. In order to detect a coincidence event, the two photons must cross different tissues to reach two opposite detectors. If μ is the linear attenuation coefficient of 511 keV photons (travelling in the same organs or tissues) and *d1* and *d2* are the different tissue thickness, then the probability *P* of a coincidence detection is given by:

$$P = e^{-\mu d_1} * e^{-\mu d_2} = e^{-\mu(d_1+d_2)} = e^{-\mu D} \qquad \textit{(Eq. 7)}$$

where *d* is the total body thickness. When photons travel through different organs or tissues then the above equation becomes:

$$P = e^{-\sum_{i=0}^{n} \mu_i d_i} \qquad \textit{(Eq. 8)}$$

where μi and *di* are the linear attenuation coefficient and thickness of the organs or tissues, *n* is the number of organs or tissues that the

photon travels through. The most common method for the correction of attenuation is through direct measurements. Usually, a transmission source, either a rotating rod source or a set of ring sources, is placed in the FOV of the scanner so as to measure all the attenuation factors in all LORs in a single scan. Initially a blank scan is acquired without an object in the scanner and then a transmission scan is acquired with the object in the scanner. The attenuation correction factors (ACF) for each LOR are given by:

$$ACF_i = \frac{Blanc_i}{Trans_i} \qquad (Eq.\ 9)$$

where i is each LOR and $Blanc_i$ and $Trans_i$ are the counts in the blank and transmission scan respectatively. With the advent of dual modality systems, such as PET/CT scanners, there have been considerable efforts to correct attenuation using computed tomography (CT) data. CT images must be segmented into a discrete set of tissue types, CT data must be scaled and images should be smoothed in a PET resolution before calculation of attenuation coefficients takes place. This method however, imposes some problems that may lead to artefacts in the reconstructed images (movement of the patient between the two scans, conversion of Hounsfield units to μ values, missing data due to the transaxial FOV of the CT scanner, etc) (Zanzonico 2004, Tarantola 2003, Muehllehner 2006).

c) Scatter Correction

Scatter results in diffuse background counts in the final reconstructed PET image and therefore reducing contrast and distorting activity concentration. In 2D PET scatter correction is straightforward. The use of septa in multi-ring PET systems removes additional scattered events, whereas in 3D PET they become more problematic because of the absence of septa.

The counts outside of the FOV do not contain true coincidence events only random and scatter, so by just taking these counts, scatter correction can be achieved. After subtracting the random counts, the scatter counts are subtracted from the prompt counts across the FOV and give rise to the true counts (uniform scattering) (Zanzonico 2004). This approach works reasonably in 2D PET but in 3D PET is not adequate. Other methods for scatter correction in 3D PET include convolution/deconvolution-based approaches (Bailey 1994), Monte Carlo simulations by directly estimating the scatter distribution (Levin 1995) and iterative reconstruction-based scatter compensation methods (Zaidi 2000).

d) Random Coincidences

Random coincidences increase the detected coincidence count rate by contributing false events in the image and raise the background. They increase with increasing the width of the energy and coincidence window and with increasing activity. They may lead to loss of image contrast and incorrect activity concentration. The standard approach to correct for random counts in a PET image is by the “delayed window” method (using the same energy window in a

standard time window -coincidence window- and in a delayed time window). The counts that are in the standard time window include randoms and trues, whereas the delayed time window includes only randoms. Thus, real-time subtraction of the delayed window counts from the coincidence window counts for each LOR correct for randoms (Zanzonico 2004, Badawi 1999).

e) Dead Time

In PET scanners, a minimum amount of time must be elapsed between successive events so as to be registered as separate events. Since radioactive decay is a random process, there is always a probability that successive events will occur within this minimum amount of time. At high count-rates, the fraction of the events falling in this category is significant. The parameter that characterizes the counting behavior of the system at high count rates is known as "*dead time*" (Bailey 2004). It is the length of the time required for a counting system to fully process and record an event, during which additional events cannot be recorded (Zanzonico 2004). Dead time models usually treat system dead time as "paralysable" and "non-paralysable". The paralysable dead time describes the situation where the system is unable to process events for a fixed amount of time τ after each event, regardless of whether the system is "dead" or not. In the non-paralysable case the system is considered again "dead" for a time τ after each event, but while the system is "dead", further events have no effect (Casey 1995). Dead time correction is made by empirical measurement of observed count rates as a function of the

increased concentrations of the activity by scaling up the measured count rate, either per LOR or globally.

f) Partial Volume Effect (PVE)

PET produces quantitatively accurate measurements of tracer concentrations *in vivo*. There are large quantitative biases that are introduced by the partial-volume effect (PVE) (Buvat 2007). PVE refers is a combination of two factors, the limited spatial resolution of PET and image sampling. Since PET scanners are limited by the spatial resolution, the resulting blurring causes spill-over (cross-contamination) between regions. That is, "hot" spots relative to "cold" background, which are smaller than twice the full width half maximum, show partial loss of intensity. The activity around the structure appears to be smeared over a larger area than it occupies in the reconstructed image (spill-out). So, the object appears to be larger than it is and has a lower activity concentration than it actually has. "Cold" spots relative to "hot" background appear to be smaller and have higher activity concentration than they actually have (spill-in). This underestimation and overestimation of activities reduces the contrast between high and low uptake regions (Erlandsoson 2012, Saha 2010).

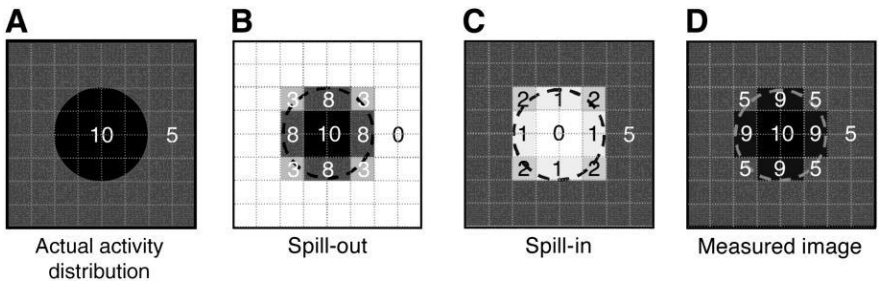

Figure 9. The measured image (D) of activity distribution (A) results from the sum of spill out (B) and spill in (C) (Soret 2007).

The partial volume effect is a concerned issue, especially for small structures in the images and correction factors need to be applied for the overestimation or underestimation of the images. One of these factors is called recovery coefficient (RC) and is the ratio of the measured peak activity concentration over the true activity concentration. Figure 10 represents the recovery coefficients for objects of different sizes and for various spatial resolutions of the system. For large objects the RC value is 1 and it means that the PVE has no effect on them.

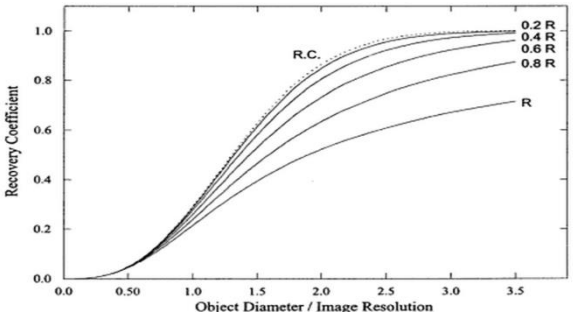

Figure 10. Recovery coefficients as a function of object size for various spatial resolutions of the system (R). (Phelps, 2004)

Other correction methods, based on image deconvolution using the point spread function (PSF) of the PET system (Teo 2007) and pixel-based methods using iterative reconstruction algorithms (Comtat 2002, Defrise 2006), have been investigated but with limited success.

1.3.4 Image Reconstruction

The goal of image reconstruction is to provide quantitatively accurate cross-sectional images of the distribution of positron-emitting radiopharmaceuticals in the object that is being scanned using externally detected radiation along mathematical algorithms of computed tomography (CT) (Defrise 2006). The collection of projection (p) profiles forms the sinogram, which is used to reconstruct the image through analytical methods such as *Filtered Back Projection (FBP)* or iterative approaches. The analytical methods utilize the mathematics of computed tomography, whereas the iterative methods model the data collection and through a series of iterations, a final image consistent with the measured data, is reconstructed (Defrise 2006, Zeng 2001). Both methods are based on the backprojection of projection profiles, which is the principle employed to reconstruct the images from acquired LORs. When a reconstruction matrix of a chosen size is selected, the counts along a LOR are projected back along the line from which they originated. This is repeated for all LORs until a reconstructed image from all backprojected data is formed.

The backprojection gives a blurred image of the actual object. This effect can be minimized by applying a filter (*ramp filter*) to the acquisition data so as to produce an image more representative of the original object being imaged. This method is called Filtered Back Projection (FBP) and is accomplished by the Fourier Transform (FT) or the central section theorem, which is that the 1D Fourier transform of a projection at an angle υ is equivalent to the 2D Fourier transform

of the object evaluated along a radial profile at the same angle. Then, by using the FT or the central slice theorem, the projection data obtained in the spatial domain can be expressed in terms of Fourier series in the frequency domain (*Fourier Transform*). The backprojection is then applied, incorporating the modified filtered projections so as to obtain the actual image of the object. Although FBP reconstructs accurately the objects, in real applications, where there is always noise in acquired data, it produces artifacts in the final image since the ramp filtered enhances high spatial frequencies.

Iterative methods of image reconstruction are based on the iterative comparison of estimated and measured data. An initial estimation of the image is made and the projections are computed from the image and compared with the measured projections. The measured projections are obtained through a transition matrix, whose elements consist of the different propabilities that a photon, which is generated in a determined voxel of the reconstructed matrix, can be detected in a specific bin of the sinogram. Differences between estimated and measured projections are used to improve the estimation and the process is iterated, until a good agreement between the two sets of projections is reached. One advantage of these methods is that corrections of the physical aspects of the imaging system can be incorporated in the process of reconstruction.

The most widely used iterative algorithms used in PET are the maximum likelihood expectation maximization (MLEM) algorithm (Shepp 1982) and the ordered subset expectation maximization

(OSEM) algorithm (Hudson 1994). The MLEM algorithm uses many iterations to achieve an acceptable agreement between estimated and measured projections and a long computational time. The OSEM is a modification of the MLEM where projections are grouped into subsets around the object to be imaged separated by a fixed angle.

There is also the 3D reconstruction method in which the projections are 2D line integrals with azimuthal angle θ and oblique, or polar, angle ζ. The full 3D projection data are then represented as a set of sinograms, with one sinogram per polar angle ζ. The algorithm most widely used in 3D reconstruction is the 3D re-projection algorithm (3DRP) (Colsher 1980, Kinahan 1989), which is an extension of the 2D FBP algorithm. 3D reconstruction algorithms are computer intensive and data sets are far larger than 2D ones. It is preferable to reduce 3D data by re-binning of the 3D set of oblique sinograms to 2D direct sinograms. The most common method to achieve that is the *single-slice re-binning* (SSRB) (Daube-Witherspoon 1987) and the *Fourier re-binning* (FORE) (Defrise 1997), which is based on the 2D Fourier transform of the oblique sinograms.

1.4 Performance of PET systems

The major goal of PET systems is to obtain good quality of detailed images of an object and also to perform well on image formation. There are several parameters that are associated with the scanner's good image formation and general performance, which include spatial resolution, energy resolution, sensitivity, scattered radiation, noise and contrast.

Spatial Resolution. The spatial resolution of a PET scanner is the ability of the device to distinguish two radioactive sources placed at a small relative distance. It is characterized by measuring the width of the profile obtained when an object smaller than the spatial resolution of the system (less than half) is imaged. This blurring is referred to as spread function. In order to measure the width of the profile, a small point source (giving the *point spread function,* PSF) or a line source (giving the *line spread function,* LSF) are used. The resolution of the system is expressed as the *full width at half maximum* (FWHM) of the profile. A good approximation for this profile is often a Gaussian function (Bailey 2004). The typical range of values of the spatial resolution in PET is around 5-10 mm FWHM. There are many factors that affect the resolution of a PET system. These include positron range, non-colinearity of annihilation photons, detector size, stopping power of the scintillator (detection efficiency), the depth of the interaction (DOI), the reconstruction methods employed and more.

Resolution in PET is specified in axial and transaxial directions across the FOV of the system. Transaxial resolution is subdivided into radial and tangential components for measurements from the center of the field of view as these vary in a ring configuration of a PET system due to differential detector penetration at different locations in x-y plane.

Energy resolution. Is the precision with which the system can measure the energy of incident photons. For a source of 511 keV photons the ideal system would demonstrate a well-defined peak

equivalent to 511 keV. There are two possible ways to define energy resolution for a PET scanner: the *single* event energy resolution and the *coincidence* energy resolution. It is usually measured by stepping a narrow energy window, or a single lower-level discriminator, in small increments over the energy range of interest while a source is irradiating the detectors. Good energy resolution is necessary for PET detectors in order to reduce background counts, scatter and achieve good contrast.

System Sensitivity. The sensitivity of a PET scanner is defined as the number of counts per unit time detected by the device for each unit of activity present in the source. It is normally expressed in counts per second per microcurie or kilobequerel (cps/μCi or cps/kBq). It depends on the scintillation crystal's efficiency, the scanner geometry and the dead time of the system. It can be determined by the combination of the geometric efficiency and the intrinsic efficiency. The geometric efficiency is equivalent to the fractional solid angle at the source subtended by the detector. For a ring detector of diameter D and depth d, the geometric efficiency (g) decreases linearly from d/D at the center to 0 at the end of the ring. The average geometric efficiency is given by d/2D (Cherry 2003). Small diameter scanners with a large axial extension usually have higher sensitivities. The efficiency of the scintillator material depends on its density, atomic number and thickness. Usually scintillation detectors offer high stopping power with good energy resolution. The intrinsic detection efficiency e, of an individual detector is given by:

$$e = (1 - e^{-\mu d}) \qquad \textit{(Eq. 10)}$$

where μ is the linear attenuation coefficient of the detector material and d is the thickness of the detector (in cm). For coincidence detection the intrinsic efficiency is given by e (Zanzonico 2004). A valid event requires that both photons be detected in opposing detectors and be within the appropriate energy range, given by the energy windows (typically between 350-650 keV).

Noise Equivalent Count Rates. The noise of PET data is indicated by the noise equivalent count rate (NECR), which is an important parameter demonstrating the impact of randoms, scatter and dead time of the system on actually measuring the true count rate. It is defined by:

$$\mathrm{NECR} = \frac{T^2}{T+S+R} \qquad \textit{(Eq. 11)}$$

where T, S and R are the true, scatter and random rates respectively. The value of NEC varies in fuction to the activity of the source used. The optimal count rate is given when NECR reaches its maximum by placing a decaying radioactive source in the centre of the FOV of the scanner. In 2D PET systems septa between the detectors reduce random and scatter count rates so NEC rate is equivalent to true count rate giving no optimal count rate. In 3D PET systems though, where no septa are used, true and scatter count rate are proportional to the activity, while random count rate is proportional to the square of the activity. By this, an optimum activity for 3D scanners exists (Zanzonico 2004, Tarantola 2003).

Scatter Fraction. The scatter fraction (SF) in PET data represents the fraction of coincidence events in which at least one of the two emitted photons has been scattered before detection. It is a critical component of NEC and can decrease image contrast. It is given by:

$$SF=\frac{S}{R_p} \qquad \textit{(Eq. 12)}$$

where, S are the scattered events and Rp is the prompt count rate. There are various sources of scatter such as scatter in the object, at the detectors, the gantry and the surrounding environment.

1.5 NEMA Standards

Various parameters specified by the manufacturer of a PET system should be verified according to some acceptance tests in order to establish the compliance of the specifications of the device. These specifications are referred to the parameters associated with the performance of PET systems, like the spatial resolution, the scatter fraction, the sensitivity and noise, as described above, as well as the image quality of a system. Specific measurement tests should be followed in order to have a standard procedure for performing these tests, especially if a meaningful comparison between scanners from different manufacturers is required, independently of camera design. The National Electrical Manufacturers Association (NEMA) has developed guidelines on how certain performance parameters should be obtained. These standards define a product, process or procedure with reference to the composition, construction, tolerance, operating characteristics etc (Standardization Policies and Procedures of the National Electrical Manufacturers 2008).

In 1991, the Society of Nuclear Medicine (SNM) established a set of standards for performing these tests (Karp 1991) but in 1994 the NEMA published a document with improved standards for performing these tests (NEMA 1994). As technology in PET research and development improved, modern whole body PET systems had essential differences in design and detector technology with earlier ones. This was the reason that NEMA has published in 2001 a new set of standards (Watson 2004) with corresponding new phantoms. In 2007, Watson et al. (Watson 2004) recommended modifications in the standards for the performance tests so as to include the intrinsic radioactivity of LSO or LYSO detectors in PET scanners, which may cause errors in the performance of the scanners. Accordingly, NEMA has published the NEMA NU 2-2007 (NEMA 2007) standards for PET systems with Lu-based detectors. In 2012 a new set of standards for PET systems, the NEMA NU 2-2012 (NEMA 2012), has been published in order to include time of flight instruments, discrete and continuous detector designs, single and multiple slice devices and multiplanar and volume reconstruction models. A standardized methodology for evaluating the performance of small animal PET systems has also been published in 2008 (NEMA 2008) from the NEMA. By this, the capabilities of small-animal PET scanners were optimized and their performance can be evaluated according to a standardized methodology. Up to then, all small animal PET imaging systems, were evaluating their performance according to the human NEMA standards by adopting the measurements and the corresponding phantoms to the small physical dimensions of such

systems, like for the microPET P4 (Tai 2001) and for the quad-HIDAC (Missimer 2004) system.

1.6 Small Animal PET

The success of imaging modalities in the clinical setting along with the need to study *in vivo* different biological processes at the cellular level has spurred the interest in molecular imaging in small laboratory animals (Hengerer 2002).

Small animal models (especially mice and rats) have been, and still are, an important part in molecular imaging since they can host a large number of human diseases because of their genetic resemblance with humans. Collection of important scientific preclinical data plays a significant role in biomedical research. For a long time, preclinical data were collected by means of *ex vivo* methods, which included organ dissection, tissue counting (Williams 1988) and whole body cryosection followed by digital autoradiography (Kanekal 1995). The major drawback of these methods was that the analysis was taken place for one given time and in one animal. The lack of repeatedly study the same animal during and after an intervention caused limitations in biomedical research and the need to develop novel imaging technologies has created.

Of the several imaging modalities available today, PET is a non-invasive technique used for *in vivo* studies of research in small animals with the use of small amounts of positron-labeled molecular imaging probes to image and assay biochemical processes of cellular and molecular functions in a single living subject (Chatziioannou 2002).

Since the mid 1990s, small animal PET has been extensively used in modern biomedical research since the spatial resolution of clinical PET systems, used earlier, did not allow their use within the framework of small animal research (Yao 2012). Amongst the advantages of the use of small animal PET systems, were the reduction in the number and cost of laboratory animals and the reduction in drug development costs. Physiological changes and molecular abnormalities can be studied by measuring the biodynamic distribution of a labeled compound in the same subject and in one scan.

1.6.1 Challenges and Limitations of Small Animal PET Systems

The most important challenge for small-animal PET systems is to obtain a high signal and localize it as accurately as possible with minimum amount of probe in the least amount of time.

The accurate spatial location of counts depends on the spatial resolution of the system, the detection efficiency of the detectors and the solid angle coverage. The coincidence timing window also plays an important role in order to minimize the noise from accidental coincidences.

So, the design of the probes, the optimization of PET systems so as to provide maximum sensitivity and spatial resolution are one of the challenges in PET imaging technique.

a) Spatial Resolution

Mice and rats are the animals of choice to investigate and understand mammalian biology. The differences of physical sizes between small animals and humans are vast since human weight is in the order of ~70-80 kg and of small animals in the order of ~300 g for rats and ~30 g for mice. The brain in mice and rats is 8-14 times smaller than in human subjects (Laborina 2006). Because of these differences, small animal PET scanners must have very high spatial resolution so as to achieve the same level of detail and accuracy as in clinical PET systems. This suggests that the reconstructed resolution should be in the order of ~1 mm in all directions in comparison with the ~10 mm in whole body work for humans (Chatziioannou 2002). Derenzo and Moses (Derenzo 1993) have developed a parameterized expression of PET spatial resolution in order to relate the different contributions of factors, which affect spatial resolution in PET imaging systems:

$$FWHM = \alpha \left[(\frac{d}{2})^2 + b^2 + (0.0022D)^2 + r^2 \right]^{1/2} \qquad \textit{(Eq. 13)}$$

where *d* is the dimension of the square face of the crystal, *b* represents the uncertainty associated with identifying individual crystals with secondary detection devices, such as PMTs. This contributes a few millimeters to the spatial resolution. The factor $[(0.0022D)^2]$ describes the non-colinearity of the 511 keV photons, where *D* is the detector of the PET scanner. *r* relates to the effective size of the object being imaged. The multiplicative factor α accounts for any resolution degradation that occurs in image reconstruction.

In most of PET systems, the size of the crystal is considered the most important component of the achievable spatial resolution. The intrinsic spatial resolution of the detector is approximately one half the crystal size. The noncolinearity is dependent on the spacing between the detectors which are in coincidence and depends on the scanner diameter. In small animal PET scanners, this is less than 0.5 mm FWHM. In order to increase PET spatial resolution, the size of the crystal detector and the diameter of the scanner should be designed as small as possible. New innovative solutions should be explored so as to build systems with improved spatial resolution. One component that has a dominant effect on spatial resolution is the positron range. Levin C.S. and Hoffman E.J. (1999) have developed a Monte Carlo simulation model of positron trajectories and calculated the distribution of the end point coordinates in water for the most common PET isotopes used: 18F, 11C, 15O and 13N (Figure 11). They have found that the spatial resolution of a PET system is degraded by positron range for nearly 1 mm FWHM for a 10-20 cm diameter system used for typical animal studies using 18F to 4 mm FWHM for an 80 cm diameter system used for human imaging using 15O. Also, they have concluded that the detector size and the photon non-colinearity also degrade spatial resolution.

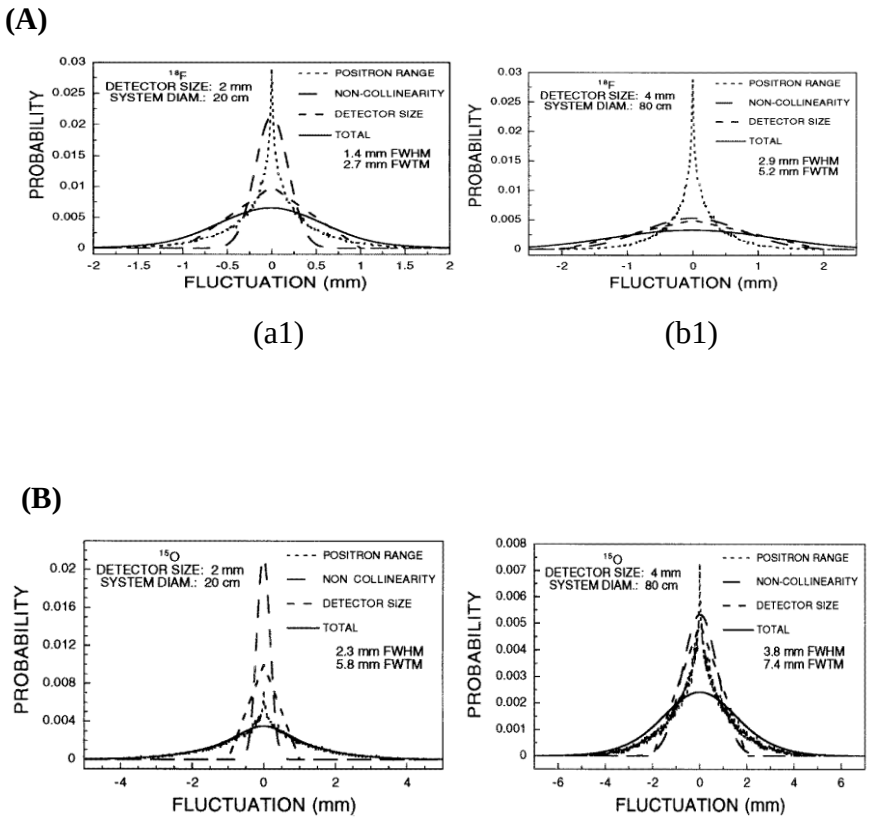

Figure 11. Calculated spatial resolution blurring factors and their combination for 18F (A) and 15O (B) with 20 cm system diameter and 2 mm wide detectors (a1) (b1), and 80 cm system diameter with 4 mm wide detectors (a2) (b2) (Levin 1999).

b) Sensitivity

The sensitivity of a small animal PET system must be as high as possible because it is a measure of the efficiency of the system and it directly determines the signal-to-noise ratio (SNR) levels of the

reconstructed image. If higher sensitivity is achieved, larger number of detected events will occur within less acquisition time.

Whole body human PET scanners detect in the order of 0.3-0.6% of the coincident annihilation events in 2D mode and 2-4% in 3D mode. In order to preserve the amount of counts per resolution element, the sensitivity for mouse imaging would need to be improved by a factor of 1000 relative to the sensitivity of human imaging, which is not attainable (Chatziioannou 2002). One could inject higher amounts of radioactivity in the subject in order to achieve more counts, but this poses other challenges. Another approach could be to develop and use more sophisticated reconstruction algorithms that make better use of the detected counts. It remains a major challenge to improve system sensitivity compared to human PET systems, while maintaining high spatial resolution at the same time.

c) Specific Activity

The amount of activity injected in a small animal during a study is limited by the specific activity of the radiochemical, the toxicity of the radiotracer, the total volume that can be injected into the small animal and by the counting rate capability of the PET system. If increases in specific activity were achieved, more radioactivity would be injected into the animal and better SNR in the images would be gained together with improved statistics. Of course, the tracer mass injected into a small animal must be sufficiently low so that the natural physiologic state of the animal is not affected. The rule of thumb is that the tracer mass will cause a maximal receptor occupancy of 1%.

Because the tracer specific activity (Bq/g) is typically fixed, the allowed tracer activities are limited. For example, it was estimated that the maximal injected radioactivity of 11C labeled raclopride, a PET ligand for D2-dopamine receptor, is 5.2 MBq in rats and 0.3 MBq in mice (Hume 1998). Another constraint on the use of radiotracers in small animals is that the injection volume should be less than 10% of the animal's total blood volume, which is 30 and 2.5 mL, respectively, for rats and mice. Hence, the commonly used tracer dilution for clinical applications in humans may not be appropriate and sometimes needs to be adapted for small animal imaging (Yao 2012).

However, Jagoda et al. (Jagoda 2004) showed that if small animal imaging studies in rodents are to have the same "quality" as human PET studies, the same number of coincidence events must be detected from a typical rodent imaging voxel as from human imaging voxel. This can be achieved only by using the same total amount of radiopharmaceutical to a rodent and to a human subject. More in concrete, this study showed roughly, through a mathematical model, that if the same drug (i.e. the same specific activity) is to be used to image both rat and human, the drug concentration in the target tissue of the rat must be 84 times higher than in the human subject in order to obtain the same statistical image quality in the same imaging time for the same study. Also, in order to make the concentrations equal, in both rat and human studies, the specific activity-detection efficiency product must be some 84 times greater than for the human study.

One could increase the amount of injected activity causing an increase in the detected counts. If the specific activity of compounds and/or the sensitivity of small animal PET systems are not increased relative to human studies, the "true" tracer distribution will not be correctly portrayed in small animal PET imaging.

d) Other Challenges

Factors such as dead time characteristics, energy resolution, attenuation and scatter correction, as well as detector design should also be taken into account. Since the system design may affect the implementation of correction techniques and affect the quantification accuracy of the results, it is really important to bear in mind two other practical challenges in PET technology. Small animal PET systems are required to have high spatial resolution and high sensitivity but they also need to cost less than human PET scanners. It is also important to understand that one PET system is not optimal for all kind of studies. That is why state-of-the-art animal PET systems are been developed with differences in the design and performance.

1.6.2 Small Animal PET Scanners

The first animal PET tomographs were designed for imaging non-human primates and were constructed in 1990s. The spatial resolution of these systems permitted only imaging of large tissues in rats and mice.

The development of the first dedicated small animal PET scanners was underway while new materials and innovation techniques were under development.

The Hamamatsu SHR-2000 (Watanabe 1992) was the first commercially-available PET scanner that developed in Japan and was installed in their Central Research Laboratory. Other systems developed at that time were the RATPET (Bloomfield 1995), which was designed at the MRC Cyclotron Unit, London and was built with the collaboration of CTI, Knoxville, TN, USA, the ECAT-713 (Cutler 1992), which was developed by CTI PET Systems Inc., Knoxville, and installed at UCLA.

These systems were the ones that provided the bridge of scanning small animals in clinical scanners and dedicated systems. This initial effort of developing PET systems for small animals was based on the use of standard hardware components, using existing detector technology based on BGO scintillator crystals coupled to PMTs. Due to the limited light output of the BGO and the low spatial resolution of the systems, soon began an effort to improve the detector resolution.

The Sherbrooke Animal PET system (Lecomte 1994, 1996) was developed at the University of Sherbrooke, in Canada, and was the first to replace the PMTs with solid state photon detectors. The BGO scintillator crystal was coupled to its own avalanche photodiode (APD) photon detector. The high detection efficiency of the APD together with its compact size were the advantages that made it attractive for PET applications. The disadvantage was the low gain of the APD which required a fast low noise preamplifier on each APD output.

With the introduction of LSO detectors, with higher light output than BGO, and the optical fibers which transfer the scintillation light from

the crystal to the multi channel PMTs, small animal scanners with higher resolution were developed. The UCLA microPET (Chatziioannou 1999) was the first high resolution animal tomography developed at UCLA with no inner septa and operation at 3-D mode. The detector consisted of an 8 x 8 array of individual LSO scintillator crystal coupled to a 64 channel PMT. The imaging FOV was 11.2 cm and 18 mm in transverse and axial direction equivalently.

Concorde Microsystems Inc. (Knoxville, TN) based on the technology used by UCLA and developed two microPET systems increasing the axial FOV to 8 cm. The microPET R4 (Knoess 2003) and the microPET P4 (Tai 2001) were the two animal scanners used for rodent and primate studies. The P4 had a 27 cm ring diameter to accommodate brain imaging, while the R4 had a 15 cm ring diameter. They both had high resolution and sensitivity.

A very similar tomograph to the above was the YAP-PET (Del Guerra 1998), which was developed at the University of Ferrara with 30 mm long crystals and 1.7% sensitivity. The MAD-PET (Pichler 1998) system was developed by the Max-Plank Institute in Munich and was based on the on the coupling of LSO detectors to APDs.

The Siemens microPET FocusTM 120 (Tai 2005) and GE eXplore Vista (Wang 2006) were two small animal PET systems, which were developed on LSO detectors and optical fiber readouts. Both systems represent the state-of-the-art in high resolution small animal PET scanners with very good sensitivity. The GE eXploreVista used the phoswich technology to limit the parallax error with 4% sensitivity,

while the microPET Focus had 6.5% sensitivity. Both systems kept the spatial resolution as constant as possible over the whole FOV.

The ATLAS (Advanced Technology Laboratory Animal Scanner) (Seidel 2002, 2003) small animal PET scanner was designed to image animals like mice and rats, in Bethesda, Maryland. This was the first system to use DOI capability and the first to use iterative resolution recovery algorithms for image reconstruction. The rPET (Vaquero 2005) small animal system was designed with MLS crystals optically coupled to PS-PMT flat panel. The average intrinsic resolution was 1.5 mm and the sensitivity of the system for a pair of detectors in coincidence was 1%.

The quadHIDAC (Schafers 2005) is a commercial small animal PET system, which was developed in UK and it was based on gas multiwire proportional chambers (MWPC). The gas detectors were coupled to lead converters, which provided high 3-dimensional spatial resolution and high level of sensitivity. The detectors of the system provided also depth of interaction information.

Small animal PET has established its position in molecular imaging with the detector technologies mentioned above. Nevertheless, new technologies and demands in research and clinical practice have pushed the limits of technology to a new level.

The first attempt was made with the integration of small animal PET systems with CT systems, although its development started out in clinical systems.

Fusion of anatomic and functional imaging was achieved together with the use of CT images to correct the attenuation factors of PET (Kinahan 1998). Hybrid small animal PET/CT systems have been

developed, living the animal at the same position during the scans (Saoudi and Lecomte 1999, Magota 2011).

The ARGUS PET/CT system by Sedecal (formerly GE eXplore Vista) was designed using LYSO/GSO detectors with a peak detection efficiency of 4.32% (Goertzen 2012). The new SuperArgus PET/CT system combined the phoswich DOI technology with sensitivity less than 11% and a central spatial resolution of 1.2 mm (http://pmod.jp/pdf/08sedecal/supera-rgus-datasheet.pdf).

Given that the integration of PET/CT in preclinical and clinical imaging provided much strength in multimodality imaging, new breakthrough developments focus on the integration of PET with magnetic resonance (MR). The absence of ionizing radiation and the high level of soft-tissue contrast in MR marked a new path in multimodality imaging by the development of small animal PET/MRI systems.

The advantages of this integration was the reduced exposure of the animal to radiation, compared to PET/CT, the easy access to metabolic disease patterns and the multi-parametric image formation through MRI (Nicol 2009). Many PET/MR small animal systems (Beyer 2011, Garlick 1997, Raylman 2006, Lucas 2006, Woody 2007, Nagy 2013, Maramraju 2011, Yamamoto 2010) have been developed and used giving new insights into molecular and cellular biology.

1.6.3 Applications

Small animal PET systems have been used for a wide range of applications typically in research laboratories rather than in clinical

use. The primary application of small animal PET was in oncology (Tatsumi 2003, Gambhir 2002, Michalski 2011, Lewis 2002, Tenbaum 2012, Puig 2013). The greatest use was the monitoring of glucose metabolism with 18F-FDG (Gambhir 2001, Michaelides 2010), which is used clinically for the detection and staging of the disease. Other uses in the field of oncology include gene expression (Blasberg 2002, Gambhir 200), cell proliferation (Bading 2008), tumor angiogenesis (Niu 2009), tumor apoptosis (Madar 2009) and hypoxia (Lapi 2009).

In cardiology, small animal PET has been used to study cardiac physiology, metabolism and heart disease conditions (Welch 2006, Thomas 2008). Quantitative cardiac function parameters can be obtained by PET images, which provide insights in cardiac disease. Hypertension (Lavoie 2004), effects of exercise (Bernstein 2003) and atherosclerosis (Daugherty 2002) are more examples of the use of small animal PET in cardiology.

Another field of application for small animal PET is neurology. Many PET radiotracers have been used to study drug mechanisms in the brain (Rojas 2013), neuroreceptor mapping (Burokas 2014, Hoekzema 2012) as well as pathophysiology. An example of these radiotracers are H215O for cerebral blood flow, 11C-raclopride for postsynaptic D2 receptor level, 11C-(R)- (-)-RWAY for 5-hydroxytryptamine receptor 1A, 11C-flumazenil for GABA(A) receptor. Also it has been used to study the effect of stroke (Rojas 2007, 2011).

PET has been used also in pharmacology for the distribution of nanoparticles (Rojas, Gispert et al. 2011) and in toxicology (Perez-Campana 2014).

The role of transgenic mice has nowdays been established and offers many possibilities for studying the molecular and cellular basis of diseases and biology with the use of high-resolution small animal PET.

Since small PET covers a wide range of biological applications it should be easy-to-use, flexible and low-cost. These systems should be able to achieve very small spatial resolution, high sensitivity and excellent detection efficiency.

1.7 Monte Carlo Simulations

The Monte Carlo (MC) methods are numerical calculation methods based on stochastic processes. The name comes from the Monte Carlo casino in Monaco, which was the most famous centre for playing games involving random drawing. Due to the stochastic nature of radiation emission and detection, the Monte Carlo simulation method is of interest for medical physics in areas such as radiotherapy, nuclear medicine, diagnostic x-rays and radiation protection (Andreo 1991).

In Nuclear Medicine, particularly in PET and SPECT (single photon emission tomography), MC simulations are considered to be a powerful research tool to predict the performance of new detectors, optimize the design of new systems and to study their response (Zaidi 1999). They have also been used to develop and validate image reconstruction techniques (Rafecas 2004, Zhang 2010), to assess

correction methods such as scatter (Lewin 1995) and attenuation (Xiao 2007) and to validate quantification methods (Casciari 1995, Bowen 2012).

The basic idea behind MC simulations is to create a model as similar as possible to the real system and to simulate the interaction with that system based on *a priori* known probabilities of occurrence through Probability Density Functions (PDFs), which are functions that describe the relative likelihood for a random variable to take on a given value. Photon emissions are generated within the phantom and transported through the scattering medium and the detection system. They may be absorbed by the detector crystal or not. This process is done by the sampling of photons using the PDFs.

1.7.1 Random Numbers

Monte Carlo simulations employ random numbers, which, in theory, cannot be predicted or calculated. The most common approach to have access to random numbers is to use pseudo-random numbers. These are calculated by algorithms which use an initial number or a seed as a starting point to initiate the random number sequence. When two seeds of identical value are used in two different simulations, the results are identical and therefore different initial numbers must be used in the simulations.

1.7.2 Variance and Error Estimation

Typically, the statistical error in the Monte Carlo method is estimated by the standard deviation (σ), which measures the amount of variation or dispersion from the average value. The standard

deviation of a random variable or probability distribution is the square root of its variance. In probability theory and statistics, the variance is a measure of the statistical dispersion of a random variable and indicates how far the possible values of the random variable have spread around from the expected value. The standard deviation gives an indication of the possible deviations from the mean. If $\mu = E(X)$ is the expected value (mean) of the random variable X, then the variance is:

$$Var(X) = E((X-\mu)^2) \qquad \textit{(Eq. 14)}$$

or simply as: $Var(X)$, σ^2.

1.7.3 Variance Reduction Techniques

Variance reduction techniques, also called non-analog sampling, are methods, which are used to reduce the variance (i.e. the error) in the estimated solution in order to reduce the increased computation time in MC simulations. The scope is to potent the random events so as to be more likely to be detected. A "weight", *W*, is attached to each photon history, which represents the probability that this photon will follow a specific path or will undergo a particular interaction. This "weight" is calculated for each particle history and when an event occurs, the "weight" is added on the counter and it is multiplied by the appropriate weight factor for each variance reduction technique used.

Detailed description of some variance reduction techniques can be found in Andreo 1991 and Salvat 1999.

1.7.4 Monte Carlo in Nuclear Medicine

There are several Monte Carlo simulation codes for the simulation of radiation transport available for public use. There are two types though of Monte Carlo codes used in Nuclear Medicine, for SPECT and PET applications: the *general purpose* codes, developed for high energy physics or dosimetry and they simulate particle transport and the *dedicated codes*, designed specifically for PET and SPECT simulations.

The general purpose simulation codes are accurate and versatile packages as EGS4 (EGS 2011), MCNP (https://mcnpx.lanl.gov/), Geant4 (Agostinelli 2003) and Penelope (Baró 1995). They have been widely used and extensively tested for various applications. There is a continuous development and support when using these codes although computer skills are always required by the end-user. The dedicated simulation codes are Sim-SPECT (Belanger 1998) derived from MCNP transport code, PET-EGS (Castiglioni 1999) based on EGS4 code, GATE (Jan 2004), SimSET (Harrison 1993), PeneloPET (Espana 2009), SORTEO (McLennan 2009) and SIMIND (Toossi 2010).

SimSET, GATE and PeneloPET are considered to be the most powerful simulation codes for clinical and pre clinical applications in PET and SPECT. They efficiently simulate physical phenomena and detector designs but they also appear limitations. There are major differences between the codes in the modeling of the detector components and the interactions within them.

There is no doubt that Monte Carlo methods are a powerful tool in many fields of Nuclear Medicine since they have been tested by a large number of researchers around the world in different fields.

It is important when choosing a dedicated MC simulation code to look for its accuracy, flexibility and efficiency, as well as if it has been validated and whether the code has extensively tested for debugging.

With the advent of technology in the computer area, the use of parallel simulation has been implemented. By this, a reduction in computational time has been achieved, which is one of the most important issues in Monte Carlo simulations. Parallelisation does not interfere with the final result and cannot alter the accuracy of the code.

Well-written documentation is also an important issue when using Monte Carlo codes, either general purpose or dedicated ones as it is key feature determining the long-term existence of the code.

2 | Aim of the thesis

2.1 Statement of the problem

Small animal PET systems have been used extensively in biomedical research. By allowing in vivo pharmacokinetic and dynamic studies they permit studies of metabolism, gene expression, pharmacokinetics, disease progression and therapeutic response among others.

Technical aspects are becoming increasingly relevant as new probes are being developed. From the detector technology point of view, small animal PET systems face the challenge of spatial resolution and sensitivity in order to detect and quantify nanomolar and picomolar concentrations of molecular probes.

Many small animal PET systems have been developed and made commercially available since the first generation of animal scanners. Their performance though is being improved every time that new equipment are being developed so as to provide images with quality equivalent to those of humans. Scanners differ in design and characteristics and therefore a standardization protocol and reconstruction methods are needed in order to optimize their capabilities. By using standardized methodologies, comparison between animal scanners can also be achieved, helping potential users to choose between scanners according to their needs.

The National Electrical Manufacturers Association (NEMA) has published a set of standards, the NEMA NU 4-2008, which provide a full protocol for the performance evaluation of small animal PET

scanners that did not exist up to now and evaluations were done by using adapted clinical PET standards.

These standards can also be used in order to evaluate the accuracy of dedicated Monte Carlo simulation codes, which are used in Nuclear Medicine extensively. GATE and PeneloPET have been used only for PET and small animal PET applications and have been validated in terms of performance parameters, such as sensitivity and scatter fraction. Although both codes are been used extensively, no code can be considered a gold standard for PET applications and therefore each code may be suitable for specific applications.

2.2 Aim

The general objective of the thesis was twofold; on one hand to compare the new NEMA NU 4-2008 standards for small animal imaging to the adapted clinical NEMA NU 2-2001 standards for the evaluation of the microPET R4 system and on the other hand to compare the use of GATE and PeneloPET MC codes, for the determination of the performance characteristics of the microPET R4 system uzing the NEMA NU 4-2008 standards. More in concrete:

A) Performance Evaluation of the microPET R4 scanner.

i) To characterize the performance evaluation of the microPET R4 small animal system in terms of spatial resolution, sensitivity, scatter fraction, count rate performance and image quality, according to the new NEMA NU 4-2008 standards for small animal systems.

ii) Compare this performance evaluation to its previous using the adapted clinical NEMA NU 2-2001 standard.

B) Monte Carlo Simulations in the NEMA NU 4-2008 framework.

i) To compare in detail the performance of two dedicated Monte Carlo codes (GATE and PeneloPET) against experimental data following the NEMA NU 4-2008 standards for small animal PET systems.

ii) Evaluate their strengths and weaknesses in terms of accuracy, flexibility, efficiency and ease of use from an end user point of view.

3 | RESULTS

The scientific results are presented in the form of research papers.

3.1 Publication 1

Fotini D. Popota, Pablo Aguiar, J. Raúl Herance, Deborah Pareto, Santiago Rojas, Domènec Ros, Javier Pavıa, and Juan Domingo Gispert. **Comparison of the Performance Evaluation of the MicroPET R4 Scanner According to NEMA Standards NU 4-2008 and NU 2-2001.** IEEE Trans Nuc Science, vol 59(5), 1879-1886, 2012.

3.2 Publication 2

Fotini D. Popota, Pablo Aguiar, Samuel España, Cristina Lois, Jose M. Udias, Domènec Ros, Javier Pavıa, and Juan Domingo Gispert. **Monte Carlo simulations versus experimental measurements in a small animal PET system. A comparison in the NEMA NU 4-2008 framework.** Phys Med Biol (Under review).

Comparison of the Performance Evaluation of the MicroPET R4 Scanner According to NEMA Standards NU 4-2008 and NU 2-2001

Fotini D. Popota, Pablo Aguiar, J. Raúl Herance, Deborah Pareto, Santiago Rojas, Domènec Ros, Javier Pavía and Juan Domingo Gispert

***Abstract*—The purpose of this work was to evaluate the performance of the microPET R4 system for rodents according to the NU 4-2008 standards of the National Electrical Manufacturers Association (NEMA) for small animal PET systems and also to compare its performance evaluation against its previous evaluation according the adapted clinical NEMA NU 2-2001. The performance parameters evaluated here were spatial resolution, sensitivity, scatter fraction, counting rates for rat- and mouse-sized phantoms and image quality. Spatial resolution and sensitivity were measured with a ^{22}Na point source, while scatter fraction and count rate performance were determined using a mouse and rat phantoms with an ^{18}F line source. The image quality of the system was assessed using the NEMA image quality phantom. Assessment of attenuation correction was performed using γ-ray transmission and CT-based attenuation correction methods. At the center of the field of view, a spatial resolution of 2.12 mm at full width half maximum (FWHM) (radial), 2.66 mm FWHM (tangential) and 2.23 mm FWHM (axial) was measured. The absolute sensitivity was found to be 1.9% at the center of the scanner. Scatter fraction for mouse-sized phantoms was 8.5 % and the peak count rate was 311kcps at 153.5 MBq. The rat scatter fraction was 22% and the peak count rate was 117 kcps at 123.24 MBq. Image uniformity showed better results with 2D FBP, while an overestimation of the recovery coefficients was observed when using 2D and 3D OSEM MAP reconstruction algorithm. All measurements were made for an energy window of 350-650 keV and a coincidence window of 6 ns. Histogramming and reconstruction parameters were used according to the manufacturer's recommendations. The microPET R4 scanner was fully characterized according to the NEMA NU 4-2008 standards. Our results diverge considerably from those previously reported with an adapted version of the NEMA NU 2-2001 clinical standards. These discrepancies can be attributed to the modifications in NEMA methodology, thereby highlighting the relevance of specific small animal standards for the performance evaluation of PET systems.**

***Index Terms*—NEMA, spatial resolution, scatter fraction, uniformity**

Manuscript received April 12, 2012; revised June 28, 2012; accepted July 10, 2012. Date of publication August 20, 2012; date of current version October 09, 2012. This work was supported in part by the Fondo de Investigación Sanitaria (FIS) of the Instituto de Salud Carlos III under Grants PS09/02620 and PS09/ 02217, the CDTI as part of the CENIT Program (AMIT Project), the Ministerio de Ciencia e Innovación under Project No. SAF2009-08076, and the Spanish Ministry of Economy and Competitiveness.

F. D. Popota is with the Institut d'Alta Tecnologia-PRBB, CRC Corporacio Sanitaria Barcelona, CO 08003, Spain, and also with the Unitat de Biofisica I Bioenginyeria, Universitat de Barcelona, Barcelona 08036, Spain. P. Aguiar is with theMolecular Imaging Group, Foundacion IDICHUS/IDIS, Santiago de Compostela 15706, Spain. D. Pareto, R. Herance, S. Rojas, and J. D. Gispert are with the Institut d'Alta Tecnologia-PRBB, CRC Corporacio Sanitaria Barcelona, Barcelona 08003, Spain, and also with the CIBER en Bioengenier´ıa, Biomateriales y Nanomedicina (CIBER BBN), Barcelona 50018, Spain (e-mail: jdgispert@fpmaragall. org). D. Ros is with the Unitat de Biofisica i Bioenginyeria, Universitat de Barcelona, Barcelona 08036, Spain, and also with the CIBER en Bioingenieria, Biomateriales y Nanomedicina, Zaragoza 50018, Spain, and the Institut d'Investigacions Biomediques Agust Pi i Sunyer (IDIBAPS), Barcelona 08036, Spain. J. Pavia is with the CIBER en Bioingenieria, Biomateriales y Nanomedicina, Zaragoza, Spain, and also with the Servei deMedicina Nuclear, Hospital Clínic, IDIBAPS, Barcelona 08036, Spain Digital Object Identifier 10.1109/TNS.2012.2208760

I. INTRODUCTION

OVER the last two decades positron emission tomography (PET) has been used to measure concentrations of positron emitter ligands for diagnostic purposes, to evaluate therapeutic agents and to provide insight into disease biology. Applied to laboratory animals, this technique permits the use of experimental approaches impracticable for humans and constitutes a powerful tool for translational research. Small animal PET applications range from investigations of receptor-ligand interactions, metabolism, gene expression, cell therapy, development of new drugs [1] and cell proliferation and migration [2]. With the use of these dedicated systems, molecular biology and in vivo imaging were intersected so as to establish molecular imaging [3]. The visualisation and follow-up of all molecular processes in living organisms has opened up huge potential in the fields of oncology, neurological and cardiovascular diseases [4].

As new probes are being developed, technical aspects are becoming more relevant depending on the specific application. Due to the significant difference in size compared to humans, small animal PET systems face the challenge of achieving suitable sensitivity and spatial resolution without any increased cost. PET detector technology has thus pushed the limits to detect and accurately quantify nanomolar or picomolar concentrations of molecular probes. Since the first generation of animal scanners [5], [6] many other systems have been developed and made commercially available [7] – [11]. This made preclinical PET systems popular for a large number of animal imaging studies because they reduced the cost of detectors and electronics.

The last few years, many efforts have been made to improve system performance by enhancing organ uptake quantification and providing images with quality equivalent to those of humans. The knowledge of the physical characteristics of each system, expressed in terms of spatial resolution, sensitivity, scatter fraction and count rate performance, image quality and accuracy of corrections, is the key point when making decisions

about the most appropriate scanner to be used for particular experiments.

Scanners differ in design and characteristics and as a consequence, a standardization of acquisition protocols and reconstruction methods is needed to compare their performances. Thus to optimize the capabilities of small animal PET scanners, their performance has to be evaluated according to a standardized methodology. Until recently, the clinical standards of the National Electrical Manufacturers Association (NEMA), such as NEMA NU 2-1994 [12] or NEMA NU 2-2001 [13], were adapted for small animal PET scanners. For example, the microPET P4 [10] and the quad-HIDAC [14] were characterized according to human clinical NEMA standards but their performance using non-standardized phantoms and experimental procedures may lead to variations on the results provided.

The NEMA published its NEMA NU 4-2008 standards, which provide a full protocol for the performance evaluation of small animal PET scanners [15]. So far, not many scanners have been evaluated according to these standards apart from the Inveon preclinical tomograph [16], the FLEX Triumph X-PET scanner [17], the Mini PET II small animal scanner [18], the microPET Focus 120 scanner [19] and the coplanar multimodality scanner for rodent imaging [20].

The microPET R4 system (Concorde Microsystems Inc.) is a dedicated system for imaging mice and rats. It has been one of the first small animal PET scanners with an axial field of view (FOV), which provides whole-body scans of rodents that permit longitudinal studies. Its performance has previously been evaluated by Knoess C, et al [21] according to the NEMA NU 2-2001 for clinical PET scanners.

In this work, we report the performance evaluation of the microPET R4 scanner using the recently published NEMA NU-4 standards for small animal PET systems. The scope of this standard is to provide a standardized methodology for the evaluation of the performance of small animal PET systems which did not exist up to now and evaluations were done adopting clinical PET standards. Therefore, one of our primary goals was to assess any significant differences between the results obtained with NEMA NU 2-2001 and NEMA NU 4-2008 that which would justify any possible re-evaluation of small animal PET systems.

II. Materials and Methods

A. System Description

The microPET R4 scanner is a dedicated PET system for imaging rodents. The scanner's detectors are made of Lu2(1-x)Ce2x(SiO4)O - (LSO), which has high stopping power for 511 keV photons, a high light output and a fast decay time of 40 ns [22], [23]. A scintillation block of 19x19x10 mm^3 is sawed to an 8x8 crystal array with 9 mm depth cuts,

leaving a 1 mm thick layer of LSO at the bottom to hold the block. The crystal size is 2.1x2.1x10 mm^3 with an axial and transaxial pitch of 2.423 mm and 2.423 mm, respectively, and the cuts are filled with a reflective material after polishing [24]. Each block is coupled to a position sensitive photomultiplier (PS-PMT, Hamamatsu R5900-C8) via a 10 cm fiber optic bundle. Four blocks of detector comprise one axial detector module, providing 32 detector rings in total. The scanner's diameter is 148 mm, the axial length is 78 mm and the effective FOV is restricted to 100 mm transaxially. A coincidence timing window of 6 ns and a 350-650 keV energy window were used for all the measurements. The average energy resolution of the system is 23% [21].

The performance characteristics of the system that were evaluated here, following the NEMA NU-4 2008 standards, were the spatial resolution, sensitivity, scatter fraction, counting rates and image quality. A brief description of the experiments is provided below for each parameter.

B. Spatial Resolution

The spatial resolution of the system is the ability to distinguish between two points after image reconstruction. This is typically measured by the width of the reconstructed point spread function of a point source, and the degree of spreading (blurring) of the point object is a measure for the quality of the imaging system. For these measurements a 1-mm ^{22}Na point source of 166 kBq was placed at various radial distances (5, 10, 15 and 25 mm) from the axial center of the FOV and at ¼ of the axial FOV. Data were acquired for 60 s in order to collect at least 10,0000 prompt counts. List-mode data of each location were histogrammed into 3D sinograms which were rebinned into 2D sinograms using Fourier rebinning with a span of 3 and a ring difference of 31, which is the maximum ring difference (MRD) of the microPET R4 scanner. The spatial resolution was determined by forming one-dimensional response functions through the peak of the image volume in three orthogonal directions. The image pixel size was made one fifth of the expected full width half maximum (FWHM) in the transverse dimensions.

The volumetric resolution of the system was also calculated here by the product of the three components of the spatial resolution; i.e. radial, tangential and axial resolution. Although NEMA standards do not include this calculation, we consider it a means to indicate the element with the smallest volume that can be resolved accurately with the device.

C. Scatter fraction, count losses and random coincidence measurements

The purpose here was to measure the relative system sensitivity to scattered radiation and the effects of dead time and random events at

various levels of activity. We used two cylindrical high density polyethylene phantoms representing rodents; mice and rats. The mouse-sized phantom was 25 mm ± 0.5 mm diameter and 70 mm ± 0.5 mm long. A cylindrical hole of 3.2 mm was drilled parallel to the center axis, at a radial distance of 10 mm. The rat-sized phantom was 50 mm ± 0.5 mm diameter and 150 mm ± 0.5 mm long, with a cylindrical hole drilled at a radial distance of 17.5 mm. Line sources were 10 mm shorter than the cylindrical phantoms. Both phantoms were centered in the axial and transaxial direction of the scanner. The initial activity for the mouse-sized and rat-sized phantom was 8.5 mCi (314.5 MBq) and 6.5 mCi (240.5 MBq) [18F]-FDG respectively. Since the microPET R4 system presents intrinsic radioactivity (^{176}Lu), a measurement of the intrinsic true count rate was also made without any activity in the test phantom line source. The duration of each frame was 1.600 s with a total acquisition time of 43.200 s. The total event rate, true event rate, random coincidences, scatter coincidences and noise equivalent count (NEC) rate were calculated as a function of the phantom activity. Furthermore, the scatter fraction of the system was calculated by the last frames due to the low activity concentration in the FOV, with count-loss rates and random-event rates below 1.0% of the true event rate. No corrections of scatter, random, dead time or attenuation were performed. Single slice rebinning (SSRB) was performed in 3D sinograms to obtain 2D data sets.

D. Sensitivity

The ability of the scanner to detect positron annihilation γ-rays was measured as a fraction of the coincidence photon pairs emitted from the source and detected by the equipment. This is an important parameter that needs to be evaluated for each system especially when using dynamic imaging with frames of short duration or tracers that can only be injected in extremely low amounts, such as [11C]- Carfentanil [25].

We used the same ^{22}Na point source as in the case of spatial resolution. The source was placed in the center of the FOV axially and trasaxially. Acquisitions were performed for 60 s at each position while the source was stepped axially to the either end of the scanner's FOV so as to collect 10,000 true events. The step size was identical to the thickness of the sinogram slice; 1.21 mm. Background true event rates were also determined by acquiring a dataset with no source in the FOV for 60 s. SSRB was used to assign counts in oblique LORs to the image slice where the LOR crosses the scanner axis, so that each slice is represented by one sinogram. For each row of the sinogram, the highest value was located and all pixels greater than 1 cm from this peak value were set to zero. Sensitivity for each slice was calculated by dividing the total counts of each slice by the total activity of the source, correcting for the branching ratio of ^{22}Na.

E. Image Quality

The purpose of this measurement was to produce images simulating those obtained in a total body imaging study of a small rodent with hot lesions and with uniform hot and cold areas. Three different measurements are computed to describe different quality aspects of reconstructed images: i) uniformity, as a measure of statistical noise in both hot and cold regions; ii) the recovery coefficient, which reflects quantitative accuracy and is known to be highly influenced by spatial resolution in small objects; and iii) spill – over ratio as another indication of the spatial resolution achieved for the images.

A NEMA phantom was specifically designed to perform these measurements. This consists of three main parts made of polymethylmethacrylate with internal dimensions of 50 mm in length and 30 mm in diameter. The main phantom body was composed of a fillable cylindrical chamber with 30 mm diameter and 30 mm length. The remaining 20 mm of the length of the phantom body was solid, with 5 fillable rods with a diameter of 1, 2, 3, 4 and 5 mm each. A lid attached to the large uniform end region of the phantom supported the two cold region chambers. One of these chambers was filled with non-radioactive water and the other was left with air inside. Both these chambers were composed of hollow cylinders of 15 mm in length and 8 mm in internal diameter, 10 mm in outer diameter and 1 mm wall thickness. The whole phantom was filled with 114 μCi 18F-FDG for a 20 min acquisition scan. The phantom was placed on the tomograph bed in such a way that the axis of its main cylindrical compartment was aligned with the axis of the tomography FOV.

We evaluated two methods to correct attenuation of the data; a radionuclide-based transmission scan and an x-ray CT-based transmission scan. NEMA standards do not specify a radionuclide-based transmission scan but in the case of the microPET R4 this is the method provided by the manufacturer. A 68Ge line source was used through a transmission scan so as to measure the attenuation along all the lines of responses (LOR). We also performed a reference scan, called blank scan, before the transmission scan to ensure that the ratio of the blank counts to the transmission counts yielded a correction factor for each emission LOR. Images were reconstructed to pixel sizes of 0.84 mm (radially and transaxially) using 2D FBP with no axial filter, FORE+2D+OSEM with 4 iterations and 16 subsets, and finally 3D-OSEM with 12 subsets, 2 iterations and 18 MAP iterations. All reconstruction parameters were left to their default values, which are the ones recommended by the scanner´s manufacturer.

CT scan was obtained by using the Discovery ST PET/CT (GE) system with a tube voltage of 120 kV and 100mA. Images were reconstructed with a voxel size of 0.1875x0.1875x0.625 mm3 providing an image volume of

512x512x153 mm3. The CT image was down-sampled to the microPET image bin size using the software provided with the microPET R4 scanner. The same software was used to convert CT Hounsfield numbers to linear attenuation coefficients at 511 keV. Different regions representing different tissues were segmented and then assigned with the appropriate μ-value. An attenuation sinogram was subsequently created using the attenuation wizard of the microPET R4 and a re-scale of the μ-map image to the actual μ-values and segmentation by thresholding of the μ-values took place. The next step was to perform Fourier rebinning for the same span and ring difference as the microPET images.

The data evaluated here after the reconstruction of the image, were the image uniformity, recovery coefficient values and accuracy of corrections. Uniformity was calculated by applying a volume of interest (VOI) of 22.5 mm in diameter by 10 mm in length over the center of the uniform region of the image quality phantom. The mean value of this uniform region indicates the true isotope concentration. Recovery coefficients (RC) were calculated on the image slices covering the central 10 mm length of the rods, which were averaged to obtain a single slice of lower noise. Circular regions of interest (ROIs) were drawn on this image around each rod with diameters twice the rods´ physical diameter. The maximum values in each of these ROIs were recorded and used to create line profiles along the axial direction the rods. The isotope concentration was measured from the mean pixel value along each of the profiles in the axial direction. The standard deviation was calculated as:

$$\%\text{STDRC} = 100 * \sqrt{\left(\frac{STD_{lineprofile}}{Mean_{lineprofile}}\right)^2 + \left(\frac{STD_{background}}{Mean_{background}}\right)^2}$$

Attenuation correction was evaluated by defining VOIs of 4 mm in diameter and 7.5 mm in length in the water- and air- filled cylindrical inserts of the image quality phantom. The ratio of the mean in each cold region to the mean of the hot uniform area was reported as the spill-over ratio (SOR). The standard deviation was calculated in the same way as that of the RCs.

III. RESULTS

Spatial Resolution At the center of the FOV the radial, tangential and axial resolutions in terms of FWHM (mm) were 2.12 mm, 2.66 mm and 2.23 mm respectively. Figure 1 shows the results obtained according to the NEMA NU 4-2008 standards for the spatial resolution of the microPET R4 system in terms of FWHM (Fig. 1A) and FWTM (Fig. 1B). Fig. 2 represents the volumetric resolution of the system.

Scatter fraction, count losses and random coincidence measurements

Fig. 3 shows the counting rate performance of the microPET R4 scanner. The scatter fraction was 8.5% for the mouse-sized phantom, while the peak count rate was 311kcps at 153.5 MBq (Fig. 3A). In the case of the rat-sized phantom the scatter fraction was 22% and the peak count rate was 117 kcps at 123.24 MBq (Fig. 3B).

Sensitivity The absolute system sensitivity at the center of the FOV was measured to be 1.9% (16.66 cps/kBq) for sinograms encompassing the central 7 cm (mouse-sized phantom) and 15 cm (rat-sized phantom). The axial FOV of the microPET R4 is 7.8 cm and therefore sinograms of the rat-sized phantom encompassed the same axial length as the sinogram of the mouse-sized phantom. Figure 4 displays the axial absolute sensitivity profile along the z-axis of the microPET R4 scanner.

Image Quality The reconstruction of the NEMA image quality phantom (Fig. 5) took place using the three reconstruction algorithms provided with the microPET R4 scanner. The pixel size was 0.84 mm (radial and axial) and in 2D FBP no axial filter was used. Table I summarizes the uniformity results without attenuation correction and with transmission and CT attenuation correction.

The recovery coefficients in function of the rod diameters are represented in Fig. 6.

The spill-over ratios measured in the air- and water-filled cylindrical inserts of the NEMA image quality phantom are indicated in Table 2 for data without correction of attenuation and with transmission-based and CT attenuation correction. The ratio of the reconstructed count density to the true count density of the ROI and the Standard Deviation (%STD) was estimated from the water and air-filled compartments of the image quality phantom. The results shown below represent the spill-over ratio and the %STD without correction of attenuation, with 68Ge transmission based attenuation correction (TX-AC) and with CT attenuation correction (CT-AC).

IV. DISCUSSION

The performance evaluation of the microPET R4 scanner in function of spatial resolution, sensitivity, scatter fraction, count rate performance and image quality according to the NEMA NU 4-2008 standards for small animal PET systems has been studied.

The system´s spatial resolution in the tangential direction was constant but it slightly deteriorated after 10 mm radial distance when moving away from the CFOV. This finding can be attributed to the parallax error, which causes degradation of the radial resolution at radial offsets. This well-known geometric error, also referred to as depth of interaction (DOI), derives from the determination of the exact position at which the photon

hits the crystal, so crystal penetration is more likely to occur for photons with an increasing incident angle [26]. The axial resolution also deteriorated at the end of the FOV ranging from 2.55 mm FWHM at 5 mm radial distance to 3.23 mm FWHM at 25 mm radial distance. Due to the fact that the maximum ring difference of the microPET R4 scanner was used to histogram the 3D sinograms to 2D sinograms and then FORE + 2D FBP reconstruction algorithm was used, may explain these results [27]. The system´s volumetric resolution was found to be 11.55 mm^3 at the CFOV and 15.08 mm^3 at 5 mm radial distance. Our results of spatial resolution do not significantly depart from those obtained by Knoess et al [21].

Generally, the spatial resolution of a PET system is measured with a point source placed at various distances across the whole FOV. The reproduction of the spatial details in the image is expressed through the point spread function (PSF) and after reconstruction profiles are fitted through the reconstructed image normally with a Gaussian spread function fitted to the PSF. Then the width at half of the maximum value of the PSF, and at tenth of the maximum value of the PSF, is measured. It has to be highlighted that the spatial resolution depends on the shape and the material of the source, the isotope used and the reconstruction method followed. There are various reconstruction methods used in PET ranging from simple 2D and 3D FBP to iterative methods such as ML-EM. Rebinning methods are also used referring either to the axial rebinning of the data (SSRB) or multislice rebinning or Fourier rebinning (FORE) [28].

According to the NEMA NU 4-2008 standards, the proposed methodology for the evaluation of the spatial resolution should be done by 2D or 3D FBP reconstruction with no smoothing applied. In this aspect, it should be considered that one of the major limitations of FBP is the statistical noise, so a smoothing filter should be applied prior to reconstruction in order to control it. Of course, on the other hand, in case of applying a smoothing filter, resolution would degrade because of the reduction of variance in the image [29]. This did not take place during the processing of the spatial resolution and therefore the effect of noise in FWHM and FWTM may explain the relatively high variability in our measurements. Furthermore, NEMA NU 4-2008 standards indicate that the FWHM should span at least five pixels; some scanners are unable to fulfill this requirement and therefore cannot follow the same pattern for the performance evaluation [30].

The sensitivity of the system was measured to be 1.9% at the center of the scanner's FOV using an energy window of 350-650 keV. This was calculated using the rate of emitted prompt gamma rays, meaning the true, scatter and random coincidences, coming from the ^{22}Na point source to the detectors. The axial sensitivity profile drops linearly from the center to the

edges of the FOV. The presence of the intrinsic radioactivity of LSO (^{176}Lu) affects the system´s ability to detect low activities in the FOV. In the microPET R4 scanner the activity of ^{176}Lu in the 271cm^3 of LSO is approximately 75 kBq [31] but the fact that an energy window of 350-650 keV was used, significantly reduced the amount of the intrinsic count rate and its contribution to the statistical noise.

Knoess et al., [21] followed a totally different methodology to evaluate the sensitivity of the microPET R4 scanner. They used a ^{68}Ge line source and aluminium sleeves with different diameters and wall thicknesses to create a shielding around the source for various energy windows. Sensitivity was calculated by plotting the true count rate against the total shielding thickness and by extrapolating to the equivalent unshielded line source, with no attenuation to the true count rate. System sensitivity for an energy window of 350-650 keV was found to be 12.24 cps/kBq (1.37%). They also performed an additional measurement using a ^{22}Na point source centered in the transaxial direction of the FOV. The radial direction was scanned from 0 mm to 50 mm offset in steps of 5 mm yielding a sensitivity of 24.48 cps/kBq (2.7%) for an energy window of 350-650 keV [21].

The counting rate was plotted as a function of the average activity concentration for the mouse- and rat-sized phantoms. Its maximum corresponds to the relationship between real and noise events. After reaching its maximum it slowly decreases as the number of random coincidences increases due to dead time effects. The peak NEC rate was found to be 311 kcps at 153.5 MBq for the mouse-sized phantom and 117 kcps at 123.24 MBq for the rat-sized phantom. The NECR for the mouse-sized phantom was found to be higher than the NECR for the rat-sized phantom because there is less photon attenuation forcing more photons getting out of the imaging subject. According to Knoess et al. [21] the maximal NEC ratio for the mouse phantom was 168 kcps at 91 MBq and for the rat phantom it was 89 kcps at 81 MBq for an energy window of 350-750 keV.

During the evaluation of the scatter fraction and count rate performance according to the NEMA NU 2-2001 [21], bigger phantoms were used as well as different energy windows [32]. For example, according to Knoess et al. [21] scatter fraction values were 18% (mouse-sized phantom) and 28% (rat-sized phantom) for an energy window of 350-750 keV, whereas in this work they were reduced to 8.5% and 22% respectively for an energy window of 350-650 keV. Since the ratio of rays falling into the range of 650-750 keV is expected to be very low, these differences in the results can be safely attributed to the different phantom sizes used in the experiments.

The image quality results provide estimation for a standardized imaging situation in small animal PET systems. All images were reconstructed using

the three reconstruction algorithms provided by the microPET R4 scanner. Correction of attenuation was performed in order to assess the impact of corrections in the measurements, especially when cold regions are used where scatter radiation is increased. It is known though that the problem of photon attenuation in small animal imaging is not so much of importance since the size of the animals is much lower than in the human case.

In the case of uniformity, the %STD indicated better results when using FBP reconstruction algorithm than the two iterative methods. This may be surprising but it concurs with Bahri M. et al [33] who found that the mean activity was within 99% of the expected value for FORE reconstruction methods.

However, an overestimation of the recovery coefficient in large rods of 5mm in diameter was obtained with 2D and 3D OSEM MAP reconstruction methods. This behavior might bias image quantification. It should be noted that since the spatial resolution of the system was over 2mm, the maximum cylinder diameter made it impossible to fully recover the total activity inside. The expected RC for a cylinder with a diameter 2.37 times the FWHM of the system is of about 0.95 [34]. The spill over ratio decreased with the use of 2D OSEM reconstruction algorithm. This can be attributed to an improvement in spatial resolution with iterative methods as compared to FBP. SOR values for the air compartment of the phantom were close to zero with or without attenuation correction.

When using the ^{68}Ge based transmission attenuation correction method, there was no significant change in the SOR values apart from a slight decrease in the phantom´s water compartment. The CT based attenuation correction method used in this study provided lower statistical noise and higher resolution anatomical images in comparison to the TX-AC method. A significant decrease in the SOR values of the water compartment was observed while in the air compartment values remained close to zero. No scatter correction method was applied in this study.

The evaluation of the image quality after reconstruction of the images was first introduced in NEMA NU 4-2008 standards from small animal PET systems, so no previous results exist so as to be compared with the ones obtained here.

It is worth mentioning that NEMA standards try to provide a standardized methodology for evaluating the performance of small animal PET systems and that these measurements are not absolute. They can be used for comparing different systems since the methodology provided is fairly easy to perform although there are some ambiguities in some sections of the NEMA NU 4-2008 standards. For example, it should be made clearer when calculating the sensitivity of a system as to which counts can be used when a system provides prompts and histogrammed coincidences as in the case

of the microPET R4 scanner. Also, the quality of the reconstructed image depends on the size of the object and the contrasts used. The size of the NEMA NU 4-2008 image quality phantom is more representative of a mouse's body and a rat's head; therefore the results obtained under these specifications must take into account the above statement.

Furthermore, NEMA NU 4- 2008 standards are not so appropriate for evaluating the performance of scanners that do not employ conventional cylindrical geometry, so modifications are required in order to provide meaningful results as in the case of the PETbox scanner [35].

V. CONCLUSIONS

This study evaluated the performance of the microPET R4 system according to the new NEMA NU 4-2008 standards for small animal PET systems and compared it with its previous evaluation according to [21]. Our findings highlight the importance of using specific performance evaluation tests for small animal imaging as some of the performance indicators calculated herein in accordance with the new standards diverge notably from published results using older ones.

To summarize our findings regarding reconstruction algorithms, FBP provided the best uniformity, at the expense of a mild underestimation of absolute activity concentration and the worst spatial resolution. 2D-OSEM yielded the best quantification accuracy and slightly worse uniformity than FBP. Finally, 3D-OSEM resulted in an important positive bias in quantitative measurements and the worst uniformity of the three evaluated methods, although it provided the best results in terms of spatial resolution. Here, when values are compared to previously results, variations can be noticed which could be attributed to the fact that different phantoms and energy windows were used.

ACKNOWLEDGMENT

The authors kindly thank Dr. Juan José Vaquero for providing the phantoms for the system´s count rate and scatter fraction. We also thank Ma Dolors de la Fuente for her valuable help and technical support.

REFERENCES

[1] S. R. Cherry, "Fundamentals of Positron Emission Tomography and applications in preclinical drug development", *J. Clin Pharmacol*., vol. 41, pp. 482-91, 2001.

[2] M. E. Phelps, "Positron emission tomography provides molecular imaging of biological processes", *Proc Natl Acad Sci.*, vol. 97, pp. 9226-9233, 2000.

[3] C. S. Levin, "Primer on molecular imaging technology", *Eur J Nuc Med Mol Imaging*, vol. 32(14), pp. S325-S345, 2005.
[4] C. S. Levin, H. Zaidi, "Current trends in preclinical PET system design", *PET Clin*. vol. 42, pp. 219-232, 2007.
[5] H. Zhang, S. Alyafei, T. Inoue, K. Tomiyoshi, K. Endo, "Performance stability of SHR 2000 high resolution PET for small animal research", *Annals of Nucl Med*, vol. 13(1), pp. 65-70, 1999.
[6] D. P. Cutler, S. R. Cherry, E. J. Hoffman, W. M. Digby, M. E. Phelps, "Design features and performance of a PET system for animal research", *J Nuc Med*, vol. 33, pp. 595-604, 1992.
[7] S. R. Cherry, Y. Shao, S. Siegel, R.W. Silverman, K. Meadors, J. Young, et al., "MicroPET: a high resolution PET scanner for imaging small animals", *IEEE Trans Nuc Sci*., vol. 44, pp. 1161-1166, 1997.
[8] A. Del Guerra, G. Di Domenico, M. Scandola and G. Zavattini, "YAP-PET: first results of s small animal positron emission tomography based on YAP:Ce finger crystals", *IEEE Trans Nucl Sci*. vol. 45, pp. 3105-3108, 1998.
[9] A.P. Jeavons, R.A. Chandler and CAR. Dettmar, "A 3D HIDAC-PET camera with sub millimetre resolution for imaging small animals", *IEEE Trans Nucl Sci, vol.* 46, pp. 468-473, 1999.
[10] C. Tai, A. Chatziioannou, S. Siegel, J. Young, D. Newport, R.N. Goble, R.E. Nutt and S.R. Cherry, "Performance evaluation of the microPET P4: a PET system dedicated to animal imaging", *Phys Med Biol.*, vol. 46, pp. 1845-1862, 2001.
[11] P. Vasca, C.L. Woody, D.J. Schlyer, S. Shokouhi, S.P. Stoll, J. F. Pratte, et al., "RatCAP: Miniaturized head-mounted PET for conscious rodent brain imaging", *IEEE Trans Nucl Sci.*, vol. 51(5), pp. 2718-2722, 2004.
[12] *National Electrical Manufactures Association. Performance Measurements of Positron Emission Tomogaphs.,* Rosslyn VA, 1994. Standards Publication NU 2- 1994.
[13] *National Electrical Manufactures Association. Performance Measurements of Positron Emission Tomogaphs.,* Rosslyn VA; 2001. Standards Publication NU 2-2001.
[14] J. Missimer, Z. Madi, M. Honer, C. Keller, A. Schubiger and S.M. Ametamey, "Performance evaluation of the 16-module quad-HIDAC small animal PET camera", *Phys Med Biol,.vol.* 49, pp. 2069-2081, 2004.
[15] *National Electrical Manufactures Association. Performance Measurements of Positron Emission Tomogaphs.* Rosslyn VA; 2008. Standards Publication NU 4-2008.
[16] Q. Bao, D. Newport, M. Chen, D.B. Stout and A.F. Chatziioannou, "Performance evaluation of the Inveon dedicated PET preclinical

tomograph based on the NEMA NU 4- standards", *J Nuc Med.*, vol. 50, pp. 401-408, 2009.

[17] R. Prasad, O. Ratib and H. Zaidi, " Performance evaluation of the Flex Triumph X-PET scanner using the National Electrical Manufacturers Association NU-4 standards", *J Nuc Med., vol.* 51, pp. 1608-1615, 2010.

[18] S.A. Kis, I. Latjos, M. Emri, L. Tron, G. Opposits, T. Bukki, et al., "Performance test of the MiniPET-II small animal scanner according to the NEMA NU-4 standards", *IEEE NSS Conference Record*, M09-152, 2009.

[19] M.A. Bahri, A. Plenevaux, G. Warnock, A. Luxen and A. Seret, "NEMA NU4-2008 image quality performance report for the microPET Focus 120 and for various transmission and reconstruction methods", *J Nuc Med.*, vol. 50, pp. 1730-1738, 2009.

[20] E. Lage, J.J. Vaquero, A. Sisniega, S. España, G. Tapias, M. Abella, et al., "Design and performance evaluation of a coplanar multimodality scanner for rodent imaging", *Phys Med Biol.*, vol. 54, pp. 5427-5441, 2009.

[21] C. Knoess, S. Siegel, A. Smith, D. Newport, N. Richerzhagen, A. Winkeler, et al., "Performance evaluation of the microPET R4 scanner for rodents", *Eur J Nuc Med Mol Imaging.*, vol. 30, pp. 737-747, 2003.

[22] C.L. Melcher and J.S. Schweitzer, "Cerium-doped Lutetium Oxyorthosilicate: A Fast, Efficient New Scintillator", *IEEE Trans Nuc Sci.*, vol. 39(4), pp. 502-505, 1992.

[23] F. Daghighian, P. Shenderov, K.S. Pentlow, M.C. Graham, C.L. Melcher and J.S Schweitzer, "Evaluation of Cerium Doped Lutetium Oxyorthosilicate (LSO) Scintillation crystal for PET", *IEEE Trans Nuc Sci.*, 1045-1047, 1993.

[24] S. Siegel, M. Eriksson, L. Eriksson, M. Casey and R. Nutt, "An alternative to polishing the surfaces of scintillation detectors", *IEEE MIC Conference Record.* , pp. 1212-1214, 2000.

[25] M. Titeler, R.A. Lyon, M.J. Kuhar, J.F. Frost, R.F. Dannals, S. Leonhardt, et al., "Mu opiate receptors are selectively labelled by [3H] carfentanil in human and rat brain", *Eur J Pharmacol*., vol. 22, pp. 221-8, 1989.

[26] J. Seidel, J.J. Vaquero and M.V. Green, "Resolution uniformity and sensitivity of the NIH ATLAS small animal PET scanner: Comparison to simulated LSO scanners without Depth-Of-Interaction capability", *IEEE Trans Nuc Sci*., vol. 50(5), pp. 1347-1350, 2003.

[27] E.P. Visser, A. Disselhorst, M. Brom, P. Laverman, M. Gotthardt, W.J. Oven and O.C. Boerman, "Spatial Resolution and Sensitivity of the Inveon Small Animal PET scanner", *J Nuc Med.*, vol. 50, pp. 139-147, 2009.

[28] S. Weber and A. Bauer, "Small animal PET: aspects of performance assessment", *Eur J Nuc Med and Mol Imaging*., vol. 31(11), pp. 1545-1555, 2004.

[29] A. Alessio and P. Kinahan, "PET Image reconstruction", in: Henkin RE, Bova D, Dillehay GL, Halama JR, Karesh SM, Wagner RH, Zimmer AM, eds. Nuclear Medicine. 2nd ed., vol. 1, Philadelphia, PA: Mosby-Elsevier; 2006.

[30] J.J. Vaquero, E. Lage, L. Ricon, E. Abella, E. Vicente and M. Desco, "rPET detectors design and data processing", *IEEE Nuc Sci Symp Conf Rec*., pp. 2885-2889, 2005.

[31] A.L. Goertzen, J.Y. Suk and C.J. Thompson, "Imaging of Weak-Source Distributions in LSO-Based Small Animal PET scanners", *J Nucl Med*. vol. 48, pp. 1692-1698, 2007.

[32] F.D. Popota, P. Aguiar, Y. Fernandez, C. Lois, D. Pareto, D. Ros, et al., "Comparison of NEMA NU 4-2008 vs NEMA NU 2-2001 for the performance evaluation of the microPET R4 system", *IEEE Nucl Sci Symp Conference Record*., M05-151, pp. 2706-2709, 2009.

[33] M.A. Bahri, A. Plenevaux, G. Warnock, A. Luxen and A. Seret, "NEMA NU 4-2008 Image quality performance report for the microPET Focus 120 and for various transmission and reconstruction methods", *J Nucl Med.* vol. 50, pp. 1730-1738, 2009.

[34] S. R. Cherry and M. Dalhbom, "PET: Physics, Instrumentation and Scanners", in: Phelps M, eds. PET Molecular Imaging and its Biological Applications, New York, NY: Springer Verlag Inc.; 2004.

[35] H. Zhang, Q. Bao, T.N. Vu, R.W. Silverman, R. Taschereau, B.N. Berry-Pusey, A. Douraghy, F.R. Rannou, D.B. Stout and A.F. Chatziioannou, "Performance evaluation of PETBox: A low cost bench top preclinical PET scanner" [research article], *Mol Imaging Biol.* vol. 13(5), pp. 949-961, 2011.

FIGURES:

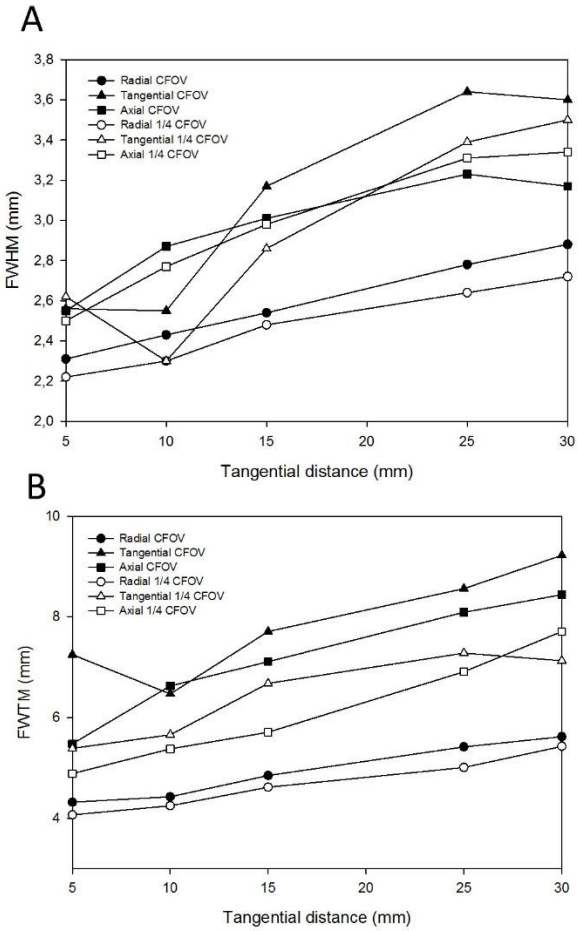

Fig. 1 Spatial resolution as a function of radial offset in terms of FWHM (A) and FWTM (B)

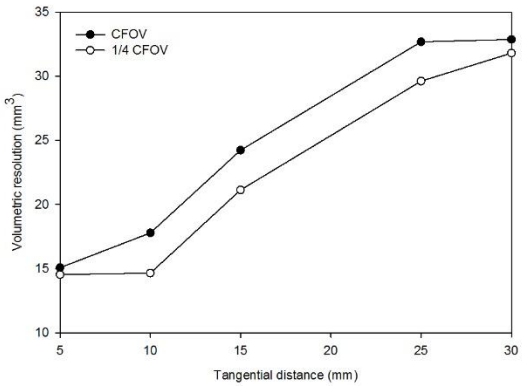

Fig. 2 Volumetric resolution at axial center and at ¼ of the axial center

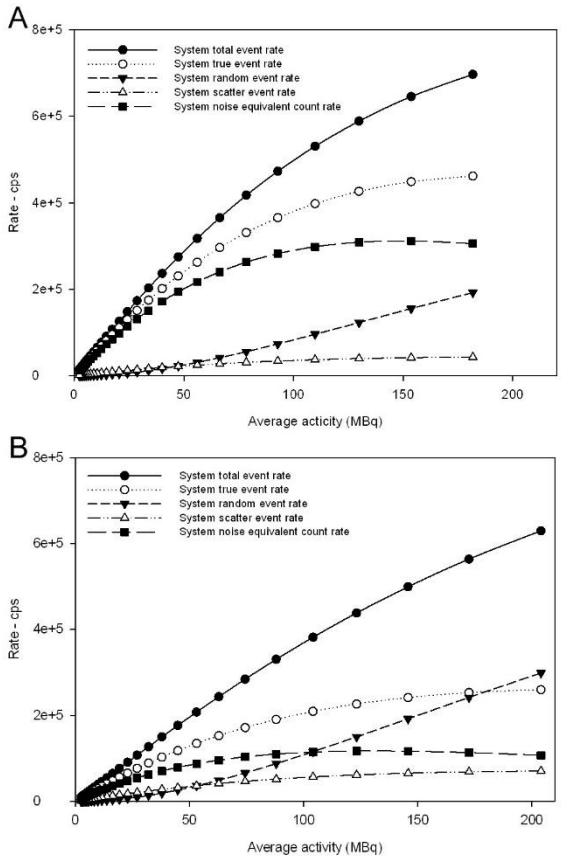

Fig. 3 Count rate performance for mouse-sized (A) and rat-sized (B) phantoms

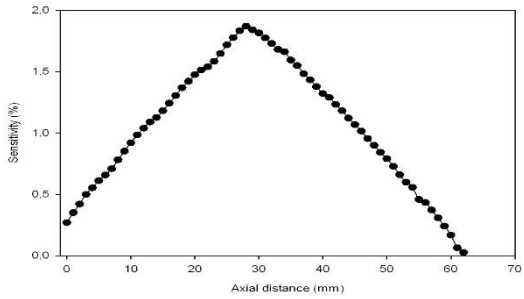

Fig. 4 Axial sensitivity profile

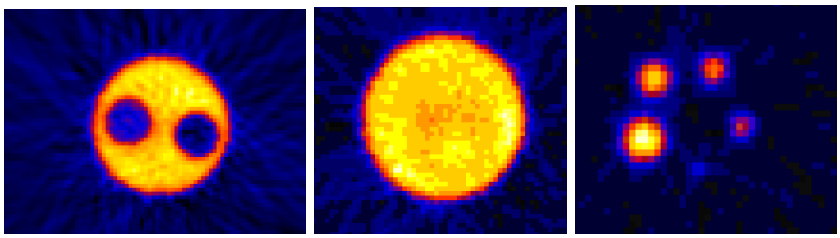

(a) (b) (c)

Fig. 5 microPET R4 transverse views of image reconstruction of the quality phantom; a) transverse view of the non-radioactive water and air chambers, b) transverse view of the uniform part and c) transverse view of the five cylindrical rods

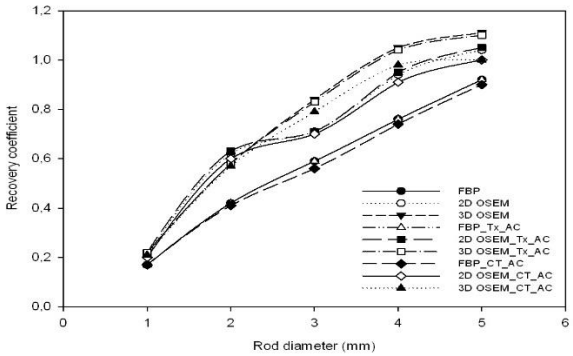

Fig. 6 Recovery coefficients using the three reconstruction algorithms of the microPET R4 with and without corrections

Reconstruction algorithms	Mean (nCi/cc)	Max (nCi/cc)	Min (nCi/cc)	%STD
FBP	4533.75	5693.45	2970.93	7.76
2D OSEM	4534.46	5779.23	2953.87	8.67
3D OSEM	4788.14	6351.49	3343.52	8.92
FBP_TX_AC	4681.77	5741.85	3076.43	7.63
2D OSEM_TX_AC	4680.87	5997.99	3060.82	8.56
3D OSEM_TX_AC	4949.35	6618.83	3486.1	8.81
FBP_CT_AC	6959.03	8753.27	4216.77	7.28
2D OSEM_CT_AC	6957.2	9106.16	4152.94	8.28
3D OSEM_CT_AC	7369.77	9960	4849.67	9.52

TABLE I Uniformity values for the microPET R4 with and without attenuation corrections

		Water		Air	
		SOR	**%STD**	**SOR**	**%STD**
No attenuation correction	**FBP**	0.23	38.86	0.05	46.27
	OSEM 2D	0.21	41.82	0.09	43.69
	OSEM 3D	0.23	58.29	0.01	123.21
Tx attenuation correction	**FBP**	0.21	38.01	0.05	43.93
	OSEM 2D	0.20	42.64	0.08	42.96
	OSEM 3D	0.22	57.76	0.01	73.79
CT attenuation correction	**FBP**	0.09	59.4	0.06	62.29
	OSEM 2D	0.15	44.18	0.10	44.12
	OSEM 3D	0.02	99.53	0.01	68.44

TABLE II SOR and %SDT for all reconstruction algorithms from the microPET R4 scanner without corrections and with transmission and CT attenuation correction

Monte Carlo simulations versus experimental measurements in a small animal PET system. A comparison in the NEMA NU 4-2008 framework.

F D Popota[1, 2], P Aguiar[3, 4, 5], S España[6, 7], C Lois[8, 9], J M Udias[10], D Ros[1, 11, 12], J Pavia[11, 12, 13] and J D Gispert[11, 14]

[1] Unitat de Biofisica i Bioenginyeria, Universitat de Barcelona, Barcelona, Spain
[2] Universidad de Pompeu Fabra, Barcelona, Spain
[3] Fundación Ramón Domínguez, Santiago de Compostela, Galicia, Spain.
[4] Servicio de Medicina Nuclear, Complexo Hospitalario Universitario de Santiago de Compostela, Galicia, Spain.
[5] Grupo de Imaxe Molecular, Instituto de Investigación Sanitarias (IDIS), Santiago de Compostela, Galicia, Spain.
[6] Advanced Imaging Unit, Centro Nacional de Investigaciones Cardiovasculares (CNIC), Madrid, Spain
[7] Ciber de Enfermedades Respiratorias (CIBERES), Madrid, Spain
[8] Grupo de Investigación en Radiofísica, Departamento de Física de Partículas, Universidade de Santiago de Compostela, Spain
[9] Madrid-MIT M+Visión Consortium, Massachusetts Institute of Technology (MIT), Cambridge, MA, USA
[10] Dpto. de Física Atómica, Grupo de Física Nuclear, Molecular y Nuclear, Universidad Complutense, Madrid, Spain
[11] Ciber en Bioengenieria, Biometeriales y Nanomedicina (CIBER-BBN), Barcelona, Spain
[12] Institut d'Investigacions Biomèdiques Agust Pi i Sunyer (IDIBAPS), Barcelona, Spain
[13] Servei de Medicina Nuclear, Hospital Clinic, Barcelona, Spain
[14] Fundació Pasqual Maragall, Barcelona, Spain

E-mail: jdgispert@fpmaragall.org

This paper is reproduced according to the original submitted version.

Abstract

In this work a comparison between experimental and simulated data using GATE and PeneloPET Monte Carlo simulation packages is presented. All simulated setups, as well as the experimental measurements, followed exactly the guidelines of the NEMA NU 4-2008 standards using the microPET R4 scanner. The comparison was focused on spatial resolution, sensitivity, scatter fraction and counting rates performance.

Both GATE and PeneloPET showed a fairly good agreement for the radial and tangential spatial resolutions at the centre of the field of view (CFOV) and at ¼ CFOV. PeneloPET was in very good agreement with the experimental data sets for the axial FWHM at the CFOV and at ¼ CFOV.

High accuracy was obtained between experiments and simulations of the system's sensitivity and scatter fraction for an energy window of 350-650 keV, as well as for the counting rate simulations. The latter was the most complicated test to perform since each code demands different specifications for the characterization of the system's dead time. Although simulated and experimental results were in excellent agreement for both simulation codes, PeneloPET demanded more information about the behavior of the real data acquisition system.

To our knowledge, this constitutes the first validation of these Monte Carlo codes for the full NEMA NU 4-2008 standards for small animal PET imaging systems.

1. Introduction

Monte Carlo (MC) simulation is a powerful tool for research on imaging systems such as Positron Emission Tomography (PET) and Single Emission Tomography (SPECT) for both clinical and small animal systems.

It can be used to address aspects that are difficult to be studied by experimental or analytical approaches (Jan *et al* 2004). It is considered to be a potent tool for the design of new medical imaging devices (Braem *et al* 2004), optimization of acquisition protocols (Zaidi 2007, Susrt and Karp 2008), development of reconstruction algorithms (Herraiz J L *et al* 2006) as well as for the implementation of correction techniques to improve image quantification (Castiglioni *et al* 1999, Barret *et al* 2005).

There are several versatile general purpose MC codes developed for high energy physics or dosimetric studies, such as EGS4 (Nelson WR *et al* 1985), MCNP (http://mcnp-green.lanl.gov/), GEANT4 (Agostinelli S *et al* 2003) and PENELOPE (Salvat *et al* 2006), which simulate radiation transport through matter and interactions of different types of particles. The use of these codes generally requires advanced programming abilities and a long learning period.

On the other hand, dedicated MC codes have been developed for simulating PET and SPECT scanners, which provide different advantages and disadvantages. The most representative codes are considered to be GATE (Jan *et al* 2004), SimSET (Harrison RL *et al* 1993) and PeneloPET (España *et al* 2009). These codes are generally easy to install and they do not require a long learning period. Each code has different characteristics, with advantages and limitations with respect to the others. In particular, there are different levels of accuracy in the description of the scanner, source distributions, physical and electronic processes, or computational efficiency that may favor one over the others to meet the requirements of certain tasks. However, it is difficult to know which one is best suited for a specific application. It is therefore of importance to evaluate the accuracy of the code through validation studies that involve the comparison between simulated and experimental data.

To this end, it is essential to rely on a set of established standards for characterizing the performance of a PET system. The National Electrical

Manufacturers Association (NEMA) has published a set of standards (NEMA 1994, NEMA 2001, NEMA 2007, NEMA 2008, Standardization Policies and Procedures of the NEMA 2008), which define a product, process or procedure with reference to the composition, construction, tolerance, operating characteristics etc.

In particular, NEMA standards for human PET and small animal systems constitute guidelines for validation studies since they describe the measurements which characterize the global system's performance in typical imaging conditions and independently of camera design.

Up to now, the available MC codes have been validated following the NEMA NU 2-2001 standards for a wide range of clinical scanners (Gonias *et al* 2007, Karakatsanis *et al* 2006, Lamare *et al* 2006, Schmidtlein *et al* 2005, 2006, Jan *et al* 2005, Stealens *et al* 2003, Carlier *et al* 2008, Assie *et al* 2004), but there is not such an extensive validation for pre clinical systems (Herraiz *et al* 2011, Merheb *et al* 2006, Rafecas *et al* 2009, Yang *et al* 2007, Lazaro *et al* 2004, Espana *et al* 2007). Following the NEMA NU 4-2008 standards, GATE has been validated in terms of sensitivity and count rate using the RRPET camera (Zeraatkar *et al* 2010) while PeneloPET has been validated in terms of scatter fraction using the ARGUS small animal PET scanner (Vicente *et al* 2010). To our knowledge only one comparative study between GATE and PeneloPET based on the NEMA NU 4-2008 standards for sensitivity and counting rates using the GE Healthcare eXplore Vista microPET scanner has been published (Liu and Zhao 2012).

The aim of this paper is to compare in detail the performance of two dedicated MC simulation codes, GATE and PeneloPET against experimental data following the NEMA NU-4 2008 standards for small animal systems in order to evaluate their strengths and weaknesses. This may help potential users to choose the code best suited for a specific application. The microPET R4 systems was used in this study, as it is likely

the commercial preclinical scanner with the largest installed base making it the most well-known and thoroughly evaluated device of its class.

We present common and specific features of the codes, and discuss their advantages and disadvantages in terms of accuracy, flexibility, efficiency, and ease of use. It is not the purpose of this paper to give a throughout understanding of the codes, but to present the differences and difficulties found from an end user point of view.

The outline of this paper is the following; in Section 2, we describe GATE and PeneloPET simulation packages and discuss features of each code. In addition, we present the experimental setup used for the validation of these codes, describing the characteristics of the
microPET R4 scanner and how it has been simulated. Then we summarize the methodology followed for the validation using the NEMA NU-4 2008 standards. In Section 3, we present the results of the validation of the codes, including simulations and experimental measurements. In Section4, a comparison among the codes in terms of accuracy, flexibility, efficiency, and ease of use is presented.

2. Materials and Methods

2.1. Description of Monte Carlo simulation codes - Overview

All MC codes share some common features such as random number generator, sample probability distributions as well as probability density functions.
PeneloPET and GATE allow the simulation of complex detector geometries such as block detectors which are arranged in cylindrical or polygonal arrangements with gaps between the block modules and shielding. The main characteristics and the differential details of each code are described below.

GATE: The GEANT 4 Application for Tomographic Emission (GATE) is a versatile and adaptable general purpose MC code written in C++ programming language (GEANT4). It is appropriate for simulation of both conventional and novel PET and SPECT systems. Both the design and development is carried out by the OpenGATE collaboration, where a large number of research groups from around the world, have publicly released this simulation toolkit after two years of software development and validation. There is a public release of GATE licensed under the GNU Lesser General Public License.

A great advantage of GATE is that it allows the description of time-dependent phenomena such as source or detector movement and source decay kinetics. With respect to other MC packages it allows a full description of a small animal PET and SPECT system. For example, a specific geometry can be modelled by combining a number of base structures such as spheres, squares, cylinders and trapezoids.

Several types of output data are included in GATE, such as ASCII, ROOT, list-mode and sinograms. ASCII data is the easiest possible output but is not compressed and the files are very large. ROOT files contain several trees in which different variables are stored and ROOT analysis software is required in order to plot the contents of the ROOT data file.

Output data can be stored under the list-mode format (LMF) developed by the Crystal Clear Collaboration (http://crystalclear.web.cern.ch) and therefore several tools enabling the reading of this format can be used. Finally, if an ECAT system is selected, as in this present work, the sinogram output can be enabled so that the coincidence events can be stored in an array of 2D sinograms, including data reduction factors such as span and mashing.

PeneloPET: PeneloPET is a MC application for simulation of geometrical PET scanners, both clinical and small animal systems (España *et al* 2009).

It is based on PENELOPE (Salvat *et al* 2006), a MC code for the generation of transport in matter of electrons, positrons and photons with energies from a few hundred eV up to 1GeV. Both codes (PENELOPE and PeneloPET) are written in FORTRAN language. The main purpose of this simulator is the optimization of the design of small animal PET systems.

The basic parts of PeneloPET are detector geometry, materials and sources definition, as well as electronic chain of detection. Four input files need to be edited by the user. All input parameters of the simulation are introduced into these four main files, which contain all the simulation parameters such as coincidence windows, energy window, scanner rotation (if needed), positron range and type of study (static or dynamic).

The modelling of the positron range used in PeneloPET generates uniform predefined positron range profiles for β^+ isotopes widely used in PET. This makes the simulations less computational expensive but still accurate.

Output data for analysis come to different levels starting from sinograrm and LOR histogramming to full list-mode data.

STIR library supports the format of the output data if reconstruction is needed for further analysis (http://stir.sourceforge.net/documentation/doxy/html/index.html). Also, data can be further explored by other programming languages, including ROOT.

The PeneloPET version used in this work was the PeneloPET v2.4, whereas for GATE was GATE 6.0.0 and Geant4 9.1.

2.2. microPET R4 scanner – detector geometry

The microPET R4 (Concorde Microsystems, Siemens), consists of four detector rings of 24 detector modules, each of 148 mm ring diameter and 78 mm axial length. Each module is composed of an 8 x 8 LSO crystal array

of 2.1 x 2.1 x 2.1 mm^3, with 2.423 mm and 2.426 mm axial and transaxial crystal pitch.

To reduce the scatter contribution of the out of FOV activity (Knoess C *et al* 2003), the front side of the animal port is confined with a 25 mm thick lead shield, whereas the back side is confined with 30 mm thick lead. Asymmetrical external shields were modelled as in the real scanner. A 6 ns coincidence window (Knoess C *et al* 2003) and a 3.2 ns time resolution (Tai *et al* 2001) were also modelled. All measurements and simulations were made for an energy window of 350-650 keV and the energy resolution was fixed to 23%. It must be noted that these are the default parameters recommended by the vendor for the normal operation of the scanner.

2.3. Performance evaluation

Following, a detailed description of the simulations with PeneloPET and GATE of the microPET R4 system according to the NEMA NU 4-2008 standards is taking place. The methodology which was used in the simulations is the same as in the experimental part (Popota *et al* 2012).

Spatial Resolution. Simulations took place reproducing a 4.48 μCi (166 kBq) ^{22}Na point source enclosed in an acrylic cylinder of 2.5 cm diameter and 0.65 cm length. The source was placed at specific radial distances, indicated by the NEMA NU 4-2008 standards, from the axial centre and at ¼ of the axial FOV. Simulation time was 60 sec for each position as in the experimental setup. Simulated 3D sinograms were converted into 2D sinogram data sets using Fourier rebinning with a ramp filter and a cut off at the Nyquist frequency. A span of 3 and a ring difference of 31 were used. Images were reconstructed by 2D FBP and the image pixel size was made one fifth of the expected FWHM in the transverse dimensions according to

the NEMA NU 4 2008 standard (NEMA 2008). Data were not corrected for attenuation, normalisation and non-collinearity.

In GATE and PeneloPET both positron range and non-collinearity were incorporated into the simulations. The non-collinearity was included in PeneloPET simulations by employing a Gaussian distribution of 0.5 degrees FWHM. Once the gamma photons arrive at the detector no light spreading on the detector crystal and the PMTs was simulated, making simulated spatial resolution perform slightly better than in a real system.
Both in GATE and PeneloPET the gamma photons that reach the detector often create multiple interactions, and consequently multiple hits, within a given crystal. For instance, a photon may interact with a single crystal by two Compton scattering events and a photoelectric absorption and all the hits that occur within the same crystal are added (electronics always measure an integrated signal). Thus, the hits per volume are regrouped so that the output is two pulses: the energy is taken to be the total of energies in each volume and the position is obtained with an energy-weighted centroid of the different hit positions. The time is equal to the time at which the first hit occurred.

Scatter fraction and NEC performance. For the estimation of the scatter fraction and NEC curves a cylindrical, high density polyethylene NEMA NU-4 2008 phantom was simulated in proportion to the mouse animal size (NEMA 2008). It was 7 cm long and 2.5 cm in diameter. The line source was placed parallel to the central axis at a radial distance of 10 mm. The fillable section was 10 mm shorter than the cylindrical phantoms with a diameter of 3.2 mm. The initial activity was 5.8 mCi (214.5 MBq). The intrinsic radioactivity of the LSO (^{176}Lu) was not simulated with any of the MC codes. A non-paralysable dead-time model was introduced in GATE and PeneloPET for the coincidence events. Simulations for the scatter fraction also included the cover shield and the bed of the real tomograph.

No corrections were applied to the simulated sinograms. Data sets were rebinned to 2D sinograms after single slice rebinning (SSRB), using a span of 31 and ring difference of 15.

In PeneloPET, we considered a coincidence time window of 6 ns, which was known by the system, a trigger dead time of 15 ns, an integration time of 120 ns and non-paralysable singles dead time of 110.4 ns (Guez *et al* 2008). In GATE, we considered a coincidence time window of 6 ns, a pile-up time of 200 ns and non-paralysable singles dead time of 110.4 ns (Guez *et al* 2008). No coincidence dead time was taken into consideration in either simulations with PeneloPET or GATE.

Sensitivity. The same point source of 4.48 μCi (166 kBq) ^{22}Na, which used for the spatial resolution, was also simulated to determine the sensitivity of the system. The source was placed at the centre of the scanner and was stepped axially to either end with a step size identical to the slice thickness (1.21 mm). Simulations lasted for 60 sec at each position. No background true event rates were determined during the simulations. Data were rebinned into 3D sinograms with span of 3 and ring difference of 31. For mouse applications, sinograms which encompass the central 70 mm of the axial FOV were kept for analysis.

3. Results

*Spatial Resolution***.** Measured and simulated spatial resolutions are shown in figures1 (a, b), 2 (a, b) and figure 3 (a, b).

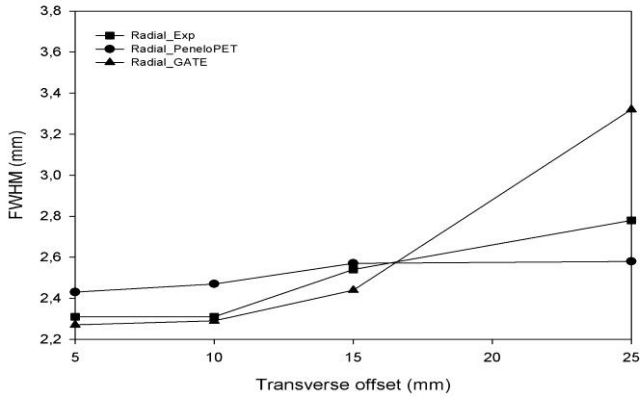

(a)

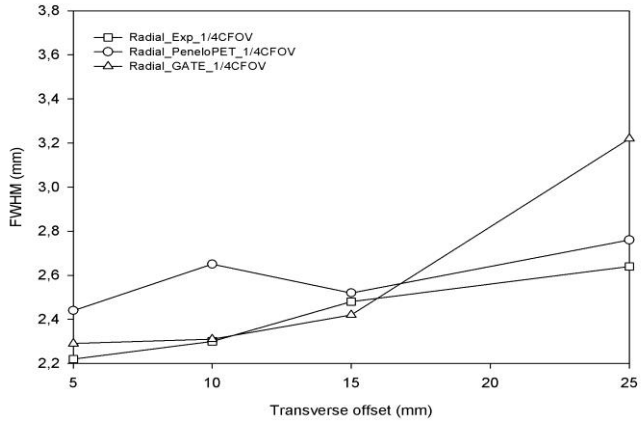

(b)

Figure 1. Radial measured and simulated spatial resolution of the microPET R4 system at CFOV (a) and at ¼ CFOV (b)

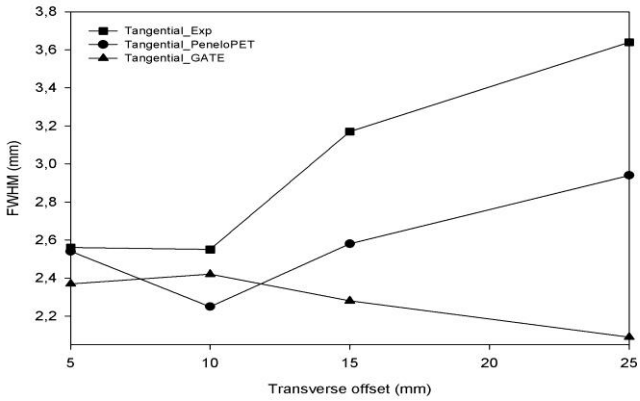

(a)

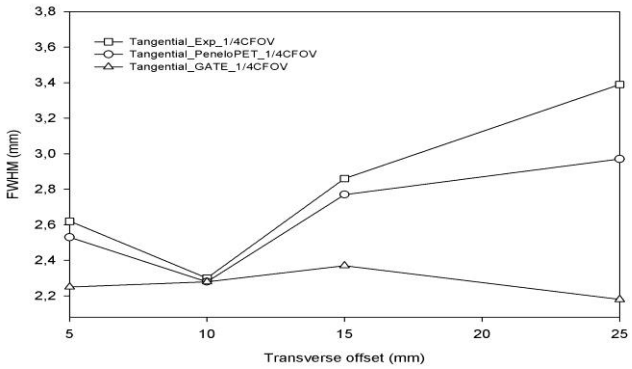

(b)

Figure 2. Tangential measured and simulated spatial resolution of the microPET R4 system at CFOV (a) and at ¼ CFOV (b)

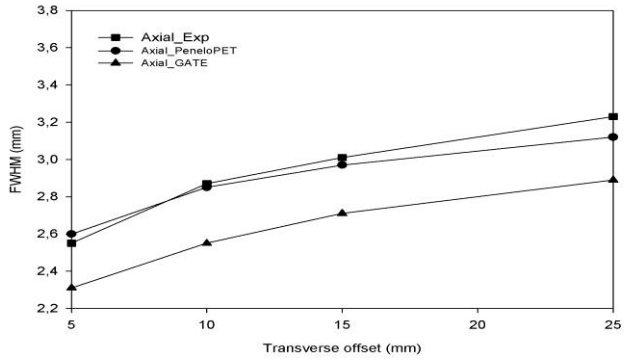

(a)

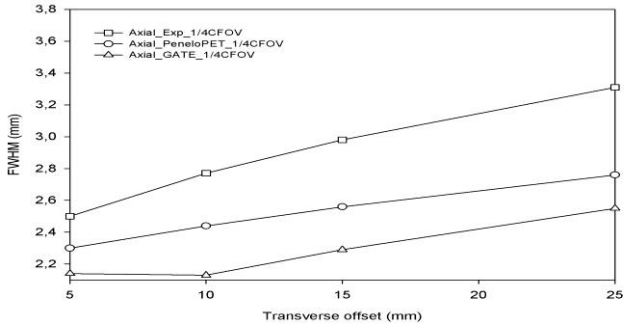

(b)

Figure 3. Axial measured and simulated spatial resolution of the microPET R4 system at CFOV (a) and at ¼ CFOV (b)

Sensitivity. Figure 4 shows the absolute system sensitivity obtained from measured and simulated data. The absolute measured system sensitivity was 1.9% at the centre of FOV using an energy window of 350-650 keV. Simulated sensitivity with GATE was 2.02%, while with PeneloPET was 2.07%.

An experimental efficiency factor of 81% was applied to the simulated data (GATE and PeneloPET) as a free parameter so as to allow the simulation to match with the efficiency of the measured data. The factor varied until

the best agreement between experimental and simulated results was obtained.

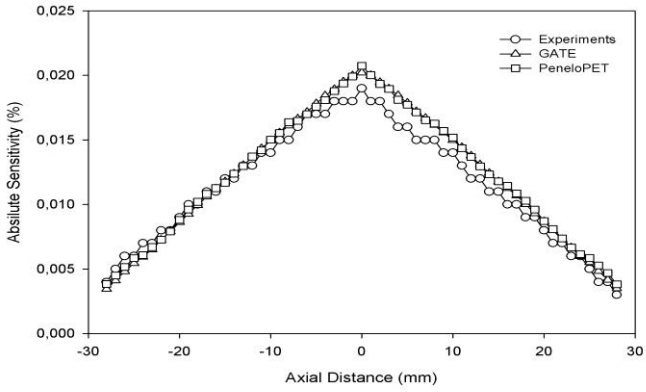

Figure 4. Measured and simulated absolute sensitivity of microPET R4

Scatter fraction and count rate performance. Scatter fractions for experimental and simulated NEMA NU 4-2008 standards are presented in Table 1.

	Scatter Fraction (%)
Experimental	8.5%
GATE	8.7%
PeneloPET	7.9%

Table 1. Scatter Fractions of the microPET R4 system of measured and simulated data using an energy window of 350-650 keV

Figure 5 compares total coincidence rate, true coincidence rate, random and scatter coincidence rate between experimental setup and simulation techniques.

Figure 6 shows experimental and simulated noise equivalent count rates (NEC). For an energy window of 350-650 keV, the experimental coincidence count rate was 311 kcps at 166.99 MBq average activity for the mouse-sized phantom. GATE coincidence count rate was 296 kcps at 166.99 MBq average activity while PeneloPET coincidence count rate was 315 kcps at 166.99 MBq average activity

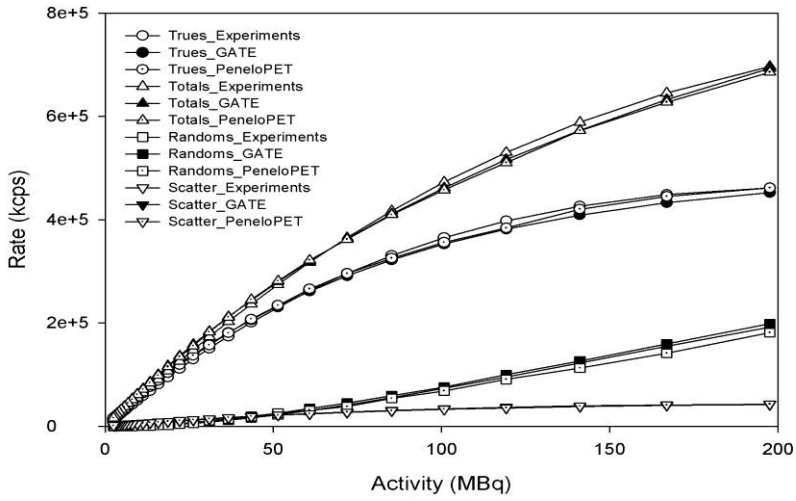

Figure 5. Experimental and simulated true, total, random and scatter coincidences for the microPET R4 system

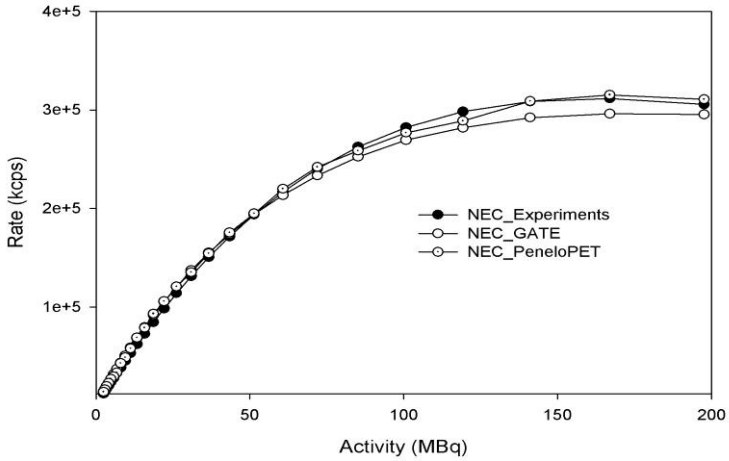

Figure 6. Experimental and simulated noise equivalent count rate (NEC) for the microPET R4 system.

In terms of CPU time, both MC codes were compared on an Intel® Core™ i3 CPU 540 @ 3.07GHz × 4 (16 Gb RAM). PeneloPET appeared to be faster than GATE. As an example, the same sensitivity simulation described in this work, involved 18 min for GATE and 13 min for PeneloPET.

4. Discussion

In this study, Monte Carlo simulation models of the microPET R4 system were developed based on GATE and PeneloPET. The proposed models were validated against experimental measurements based on the NEMA NU 4-2008 standards (Popota *et al* 2012) and mainly focused on system sensitivity, spatial resolution, scatter fraction and count rate performance.

The Monte Carlo simulations of the performance of the microPET R4 were compared in order to help potential users to choose the code that suits best each application. In this regard, it was also essential to understand

how each code differs from the other depending on the particular application, not only in relation to their performance, but also based on the strengths and weaknesses of their use.

Thus, the most important features of MC codes can be said that are these features which make the difference between them, and the features under investigation here were the accuracy, efficiency, flexibility and ease of use as an end user.

In terms of spatial resolution, PeneloPET and GATE were in good agreement for radial and tangential FWHM when compared with the experimental data at the CFOV for the different tangential distances. PeneloPET was also in good agreement with experimental data for radial and tangential FWHM at the ¼ CFOV. On the other hand, GATE showed a slight underestimation, particularly important for the tangential FWHM. In relation to the axial FHWM, PeneloPET showed good agreement with experimental results at the CFOV, whereas at ¼ CFOV both GATE and PeneloPET showed a small offset.

In terms of sensitivity, simulations were made to match the measured results by introducing a detection efficiency factor (Lazaro *et al* 2004, Latrizien *et al* 2007, Abushab *et al* 2011). This is a common procedure in order to avoid explicitly simulating light spread in the crystal, a real detector signal processing chain, optical coupling efficiencies and the PMTs. The efficiency in the emission of the photo-electrons from the cathode after the deposition of energy by a scintillation photon is referred to the efficiency factor that has been used here. Good agreement was obtained across the whole axial distance of the scanner between experiments, GATE and PeneloPET.

In terms of scatter fraction, high accuracy was obtained between simulations and experimental values, since all scattering mediums were properly incorporated in the simulation codes.

One of the most complicated simulations is that of counting rates due to the fact that an accurate model of the system's dead time is required in order to properly simulate it. Each code demands different parameters for the characterization of the dead time of the system, which sometimes are unknown or difficult to be found. However, no major discrepancies between the two codes were found.

PeneloPET has the ability to fully and accurately simulate the system's dead time since it takes into account the time that needs to be elapsed from a single trigger event until the next one can be resolved (trigger dead time). It also takes into account the time that needs to be elapsed from the trigger of one single event until the next trigger can be measured by the system. These two times must be in concordance with the rise and fall time of the crystal (integration time) and finally the time that needs to be elapsed from the trigger of a single event that is going to be integrated until new events can be measured in the detector (single dead time). All these sources of time are interconnected providing the most realistic system's dead time, which requires the use of adequate values for all of them. On the other hand though, this comes at a cost of knowing *a priori* the theoretical values of the system from the specifications of the system's components, or else, they should be used as adjustable parameters, which should be tuned to properly reproduce the actual system's dead time (Abushab *et al* 2011).

In GATE the proper timing of the simulated event sequence is an *a priori* input for modeling time-dependent processes such as count rates. A non-paralyzable dead time is modeled explicitly on an event-by-event basis. While these models represent the idealized behavior, they correctly predict the correct dead-times for a system. At the end of a digitizer chain in GATE, the coincidence sort was added to find pairs of singles that are in coincidence. Pairs of singles can be considered coincidences whenever the time interval between the singles is less than the coincidence window. Each single event is stored with its corresponding event number. If the event

numbers of the singles associated with a coincidence are different, it is considered to be a random coincidence. Multiple coincidences corresponding to more than two singles within the same coincidence window were discarded.

Apart from the performance results, it should be mentioned that both codes are freely available. PeneloPET can be obtained by request to the authors. Its installation is fairly easy and it does not require any special knowledge of computer skills. GATE's installation though can be quite demanding but help is available from the gate-user mailing list (http://www.opengatecollaboration.org).

In relation to the flexibility and ease to use, the simulations were accurately prepared by editing input files, where the exact physical parameters of the scanner and type of acquisitions were defined. Apart from the scanner, phantoms and sources used for each simulation, light guides, photomultiplier tubes and inter-crystal and inter-ring material were also defined.

More in detail, the codes allow simulation of either kind of detectors no matter whether they are continuous rings or blocks of detectors including pixelated block of crystals. Definition of shielding, surrounding material and bed were also included in the simulations. The phantoms used in the experiments were simulated in detail using the input files of GATE and PeneloPET.

Both codes provide a detailed list of all isotopes used in PET. Also, the direction of emission is made randomly and isotropically in both codes. After editing, definition of the geometry of the scanner and objects used can be visualized by tools provided by GATE and PeneloPET, which is very helpful for the end user in order to verify that the geometry of the scanner has been properly reproduced. Once everything is defined and depending on what is simulated, it is possible to split the simulation in any number of

parallel processes which reduces computational time just by using simple scripts. This improves the computational efficiency of both codes.

In terms of CPU time, PeneloPET appeared to be faster than GATE, which may be an important factor when deciding on a MC code and the simulations to be performed, especially time demanding ones.

Both MC codes, used here, have been validated against several PET systems using the NEMA NU 2-2001 standards, whereas they have not been validated using the NEMA NU 4-2008 standards. They are both considered to be accurate and efficient, whereas the practical applicability of each code depends on the preferences and particular requirements of the end user depending the simulations that are about to be performed.

5. Conclusions

We have compared the capability of GATE and PeneloPET to simulate the performance evaluation of the microPET R4 system under the established standards of NEMA NU 4-2008 standards for small animal PET systems.
The results of the study indicate that both codes can accurately simulate the main performance characteristics of the R4 system. They both use accurate models to describe the physics, the detection system and the phantoms used in each simulation.
For the simulation of sensitivity both codes provided accurate results in comparison with the experimental data once some physical phenomena not simulated in detail were effectively taken into account using an efficiency factor in both MC codes.
PeneloPET may use a thorough knowledge of the system's dead time component, if known. If these system contributions to dead time are not known *at priori* dead time simulation in PeneloPET should proceed via tuning some of the parameters of the simulation. This differentiates PeneloPET from GATE when counting rates have to be simulated since the

latter considers less parameters during dead time simulation, and thus tuning these to describe actual system behaviour is less cumbersome.

Acknowledgements

This work was supported in part by AMIT project (CEN-20101014) from the CDTI-CENIT program (Ministerio de Ciencia e Innovación) and Fondo de Investigaciones Sanitarias (PI12-00390).

References

Abushab KM, Herraiz JL, Vicente E, España S, Vaquero JJ and Udías JM 2011 PeneloPET simulations of the Biograph ToF clinical PET scanner *IEEE Nuclear Science Symposium and Medical Imaging Conference* 4420-4428

Agostinelli S *et al* 2003 Geant4—a simulation toolkit *Nuclear Instruments and Methods in Physics Research Section A: Accelerators, Spectrometers, Detectors and Associated Equipment,* **506**(3) 250-303

Assie K, Gardin I, Vera P and Buvat I 2004 Validation of the Monte Carlo simulator GATE for indium-111 imaging *Phys Med Biol* **50**(13) 3113-25

Barret O, Carpenter T A, Clark J C, Ansorge R E and Fryer T D 2005 Monte Carlo simulation and scatter correction of the GE advance PET scanner with SimSET and Geant4 *Phys. Med. Bio.* **50**(20) 4823-40

Braem A *et al* 2004 Novel design of a parallax free Compton enhanced PET scanner *Nuc Instr Med A* **525** 268-274

Carlier T, Moisan M, Ferrer L, Kraeber-Bodere F, Barbet J and Bardies M 2008 Validation of a GATE model of the Siemens Symbia system for 99mTc, 111In and 131I acquisitions *J Nucl Med* **49** (Supplement 1):405P

Castiglioni I, Cremonesi O, Gilardi M C, Bettinardi V, Rizzo G, Savi A, Bellotti E, Fazio F 1999 Scatter Correction Techniques in 3D PET: A Monte Carlo Evaluation *IEEE Trans. Nuc. Science* **46**(6) 2053-58

España S, Herraiz JL, Vicente E, Herranz E, Vaquero JJ, Desco M and Udias JM 2007 Validation of PeneloPET Against Two Small Animal PET Scanners *IEEE Nuc Sci Symp Conf Rec* **5** 3640-3643

España S, Herraiz J L, Vicente E, Vaquero J J, Desco M and Udias J M 2009 A Monte Carlo PET simulation tool based on PENELOPE: features and validation *Phys. Med. Biol.* **54**(6) 1723-1742

Gonias P *et al* 2007 Validation of a GATE model for the simulation of the Siemens PET/CT biograph 6 scanner *Nucl. Instr. Meth. Phys. Res.* **571** 263-266

Guez D, Bataille F, Comtat C, Honore P F, Jan S and Kerhoas S 2008 Counting Rates Modeling for PET Scannners With GATE *IEEE Trans Nuc Med* **55**(1) 516-523

Harrison RL, Haynor DR, Gillispie SB, Vannoy SD, Kaplan MS and Lewellen TK 1993 A public domain simulation system for emission tomography. Photon tracking through heterogeneous attenuation using importance sampling *J Nuc Med* **34**(5): 60P

Herraiz JL, España S, Vaquero JJ, Desco M and Udias JM 2006 FIRST: fast iterative reconstruction software for (PET) tomography *Phys. Med. Bio.* **51** 4547-4565

Herraiz JL, Vicente E, España S, Vaquero JJ, Jakoby BW and Udias JM 2011 PeneloPET simulations of the Biograph ToF clinical PET scanner *IEEE Nuc Sci Symp and Med Imag Conf* 4420-4428

Jan S *et al* 2004 GATE: a simulation toolkit for PET and SPECT *Phys. Med. Bio.* **49** 4543-4561

Jan S, Comtat C, Strul D, Santin G and Trabossen R 2005 Monte Carlo simulation for the ECAT EXACT HR+ system using GATE *IEEE Trans. Nucl. Sci.* **52** 627-633

Karakatsanis N *et al* 2006 Comparative evaluation of two commercial PET scanners, ECAT EXACT HR+ and Biograph 2, using GATE *Nucl. Instr. Meth. Phys. Res.* **571** 368-372

Knoess C *et al* 2003 Performance evaluation of the microPET R4 PET scanner for rodent *Eur J Nucl Med Mol Imaging* **30**737-747

Lamare F, Turzo A, Bizais Y, Le Rest CC and Visvikis D 2006 Validation of a Monte Carlo simulation of the Philips Allegro/GEMINI PET systems using GATE *Phys. Med. Biol.* **51** 943-962

Lartizien C, Kuntner C, Goertzen AL, Evans AC and Reilhac A 2007 Validation of PET-SORTEO Monte Carlo simulations for the geometries of the microPET R4 and Focus 220 PET scanners *Phys. Med. Bio.* **52** 4845-4862

Lazaro D *et al* 2004 Validation of the GATE Monmte Carlo simulation platform for modelling a CsI(Tl) scintillation camera dedicated to small animal imaging *Phys. Med. Biol.* **49** 271-287

Liu H and Zhao S 2012 Overview of PeneloPET: a PET-dedicated Monte Carlo simulation toolkit *4th Electronic System-Integration Technology Conference* 1000-1003

Monte Carlo N-Particle Code, MCNP, http://mcnp-green.lanl.gov/

Merheb C, Nicol S, Petegnief Y, Talbot JN and Buvat I 2006 Assessment of the Mosaic animal PET system response using list-mode data for validation of GATE Monte Carlo modelling *Nucl. Instrum. Meth. A* **569**(2) 220-224

National Electrical Manufacturers Association. 1994 Performance Measurements of the Positron Emission Tomographs. Rosslyn, VA Standards Publication NU 2-1994

National Electrical Manufacturers Association 2001 Performance Measurements of Positron Emission Tomographs. Rosslyn VA Standards Publication NU 2-2001.

National Electrical Manufacturers Association 2007 Performance Measurements of Positron Emission Tomographs. Rosslyn VA Standards Publication NU 2-2007

National Electrical Manufacturers Association 2008 Performance measurements of Small Animal Positron Emission Tomographs. Rosslyn VA Standards Publication NU 4-2008.

Nelson WR, Hirayama H and Rogers DWO 1985 The EGS4 Code System Report SLAC-265 (Stanford Linear Accelerator Center, Stanford, CA)

Popota FD, Aguiar P, Herance RJ, Pareto D, Rojas S, Ros D, Pavia J and Gispert JD 2012 Comparison of the Performance Evaluation of the MicroPET R4 Scanner According to NEMA NU 4-2008 and NEMA NU 2-2001 *IEEE Trans Nuc Sci* 59(5) 1879-1886

Rafecas M, Fontaine R, Rechka S and Lecomte R 2009 Development and Validation of a GATE Simulation Model for the LabPET Scanner *IEEE Transactions on Nuclear Science* **56**(6) 3672-3679

Salvat F, Fernandez-Varea J and Sempau J 2006 *PENELOPE-2006 : A Code System for Monte Carlo Simulation of Electron and Photon Transport*, 1st edition, OECD, ISBN 92-64-02301-1

Schmidtlein CR, Kirov AS, Bidaut LM, Nehmeh SA, Erdi YE, Ganin A, Stearns CW, McDaniel DL, Hamacher KA, Humm JL, Amols HI. Validation of GATE Monte Carlo simulations of the GE Advance/Discovery LS PET scanner. Med. Phys. 33 (2006) 198-208

Schmidtlein CR, Kirov AS, Nehmeh SA, Bidaut LM, Erdi YE, Hamacher KA, Humm JL, and Amols HI 2005 Validation of GATE Monte Carlo Simulations of the Noise Equivalent Count Rate and Image Quality for the GE Discovery LS PET System *Medical Physics*, **32**(6) 1900

Staelens S, Strul D, Santin G, Vandenberghe S, Koole Y, D'Asseler Y, Lemahieu I, Van de Walle R 2003 Monte Carlo simulations of a scintillation camera using GATE: validation and application modelling *Phy Med Biol* **48**(18) 3021

Standardization Policies and Procedures of the National Electrical Manufacturers. 2008. http://www.nema.org/Standards/About-Standards/Documents/SPP-2008.pdf

Susrt S and Karp J S 2008 Design considerations for a limited angle, dedicated breast, TOF PET scanner *Phys. Med. Bio.* **53** 2911-2921

Tai YC, Chatziioannou A, Siegel S, Young J, Newport D, Goble RN, Nutt RE and Cherry SR 2001 Performance evaluation of the microPET P4: a PET system dedicated to animal imaging *Phys. Med. Biol*. **46** 1845-186

Vicente E, Herraiz JL, Canadas M, Cal-Gonzalez J, Espana S, Desco M, Vaquero JJ and Udias JM 2010 Validation of NEMA NU 4-2008 Scatter Fraction estimation with ^{18}F and ^{68}Ga for the ARGUS small animal PET scanner *Nuc Sci Symp Conf NSS/MIC* **12** 3553-3557

Yang CC, Seidel J, Wang Y, Lee JS, Pomper MG, Tsui BMW 2007 Validation of GATE Monte Carlo simulation of the performance characteristics of a GE eXplore VISTA small animal PET system *IEEE Nuc Sci Symp Conf Rec* **4** 3187-3190

Zaidi H 2007 Optimisation of whole-body PET/CT scanning protocols *Biomed Imaging Inter J (Review article)* **3**(2)

Zeraatkar N, Ay MR, Kamali-Asl AR and Zaidi H 2010 A Novel Model for the Monte Carlo Simulation of the Performance Parameters of the Rodent Research PET (RRPET) Camera Based on NEMA NU-4 Standards *XII Mediterranean Conference on Medical and Biological Engineering and Computing IFMBE Proceedings* **29** 311-14

4 | DISCUSSION

In the first study, "Comparison of the Performance Evaluation of the MicroPET R4 Scanner According to NEMA Standards NU 4-2008 and NU 2-2001", the performance evaluation of the microPET R4 scanner in function of spatial resolution, sensitivity, scatter fraction, count rate performance and image quality according to the NEMA NU 4-2008 standards for small animal PET systems has been studied.

The methodology followed in this study and the results obtained are described in section 3.1. It is worth mentioning though that according to the NEMA NU 4-2008 (NEMA 2008) standards, the reconstruction of the images obtained it is done by 2D or 3D FBP reconstruction method with no smoothing applied. In this aspect, it should be considered that one of the major limitations of FBP is the statistical noise, so a smoothing filter should be applied prior to reconstruction in order to control it. By this method though, the resolution would degrade because of the reduction of variance in the image (Alessio and Kinahan 2006). This did not take place during the processing of the spatial resolution and therefore the effect of noise in FWHM and FWTM, together with the maximum ring difference used may explain the relatively high variability in the results obtained.

Also, this approach of reconstruction it appears to be problematic for systems with irregular crystal spacing such as the LabPET (Goertzen 2012) systems and the PETbox (Zhang 2010) due to the degradation of resolution and artifacts introduced by interpolation and rebinning of measured data onto projections with regural spacing. Systems with

large axial extension, such as the InveonDPET (Bao 2008), are more prone to axial and radial photon penetration at large radial offsets and large ring differences if reconstructed with FBP. An alternative choice would be the use of statistical reconstruction methods, such as Maximum a Posteriori (MAP) or the Maximum Likelihood Expectation-Maximazation (ML-EM) algorithm.
The spatial resolution of the system at small radial distances was satisfactory given the actual detector size of the R4 system.

The sensitivity of the system was measured to be 1.9% at the center of the scanner's FOV using an energy window of 350-650 keV. The presence of the intrinsic radioactivity of LSO (176Lu) affects the system´s ability to detect low activities in the FOV. In the microPET R4 scanner the activity of ^{176}Lu in the 271 cm^3 of LSO is approximately 75 kBq (Goertzen 2007) but the fact that an energy window of 350-650 keV was used significantly reduced the amount of the intrinsic count rate and its contribution to the statistical noise.

The counting rate was plotted as a function of the average activity concentration for the mouse- and rat-sized phantoms. Its maximum corresponds to the relationship between real and noise events. The NECR for the mouse-sized phantom was found to be higher than the NECR for the rat-sized phantom because there is less photon attenuation forcing more photons getting out of the imaging subject.
It should be noted that during the evaluation of the scatter fraction and count rate performance according to the NEMA NU 2-2001 (NEMA 2001), different phantoms and energy windows were used

(Knoess 2003). This may justify the differences in the results between this study and the previous evaluation of the microPET R4 system.

The evaluation of the image quality after reconstruction of the images was first introduced in NEMA NU 4-2008 standards from small animal PET systems, so no previous results exist so as to be compared with the ones obtained in this study.

The image quality results provide estimation for a standardized imaging situation in small animal PET systems. All images were reconstructed using the three reconstruction algorithms provided by the microPET R4 scanner. Correction of attenuation was performed in order to assess the impact of corrections in the measurements, especially when cold regions are used where scatter radiation is increased. It is known though that the problem of photon attenuation in small animal imaging is not so much of importance since the size of the animals is much lower than in the human case.

Our results come in accordace with Goertzen 2012, who evaluated the performance parameters of various preclinical PET systems using the NEMA NU 4-2008 standards. Among the small animal PET systems they used in this study, they included the microPET R4 system and the results obtained do not significantly depart from the ones obtained in here.

Particularly, the values of spatial resolution were in good agreement between them for all radial distances across the FOV. Sensitivity values were 1.2%, whereas in our findings was 1.9% using an energy window of 350-650 keV.

Values of scatter fraction for mouse and rat applications were almost the same in both studies (using the mouse phantom: 9.3% vs. 8.5%, using a rat phantom: 22.2% vs. 22% in Goertzen 2012 and Popota 2012 respectively). The peak NECR using a mouse phantom was 618 kcps at 156 MBq in Goertzen 2012 and 311 kcps at 153.5 MBq in this study. The value of peak NECR using a rat phantom did not significantly depart from Goertzen 2012, since our findings indicated 117 kcps at 123.24 MBq in comparison to 137 kcps at 137 MBq.
The results obtained for image quality of the microPET R4 system did not significantly varied from Goertzen 2012, using FBP as a reconstruction algorithm and attenuation corrections.

In the second study, "Monte Carlo Simulations versus experimental measurements in a small animal PET system. A comparison in the NEMA NU 4-2008 framework", a comparison between the performance of two dedicated MC codes, GATE and PeneloPET, against experimental data following the NEMA NU-4 2008 standards for small animal systems, took place. The aim was to evaluate their strength and weaknesses in order to help potential users to choose the code best suited for a specific application.

From the results obtained in the simulation study for the spatial resolution, PeneloPET has an overall better performance that GATE. GATE showed a slight underestimation particularly for the tangential FWHM at ¼ CFOV. The radial and axial reoslution losses due to photon penetration and mispotioning of the coincidence events can be modeled with MC simulation and be incorporated into a system response matrix to recover these losses (Mumcuoglu 1996).

Good agreement was obtained in the results across the whole axial distance of the scanner between experiments, GATE and PeneloPET. It should be noted here, that the detection efficiency factor (Latrizien 2007, Lazaro 2004) was introduced in the simulations in order to compensate for not simulating explicitly the light spread in the crystal, the optical coupling efficiencies and the PMTs.

The simulations for the counting rates proved to be the most complicated ones due to the fact that an accurate model of the system's dead time is required to be properly simulated.
Each simulation code demands different input parameters, which characterize the system's dead time and sometimes are very difficult to be found. PeneloPET for example, requires many parameters to be known for the full and accurate simulation of the dead time and all these parameters are interconnected between them. So, this comes at a cost of knowing *a priori* the theoretical values of the system. If this is not possible, then these values should be used as adjustable parameters which require effort and time so as to properly reproduce the actual system's dead time. However, from the results obtained in this study, no major discrepancies between the two codes were found.

It is worth mentioning that NEMA standards try to provide a standardized methodology for evaluating the performance of small animal PET systems and that these measurements are not absolute. They can be used for comparing different systems since the methodology provided is fairly easy to perform although there are some ambiguities in some sections of the NEMA NU 4-2008 (NEMA

2008) standards. For example, it should be made clearer when calculating the sensitivity of a system as to which counts can be used when a system provides prompts and histogrammed coincidences as in the case of the microPET R4 scanner. Also, the quality of the reconstructed image depends on the size of the object and the contrasts used. The size of the NEMA NU 4-2008 (NEMA 2008) image quality phantom is more representative of a mouse's body and a rat's head; therefore the results obtained under these specifications must take into account the above statement.

Regarding the availability of the codes, both MC codes used in the study, are freely available to use and install although GATE may be quite demanding in the installation process. They are both flexible with accurate protocols to be edited for the set up of the system. PeneloPET maybe fairly more user friendly although they do not lack detail in simulating the physical parameters of a scanner. Visualization tools are available in both codes for the verification of the geometry of the scanner.

PeneloPET proved to be faster than GATE, which indicates that the central processing unit (CPU) time is crusial when time demanding simulations, like the ones of counting rates, are to be perfrormed.

Both simulation codes that have been used in this study have been validated for several PET systems using the NEMA NU 2-2001 clinical standards (Lamare 2006, Jan 2005, Staelens 2003, Carlier 2008). However, there are not many MC simulation studies using the NEMA NU 4-2008 standards (Vicente 2010, Zeraatkar 2010) for small animal PET systems.

Concluding, GATE and PeneloPET are undoubtedly the dedicated MC simulation codes of choice for PET and SPECT systems either for clinical or for small animal use.

5 | CONCLUSIONS

A) Performance Evaluation of the microPET R4 scanner according to the NEMA NU 4-2008 standards.

i. The performance evaluation using specific small animal PET standards departed notably from those obtained using the adapted clinical standards.

ii. The differences were mainly attributed to the use of different phantoms and energy windows.

iii. The results regarding the image quality of the microPET R4 system could not be compared to previous ones since they do not exist from previous studies.

B) Monte Carlo Simulations of the microPET R4 scanner in the NEMA NU 4-2008 framework.

i. Both dedicated codes can accurately simulate the main performance characteristics of the R4 system, which were focused in spatial resolution, sensitivity, scatter fraction and counting rates.

ii. Accurate results were obtained for the simulation of the spatial resolution for PeneloPET, whereas GATE showed a slight underestimation for the tangential FWHM at ¼ CFOV.

iii. High accuracy was obtained for sensitivity and scatter fraction when comparison between experiments and simulation codes was assessed.

iv. No major discrepancies between experiments, GATE and PeneloPET were found for the simulation of counting rates.

v. Thorough knowledge of the system's dead time is required when PeneloPET is the code of choice, while the system's contributions to dead time must be known *a priori* or be tuned via various simulations.

vi. PeneloPET proved to be faster than GATE in terms of CPU time.

6 | REFERENCES

Agostinelli S., K. Allison, et al. (2003). "GEANT4 – a simulation toolkit." *Nuc Inst Meth In Phys Res A 506: 250-303.*

Alessio A. M., P. E. Kinahan (2006). "Improved quantitation for PET/CT image reconstruction with system modeling and anatomical priors." *Med. Phys. 33(11): 4095-4103.*

Alessio A. M. and P. E. Kinahan (2006). "PET Image reconstruction" in "*Nuclear Medicine*" by R. E. Henkin, D. Bova, G. L. Dillehay, J. R. Halama, S. M. Karesh, R. H.Wagner, andA.M. Zimmer,Eds., 2nd ed. Philadelphia, PA: Mosby-Elsevier, vol. 1.

Andreo, P. (1991). "Monte carlo techniques in medical radiation physics." *Phys Med Biol 36(7): 861–920.*

Badawi R. D. and P. K. Marsden (1999). "Developments in component-based normalization in 3D PET." *Phys Med. Biol. 44: 571-594.*

Badawi R D, M. P. Miller et al. (1999), "Randoms variance reduction in 3D PET" *Phys Med Biol 44(4): 941-954.*

Bading J. R. and A. F. Shields (2008). "Imaging of cell proliferation: status and prospects." *J Nucl Med. 49(2): 64S–80S.*

Bahri M. A., A. Plenevaux, G. Warnock, A. Luxen, and A. Seret (2009). "NEMA NU 4-2008 image quality performance report for the microPET Focus 120 and for various transmission and reconstruction methods," *J. Nucl. Med 50: 1730–1738.*

Bailey D. L., D. Townsend, P. E. Valk, M. N. Maisey (2004). "Positron Emission Tomograpgy basic sciences" London, Springer. Bailey D. L. and S. R. Meikle (1994). "A convolution-substraction scatter correction methods for 3D PET" *Phys Med Biol 39(3): 411-424.*

Baró J., J. Sempau, J. M. Fernández-Varea, F. Salvat (1995). "PENELOPE: an algorithm for Monte Carlo simulation of the penetration and energy loss of electrons and positrons in matter", *Nucl. Instrum. Meth. B 100: 31–46.*

Belanger M. J., J. C. Yanch, A. Lu, A. B. Dobrznecki (1998). "The SimSPECT photon selector and multiple angular sampling of photons", *Nuc Sci Symposium 3: 2023-2025.*

Berard P., J. Riendeau et al. (2007). "Investigation of the LabPET detector and electronics for photon-counting CT imaging." *Nucl Instr Meth A 571: 114–7.*

Bernstein D. (2003). "Exercise assessment of transgenic models of human cardiovascular disease." *Physiol Genomics 13: 217–26.*

Beyer T., L. S. Freudenberg, J. Czernin, W. Townsend (2011). "The future of hybrid imaging-part 3: PET/MR, small animal imaging and beyond", *Insights Imaging 2: 235-246.*

Blasberg R. (2002). "PET imaging of gene expression." *Eur J Cancer. 38: 2137–2146.*

Bloomfield P. M., S. Rajeswaran et al. (1995). "The design and physical characteristics of a small animal positron emission tomography." *Phys Med Biol 40(6): 1105-26.*

Burokas A., E. Martin-Garcia et al. (2014). "Relationships between serotonergic and cannabinoid system in depressive – like behavior: a PET study with [11c]-DASB." J Neurochem (*in press).*

Buvat I., S. L. Bacharach, M. Soret (2007). "Partial Volume Effect in PET Tumor Imaging", *J Nucl Med 48: 932-345.*

Carlier T., M. Moisan, L. Ferrer, F. Kraeber-Bodere, J. Barbet, M. Bardies (2008). **"**Validation of a GATE model of the Siemens Symbia system for 99mTc, 111In and 131I acquisitions." *J Nucl Med 49(1): 405P*.

Casey M. E., H. Gadagkar, D. Newport (1995). "A component based method for normalization in volume PET." *Proceedings of the 3rd International Meeting on Fully Three-Dimensional Image Reconstruction in Radiology and Nuclear Medicine, Aix-les-Bains, France.*

Castiglioni, I., O. Cremonesi et al. (1999). "Scatter correction techniques in 3D PET: a Monte Carlo evaluation." *IEEE Trans. Nucl. Sci. 46: 2053-2058.*

Chatziioannou A. F. (2002). "PET Scanners dedicated to molecular imaging of small animal models." *Review Article, Mol Imag Biol 4(1): 47-63.*

Chatziioannou A. F., S. R. Cherry et al. (1999). "Performance evaluation of microPET: a high resolution lutetium

oxyorthosilicate PET scanner for animal imaging." *J Nucl Med 40: 1164-1175.*

Cherry S. R., J. A. Sorenson, M. E. Phelps (2003). "Physics in Nuclear Medicine.", 3rd edition, Saunders.

Colsher J. G. (1980). "Fully three dimensional positron emission tomography." *Phys. Med Biol 20: 103-115.*

Comtat C., P. E. Kinahan et al. (2002). "Clinically feasible reconstruction of 3D whole-body PET/CT data using blurred anatomical labels." *Phys. Med. Biol. 47: 1-30.*

Cutler P. D., S. R. Cherry, E. J. Hoffman, W. M. Digby, M. E. Phelps (1992). "Design features and performance of a PET system for animal research." *J. Nucl. Med., 33: 595-604.*

Daube-Witherspoon M. E., G. Muehllehner (1987). "Treatment if axial data in three-dimensional PET." *J Nucl Med 28: 1717-1724.*

Daugherty A. (2002). "Mouse models of atherosclerosis." *Am J Med Sci 323: 3–10.*

Defrise M., P. E. Kinahan et al. (1997). "Exact and approximate rebinning algorithms for 3D PET data." *IEEE Trans Med Imaging 16: 145-158.*

Defrise M. and G. T. Gullberg (2006). "Image reconstruction." *Phys Med Biol 51(13): R139–R154.*

Del Guerra A., N. Belcari (2002). "Advances in animal PET scanners." *Q. J. Nucl Med 46: 35-47.*

Del Guerra A., G. Di Domenico, M. Scandola, G. Zavattini (1998). "High spatial resolution small animal YAP-PET.", *Nucl Instum Methods Phys Res (A) 409: 508-510*.

Derenzo S. E., W. W. Moses et al. (1993). "Critical instrumentation issues for <2 mm resolution, high sensitivity brain PET." *I. International Congress Series; Quantification of Brain Function: Tracer Kinetics and Image Analysis in Brain PET: 25-32.*

EGS (2011) http://rcwww.kek.jp/research/egs/

Engstrom P. W. (1978). "Photomultipliers – then and now." *RCA Eng 24(1): 18-26.*

Erlandsoson K., I. Buvat, P. H. Pretorius, B. A. Thomas, B. F. Hutton (2012). "A review of partial volume correction techniques for emission tomography and their applications in neurology, cardiology and oncology." *Phys Med Biol 57: R119-R159.*

España S., J. L. Herraiz, E. Vicente, J. J. Vaquero, M. Desco, J. M. Udias (2009). "PeneloPET, a Monte Carlo PET simulation tool based on PENELOPE: features and validation." *Phys Med Biol 54(6): 1723-1742*.

Fahey F. H. (2002). "Data Acquisition in PET imaging." *J Nuc Med Tech 30(2): 39-49.*

Fontaine R., F. Belanger et al. (2005). "Architecture of a dual-modality, high-resolution, fully digital positron emission tomography/computed tomography (PET/CT) scanner for small animal imaging." *IEEE Trans Nuc Sci 52(3): 691-696.*

Gambhir S. S., J. Czernin, J. Schwimmer, D. H. S. Silverman, R. E. Coleman, M. E. Phelps (2001). "A tabulated summary of the FDG PET literature." *J Nucl Med. 42: 1S–93S.*

Gambhir S. S. (2002). "Molecular imaging of cancer with positron emission tomography." *Nat Rev Cancer 2: 683–693.*

Garlick P. B., P. K. Marsden et al. (1997). "PET and NMR dual acquisition (PANDA): applications to isolated, perfused rat hearts." *NMR Biomed. 10: 138–142*.

Geworski L., B. O. Knoop, M. L. de Cabreias, W. H. Knapp, D. L. Munz (2000). "Recovery correction for quantitation in emission tomography: a feasibility study*." Eur J Nucl Med 27: 161-169.*

Goertzen A. L., J. Y. Suk, C. J. Thompson (2007). "Imaging of weak-source distributions in LSO-based small animal PET scanners," *J. Nucl. Med. 48: 1692–1698.*

Goertzen A. L., Q. Bao, M. Bergeron et al. (2012). "NEMA NU 2-2008 comparison of preclinical PET imaging systems." *J. Nucl. Med. 53(8): 1300-9.*

Harrison R. L., D. R. Haynor et al. (1993). "A public-domain simulation system for emission tomography: Photon tracking through heterogeneous attenuation using importance sampling." *J Nuc Med 34(5): 60P*.

Hengerer A., T. Mertelmeir (2002). "Molecular Biology for Medical Imaging*." Biomedical Imaging 5th IEEE EMBS International Summer School on.*

Hoekzema E., S. Rojas et al. (2012). “In vivo molecular imaging of GABA/benzodiazepine receptor complex in the aged rat brain.” *Nuerobiol Aging 33(7): 1457-65*.

Hudson H. M., R. S. Larkin (1994). “Accelarated image reconstruction using ordered subsets of projection data.” *IEEE Trans Med Imag 13: 601-609.*

Hume S. P., R. N. Gunn, T. Jones (1998). “Pharmacological contsrains associated with positron emission tomographic scanning of small laboratory animals.” *Eur J Nucl Med 25: 173-176*.

Hutchins G. D., M. A. Miller, V. C. Soon, T. Receveur (2008). “Small Animal PET Imaging.” *ILAR J 49(1): 54-56.*

Jan S., G. Santin, D. Strul, S. Staelens et al. (2004). “GATE: a simulation toolkit for PET and SPECT.” *Phys. Med. Biol. 49: 4543-4561*.

Jan S., C. Comtat, D. Strul, G. Santin, R. Trabossen (2005). “Monte Carlo simulation for the ECAT EXACT HR+ system using GATE.” *IEEE Trans. Nucl. Sci. 52: 627-633*.

Jacoda E. M., J. J. Vaquero, J. Siedel, M. V. Green, W. C. Eckelman (2004). “Experiment assessment of mass effects in the rat: implications for small animal PET imaging.” *Nuc Med and Biol 31: 771-779*

Kanekal S., A. Sahai, R. E. Jones, D. Brown (1995). “Storage-phosphor autoradiography: a rapid and highly sensitive method for spatial imaging and quantitation of radioisotopes.” *J Phramcol Toxicol Methods 33(3): 171-178*.

Karp J. S., M. E. Daube-Witherspoon et al. (1991). "Performance standards in positron emission tomography." *J Nucl Med 32: 2342-2350.*

Kinahan P. E. and J. G. Rogers (1989). "Analytic three dimensional image reconstruction using all detected events." *IEEE Trans Nucl Sci 36: 964-968.*

Kinahan P. E., D. W. Townsend, T. Beyer, D. Sashin (1998). "Attenuation correction for a combined 3D PET/CT scanner." *Med Phys 25(10): 2046–2053.*

Knoess C., S. Siegel et al. (2003). "Performance evaluation of the microPET R4 PET scanner for rodents." *Eur J Nucl Med Mol Imaging 30(5): 737-47.*

Knoll G. (2000). "Radiation Detection and Measurement", *Third Edition, John Wiley & Sons, Inc.*

Kuncic Z., A. McNamara, K. Wu, D. Boardman (2011). "Polarization enhanced X-ray imaging for biomedicine." *Nuc Instr and Meth (A) 648(1): S208-S210.*

Laborina M., A. Brunetti, M. Salvatore (2006). "Small Animal PET: A review of commercially available imaging systems." *Current Medical Imaging Review 2: 187-192.*

Lamare F., A. Turzo, Y. Bizais, C. C. Le Rest, D. Visvikis (2006) "Validation of a Monte Carlo simulation of the Philips Allegro/GEMINI PET systems using GATE." *Phys. Med. Biol.* 51: 943-962.

Lapi S. E., T. F. Voller, M. J. Welch (2009). "PET imaging of hypoxia." *PET Clin. 4: 39–47.*

Lartizien C., C. Kuntner, A. L. Goertzen, A. C. Evans, A. Reilhac (2007). "Validation of PET-SORTEO Monte Carlo simulations for the geometries of the microPET R4 and Focus 220 PET scanners." *Phys. Med. Bio.* 52: 4845-4862.

Lavoie J. L., R. A. Bianco et al. (2004). "Transgenic mice for studies of the renin-angiotensin system in hypertension." *Acta Physiol Scand 181: 571–577.*

Lazaro D., I. Buvat et al. (2004) "Validation of the GATE Monte Carlo simulation platform for modeling a CsI(Tl) scintillation camera dedicated to small animal imaging." *Phys. Med. Biol.* 49: 271-287.

Lecomte R., J. Cadorette, P. Richard, S. Rodrigue, D. Rouleau (1994). "Design and engineering aspects of a high resolution positron tomography for small animal imaging." *IEEE Trans Nucl Sci, 41: 1446-1452.*

Lecomte R, J. Cadorette et al. (1996). "Initial results from the Sherbrooke avalanche photodiode positron tomography." *IEEE Trans Nucl Sci, 43: 1952-1957.*

Levin C. S. (2004). "Emission tomography: The fundaments of pet and spect." *Elsevier, Chap. Basic Physics of Radionuclide Imaging, pages 53–88. 2.1.2, 2.1.3.1, 2.1.3.2.*

Levin C. S., M. Dahlbom, E. J. Hoffman (1995). "A Monte Carlo Correction for the Effect of Compton Scattering in 3D PET Brain Imaging." *IEEE Trans Nucl Sci 42(4): 1181-1185.*

Levin C. S., E. J. Hoffman (1999). “Calculation of positron range and its effects on the fundamental limit of positron emission tomography system spatial resolution”, *Phys Med Biol 44: 781-799.*

Lewellen T. K. (2008). “Recent developments in PET technology”, *Phys. Med. Biol. 53: R287-R317.*

Lewis J. S., S. Achilefu, J. R. Garbow, R. Laforest, M. J. Welch (2002). “Small animal imaging: current technology and perspectives for oncological imaging.” *Eur J Cancer 38: 2173-8.*

Liang H., Y. Yang et al. (2007). “A microPET/CT system for in vivo small animal imaging.” *Phys Med Biol 52: 3881–94.*

Lucas A. J., R. C. Hawkes et al. (2006). “Development of a combined microPET-MR system.” *Technol Cancer Res Treat. 5: 337–341.*

Madar I., Y. Huang et al. (2009). “Detection and quantification of the evolution dynamics of apoptosis using the PET voltage sensor 18F-fluorobenzyl triphenyl phosphonium.” *J Nucl Med. 50: 774–780.*

Maramraju S. H., S. D. Smith et al. (2011). “Small animal simultaneous PET/MRI: initial experiences in a 9.4 T microMRI.” *Phys Med Biol, 56(8):2459-80.*

Magota K., N. Kubo, Y. Kuge, K. Nishijima, S. Zhao, N. Tamaki (2011). “Performance characterization of the Inveon preclinical small-animal PET/SPECT/CT system for multimodality imaging.” *Eur J Nucl Med Mol Imaging 38(4): 742-52.*

McLennan A., A. Reilhac, M. Brady (2009). "SORTEO: Monte Carlo-based simulator with list-mode capabilities." *Conf Proc IEEE Eng Med Biol Soc 3751-3754.*

MCNP https://mcnpx.lanl.gov/

Melcher C. L. (2000). "Scintillation crystals for PET." *J Nucl Med 41: 1051-1055.*

Merheb C., Y. Petegnief, J. N. Talbot (2007). "Full modeling of the MOSAIC animal PET system based on the GATE Monte Carlo simulation code." *Phys. Med. Biol. 52(3): 563-76.*

Michaelides M., J. Pascau et al. (2010). "Dopamine D4 receptors modulate brain metabolic activity in the prefrontal cortex and cerebellum at rest and in response to methylphenidate." *Eur J Neurosci 32(4): 668-676.*

Michalski M., X. Chen (2011). "Molecular imaging in cancer treatment." *Eur J Nucl Med Mol Imaging 38: 358–377.*

Missimer J., Z. Madi, M. Honer, C. Keller, A. Schubiger, S. M. Ametamey (2004). "Performance evaluation of the 16-module quad-HIDAC small animal PET camera." *Phys. Med. Biol. 49: 2069–2081.*

Muehllehner G. and J. S. Karp (2006). "Positron Emission Tomography." *Phys Med Biol 51: R117-R137.*

Mumcuoglu E. U., R. M. Leahy, S. R. Cherry, E. Hoffman (1996). "Accurate geometric and physical response modelling for statistical image reconstruction in high resolution PET." *IEEE Nucl Sci Symp Conf Rec. 3:1569-1573.*

Nagy K., M. Toth et al (2013). “Performance evaluation of the small animal nanoScan PET/MRI system.” *J Nuc Med, 54(10):1825-1832*.

National Electrical Manufacturers Association. Performance Measurements of the Positron Emission Tomographs. Rosslyn, VA; 1994. Standards Publication NU 2-1994.

National Electrical Manufacturers Association. Performance Measurements of Positron Emission Tomographs. Rosslyn VA; 2001. Standards Publication NU 2-2001.

National Electrical Manufacturers Association. Performance Measurements of Positron Emission Tomographs. Rosslyn VA; 2007. Standards Publication NU 2-2007.

National Electrical Manufacturers Association. Performance measurements of Small Animal Positron Emission Tomographs. Rosslyn VA; 2008 Standards Publication NU 4-2008.

National Electrical Manufacturers Association. Performance Measurements of Positron Emission Tomographs. Rosslyn VA; 2013. Standards Publication NU 2-2012.

Niu G., Chen X. (2009). “PET imaging of angiogenesis.” *PET Clin. 4: 17–38.*

Perez-Campana C., V. Gomez-Vallejo et al. (2014). “Assessing lung inflammation after nanoparticle inhalation using 2-deoxy-2-[18F]fluoro-D-glucose positron emission tomography imaging.” *Mol Imaging Biol 16: 264-273.*

Phelps M. E. (2004). “Molecular Imaging and its Biological Applications.” Springer, New York.

Phelps M. E. (2006). “PET: physics, instrumentation and scanners.” Springer, New York.

Pichler B. J., Boning C. et al (1998). “Studies with a prototype high resolution PET scanner based on LSO-APD modules.” *IEEE Trans Nucl Sci, 45:1298-1302*.

Puig I., I. Chicote et al. (2013). “A personalized preclinical model to evaluate the metastatic potential of patient-derived colon cancer initiating cells.” *Clin Cancer Res 19(24): 6787-801*.

Rafecas M., Mosler B. et al. (2004). “Use of a Monte Carlo-based probability matrix for 3-D iterative reconstruction of MADPET-II data.” *IEEE Trans Nucl Sci 51: 2597–605*.

Raylman R. R., Majewski S. et al. (2006). “Simultaneous MRI and PET imaging of a rat brain.” *Phys Med Biol. 51: 6371–6379.*

Rojas S., J. R. Herance et al. (2013). “In vivo evaluation of amyloid deposition and brain glucose metabolism of 5XFAD mice using positron emission tomography.” *Neurobiol Aging 34(7): 1790-1798.*

Rojas S., A. Martin et al. (2011). “Positron emission tomography with 11C-flumazenil in the rat shows preservation of binding sites during the acute phase after 2 h-transient focal ischemia.” *Nueroscience 19: 182-208.*

Rojas S. A., A. Martin et al. (2007). “Imaging brain inflammation with [(11)C]PK11195 by PET and induction of the peripheral-type benzodiazepine receptor after transient

focal ischemia in rats." *J. Cereb Blood Flow Metab. 27(12): 1975-1986.*

Rojas S., J. D. Gispert et al. (2011). "Biodistribution of amino-functionalized diamond nanoparticles. *In vivo* studies based on 18F radionuclide emission." *ACS Nano 5(7): 5552-5559.*

Saha G. B. (2010). "Basics of PET Imaging: Physics, Chemistry and Regulations." *Second Edition, Springer, New York.*

Staelens S., D. Strul et al. (2003). "Monte Carlo simulations of a scintillation camera using GATE: validation and application modeling." Phy Med Biol 48(18): 3021.

Salvat, F., J. M. Fernandez-Varea, J. Sempau, J. Mazurier (1999). "Pratical aspects of monte carlo simulation of charged particle transport: Mixed algorithms and variance reduction techniques." *Radiat Environ Biophys 38: 15–22.*

Saoudi A. and R. Lecomte (1999). "A novel APD-based detector module for multi-modality PET/SPECT/CT," *IEEE Trans Nuc Sci 46: 479-484.*

Schafers K. P., A. J. Reader, M. Kriens, C. Knoess, O. Schober, M. Scahfers (2005). "Performance evaluation of the 32-Module quadHIDAC small animal PET scanner." *J Nuc Med 46(6): 996-1004.*

Schnockel U., S. Hermann et al. (2010). "Small-animal PET: a promising, non invasing tool in pre-clinical research." *Eur J Pharm Biopharm. 74: 50-54.*

Seidel S., J. J. Vaquero, M. V. Green (2003). "Resolution uniformity and sensitivity of the NIH ATLAS small animal PET scanner: Comparison to simulated LSO scanners without the depth-of-interaction capability." *IEEE Trans Nuc Med 50(5): 1347-1350.*

Shepp L. A., Y. Vardi (1982). "Maximum likelihood reconstruction for emission tomography." *IEEE Trans Med Imag MI-1 (2): 113-122.*

Standardization Policies and Procedures of the National Electrical Manufacturers (2008). http://www.nema.org/Standards/About-Standards/Documents/SPP-2008.pdf.

Tai Y. C., A. Chatziioannou et al. (2001). "Performance evaluation of the microPET P4: A PET system dedicated to animal imaging." *Phys.Med. Biol. 46: 1845–1862.*

Tai Y. C., A. Ruangma et al. (2005). "Performance evaluation of the micropet focus: A third generation micropet scanner dedicated to animal imaging." *J Nuc Med 46: 455–463.*

Tarantola G., F. Zito, M. D. Gerundini (2003). "PET Instrumentation and Reconstruction Algorithms in Whole-Body Applications." *J Nuc Med, 44(5): 756-769 Continuing Education.*

Tatsumi M., Y. Nakamoto et al. (2003). "Initial experience in small animal tumor imaging with a clinical positron emission tomography/computed tomography scanner using 2-[F-18]Fluoro-2-deoxy-D-glucose." *Cancer Res 63: 6252–6257.*

Tenbaum S. P., P. Ordonez-Moran et al. (2012). “β-catenin confers resistance to PI3K and AKT inhibitors and subverts FOXO3a to promote metastasis in colon cancer.” *Nat Med 18(6): 892-901*.

Teo B. K., Y. Seo et al. (2007). “Partial-volume correction in PET: validation of an iterative postreconstruction method with phantom and patient data.” *J Nuc Med 48: 802-810.*

Thomas D., H. Bal et al (2008). “Noninvasive assessment of myocardial viability in a small animal model: comparison of MRI, SPECT and PET.” *Magn Reson Med 59(2): 252-9.*

Turkington TG (2001). “Introduction to PET Instrumentation.” *J Nuc Med Technol 29: 1-8.*

Vaquero J. J., J. Seidel, S. Siegel, W. R. Gandler, M. V. Green (1998). “Performance characteristics of a compact position-sensitive LSO detector module.” *IEEE Trans Med Imaging 17(6): 967-978.*

Vaquero J. J., E. Lage et al. (2005). “rPET detector design and data processing.” *IEEE NSS Conf Rec 5: 2885-2889.*

Vicente E., J. L. Herraiz et al. (2010). “Validation of NEMA NU 4-2008 Scatter Fraction estimation with 18F and 68Ga for the ARGUS small animal PET scanner.” *Nuc Sci Symp Conf NSS/MIC 12: 3553-3557.*

Visser E. P., A. Disselhorst et al. (2009). “Spatial resolution and sensitivity of the Inveon small animal PET scanner.” *J. Nuc Med 50: 139–147.*

Wang Y., J. Seidel, B. Tsui, J. J. Vaquero, M. G. Pomper (2006). "Performance evaluation of the GE healthcare eXplore vista dual-ring small-animal pet scanner." *J Nuc Med 47(11): 1891–1900.*

Watanabe M., H. Uchida et al. (1992). "A high resolution PET for animal studies." *IEEE Trans. Med. Imag. 11: 577-580.*

Watson C. C., M. E. Casey et al. (2004). "NEMA NU2 performance tests for scanners with intrinsic activity." *J Nuc Med 45: 822-826.*

Welch M. J., J. S. Lewis et al. (2006). "Assessment of myocardial metabolism in diabetic rats using small-animal PET: a feasibility study." *J Nuc Med 47(4): 689-97.*

West C. M. L., T. Jones, P. Price (2004). "The potential of positron-emission tomography to study anticancer-drug resistance." *Nature Reviews Cancer 4: 457-469.*

Williams R. W., P. Rakic (1988). "3-Dimensional counting: an accurate and direct method to estimate numbers of cells in sectioned material." *J Comp Neurol 278: 344-352.*

Woody C., D. Schlyer et al. (2007). "Preliminary studies of a simultaneous PET/MRI scanner based on the RatCAP small animal tomograph." *Nuc Instr Meth Phys Res (A) 571: 102–105.*

Xiao J., T. C. de Wit, W. Zbijewski, S. Staelens, F. J. Beekman (2007). "Evaluation of 3D Monte Carlo–Based Scatter Correction for 201Tl Cardiac Perfusion SPECT." *J Nuc Med 48(4): 637-644.*

Yamamoto S., M. Imaizumi et al. (2010). “Design and performance from an integrated PET/MRI system for small animals.” *Ann Nucl Med, 24(2):89-98.*

Yao R., R. Lecomte, E. S. Crawford (2012). “Small-animal PET: What is it, and why do we need it?.” *J Nuc Med Technol 40: 157-165.*

Zaidi, H. (1999). “Relevance of accurate monte carlo modeling in nuclear medical imaging.” *Med Phys 26(4): 574–608.*

Zaidi H. (2000). “Comparative evaluation of scatter correction techniques in 3D positron emission tomography.” *Eur J Nucl Med 27(12): 1813-26.*

Zanzonico P. (2004). “Positron Emission Tomograhy: A Review of basic Principles, Scanner Design and Performance, and Current Systems.” *Seminars in Nuclear Medicine, Vol XXXIV, 2: 87-111.*

Zeng, G. L. (2001). "Image reconstruction--a tutorial." *Computerized medical imaging and graphics : the official journal of the Computerized Medical Imaging Society 25(2): 97-103.*

Zeraatkar N., M. R. Ay, A. R. Kamali-Asl, H. Zaidi (2010). “A Novel Model for the Monte Carlo Simulation of the Performance Parameters of the Rodent Research PET (RRPET) Camera Based on NEMA NU-4 Standards.” *XII Mediterranean Conference on Medical and Biological Engineering and Computing IFMBE Proceedings 29***:** *311-14.*

Zhang H., Q. Bao, et al. (2011). “Performance evaluation of PETBox: A low cost bench top preclinical PET scanner.” *Mol. Imaging Biol.13(5): 949–961.*

Zhang L., S. Staelens et al. (2010). “Fast and memory-efficient Monte Carlo-based image reconstruction for whole-body PET.” *Med Phys.37(7): 3667-76.*